BANDWIDTH EFFICIENT TRELLIS CODING FOR UNITARY SPACE-TIME MODULATION IN NON-COHERENT MIMO SYSTEM

SUN ZHENYU

A THESIS SUBMITTED
FOR THE DEGREE OF PHILOSOPHY OF DOCTORAL
DEPARTMENT OF ELECTRICAL & COMPUTER ENGINEERING
NATIONAL UNIVERSITY OF SINGAPORE
2003

Acknowledgements

I am indebted to my supervisor, Professor Tjhung Tjeng Thiang, for his leading me into this exciting area of wireless communications and for his cheerful optimitism and warm encouragemnets throughout the course of my research. I have learned from him not just how to solve complicated problems in research, but his insights, insparation and his way of conducting research and living. Without Prof. Tjhung's continuous guidance and support, the completion of this thesis would not have been possible.

I am grateful to Professor Kam Pooi Yuen, Associate Professor Ng Chun Sum and Assistant Professor Nallanathan Arumugam for being my degree committe members, and for their thoughtful suggestions and genuine concerns. I would also like to thank Dr. Cao Yewen, Dr. Huang Licheng and Dr. Tian Wei, for their comments and helps on this work. Special thanks must go to my colleagues in the Communication Laboratory, NUS, for their fellowship and the many helpful discussions.

Lastly, I want to express my gratitude to my beloved wife, Wang Wen, and my parents, for their understandings and endless supports.

Table of Contents

List of Figures

List of Tables

Abstract

A novel and important unitary space-time modulation (USTM) scheme for the non-coherent multi-input multi-output (MIMO) system where the channel state information is not known both at the transmitter and the receiver, has drawn increased attention for its potential in achieving high spectrum efficiency in data communication without the overhead of channel estimation. Therefore combined with channel coding, USTM will be a promising technique for future wireless applications. However, so far research on coded USTM is quite limited and is only in its early stage.

The aim of this thesis is to investigate and propose a large class of bandwidth efficient trellis coding schemes for the USTM in the non-coherent MIMO system. We first proposed trellis-coded USTM (TC-USTM), and performed the error performance analysis to obtain the design rules for a good trellis coding scheme. Then by exploiting the dissimilarities between distinct signal points in a constellation, we proposed and developed a systematic and universal "mapping by set partitioning" strategy for the TC-USTM. Using theoretical analysis and computer simulations, we demonstrated that TC-USTM produces significant coding gain over the uncoded USTM. We also proposed another important trellis coding scheme, namely, the multiple trellis-coded USTM (MTC-USTM), where each trellis branch is assigned multiple ($k \geqslant 2$) USTM

signal points. A systematic set partitioning scheme is developed for the k-fold Cartesian product of the USTM signals. We concluded that given the same information rates and number of trellis states, the MTC-USTM outperforms the TC-USTM, especially at high signal-to-noise ratio. We also extended the above trellis coding schemes to the differential USTM (DUSTM) constellations, which operate in a slow Rayleigh flat fading channel. Using similar analysis and manipulation, we demonstrated that the resulting TC-DUSTM has superior error performance compared to its uncoded counterparts.

Chapter 1

Introduction

1.1 Multiple Antenna Channels

Wireless communication systems, including the cellular mobile system, wireless local area network, *etc.*, have been undergoing rapid development in the past few years. The first and second generations of the wireless systems focus on *voice* communications, while the new generation (3G) focuses mainly on providing both *voice* and *data* access. The ever increasing quality and data rate provided by the wireless systems, together with its flexibility, made it possible to develop a rich collection of new wireless data applications, which promise to have great impact on people's daily life.

There are many challenges facing the realization of wireless communications, among which the limitation of the spectrum resource is the hardest to overcome. As data applications require much higher data rates and the spectrum for new data application is limited, one should maximize the data rate within a *given* bandwidth. Accordingly the *spectrum efficiency* should be maximized.

One way to meet this end is the use of spread spectrum (SS), code division multiple access (CDMA). However in a multi-user wireless network, strong signals transmitted by one user acts as strong interference to other users. Therefore it is of interest to

develop other approaches to increase the spectrum efficiency.

Multiple-antenna diversity is an important means to meet this challenge. In a wireless system with multiple transmit and receive antennas (also known as multi-input multi-output (MIMO) system), the spectrum efficiency can be greatly increased from that of the conventional single antenna system, with the same total transmission power. Research shows that the performance of MIMO systems can be greatly increased in terms of improving the reliability at a given data rate and in terms of supporting a much higher data rate. Several practical systems have demonstrated this performance gain in MIMO systems, such as the celebrated Bell Laboratories layered space-time (BLAST) system [1, 5].

Fading in the wireless environment is considered as a source of uncertainty that makes wireless links unreliable. When the channel coefficients is atypically small, *i.e.*, when deep fades happen, the transmitted signal is buried in the noise and is lost. Hence one needs to compensate against signal fluctuations in fading channels to have a steady signal strength. Multiple antennas provide independent signal paths on so-called space diversity. Each pair of transmit and receive antennas provides a signal path from the transmitter to the receiver. By sending signals that carry the same information through a number of different paths, multiple independently faded replicas of the data symbol can be obtained at the receiver end; by averaging over these replicas, more reliable reception is achieved. In a system with M transmit and N receive antennas, we define the maximal diversity gain (order) as MN.

1.2 Channel State Information

Channel state information (CSI) for the MIMO system is characterized by a $M \times N$ random matrix $\mathbf{H}$. $\mathbf{H}_{i,j}, 1 \leqslant i \leqslant M, 1 \leqslant j \leqslant N$ are the fading coefficients between transmit-receive antenna pairs. Depending on the availability of $\mathbf{H}$, the MIMO system can be categorized into *coherent* and *non-coherent* MIMO system. For the former, $\mathbf{H}$ is perfectly known at the receiver while for the latter, $\mathbf{H}$ is unknown both at the transmitter and the receiver. Channel capacity and channel coding techniques for the coherent MIMO system have been well studied in the past several years. In contrast, information-theoretic study on the channel capacity, as well as the channel coding techniques for the non-coherent MIMO system, are still in the early stages.

1.2.1 Coherent MIMO System

Channel capacity for coherent MIMO system has been treated in [1], [2], [3] and is shown to have been greatly increased, compared with that for the single-antenna system. For independent and identically distributed (i.i.d.) Rayleigh fading between all antenna pairs, the capacity gain is $\min\{M, N\}$, i.e., the channel capacity increases linearly with the minimum of the number of transmitter and receiver antennas.

To approach channel capacity, space-time coding for the coherent MIMO system has been proposed. Space-time codes can mainly be categorized into space-time trellis codes (STTC) [17] and space-time block codes (STBC) [18], [19], [21]. A big fraction of channel capacity can be achieved by following the design criteria to increase the *diversity gain (order)* and the *coding gain (advantage)* for good codes. Various concatenated space-time codes also appeared to achieve more spectrum efficiency

at the expense of the increased decoding complexity. For example, in [26], space-time block codes are assigned to the trellis branch, resulting in the so-called super orthogonal space-time trellis codes. In [27], a similar method to that in [26] was proposed independently. Turbo codes and the iterative decoding process were also combined with the space-time codes, which approach the capacity bound, even at low SNR [24, 65].

The decoding of the aforementioned space-time codes requires perfect knowledge of the CSI, which is usually obtained through channel estimation and tracking. In a fixed wireless communication environment, the fading coefficients vary slowly, so the transmitter can periodically send pilot signals to allow the receiver to estimate the coefficiens accurately. In mobile environments, however, the fading coefficients can change quite rapidly and the estimation of the channel parameters becomes difficult, particularly in a system with a large number of antennas. In this case, there may not be enough time to estimate the parameters accurately enough. Also, the time one spends on sending pilot signals is not negligible, and the tradeoff between sending more pilot signals to estimate the channel more accurately and using more time to get more data through becomes an important factor affecting performance. In such situations, one may also be interested in exploring schemes that do not need explicit estimates of the fading coefficients. It is therefore of interest to understand the fundamental limits of non-coherent MIMO channels.

1.2.2 Non-Coherent MIMO System

A line of work was initiated by Marzetta and Hochwald [4], [9] to study the capacity of multiple-antenna channels when neither the receiver nor the transmitter knows the fading coefficients of the channel. They used a block fading channel model [15]

or the piecewise constant Rayleigh flat-fading channel [4] where the fading gains are i.i.d. complex Gaussian distributed and remain constant for T symbol periods before changing to a new independent realization, where T is the coherence time of the channel. Under this assumption, they reached the conclusion that further increasing the number of transmit antennas M beyond T cannot increase the capacity. They also characterized certain structure of the optimal input distribution, and computed explicitly the capacity of the one transmit and receive antenna case at high SNR. Lizhong and Tse used a geometric interpretation, the *sphere packing in Grassmann manifold* to calculate the capacity for the non-coherent MIMO system [6]. They derived that the capacity gain is $M^*(1 - M^*/T)$ bits per second per hertz for every 3-dB increase in SNR, where $M^* = \min\{M, N, \lfloor T/2 \rfloor\}$. Hassibi and Martezza continues the work in [4] and find a closed form expression for the probability density function of the received signal.

The capacity-attaining input signal is the product of an isotropically random unitary matrix, and an independent nonnegative real diagonal matrix. In certain limiting regions [4], [6], the diagonal matrix is constant, and the message is carried entirely by the unitary matrix: a type of modulation called unitary space-time modulation (USTM) [9]. A number of practical considerations make USTM attractive for general usage.

Extensive work has been done to construct good unitary space-time (UST) constellations with reasonable complexity. A systematic design approach was proposed [10] and is widely used in the literature for its efficiency and the group structure of the constellations. In this approach, one begins with a $T \times M$ complex matrix whose columns are orthonormal to each other, and then rotates this signal matrix

successively in the high-dimensional complex space to generate other signals. In [13], Agrawal *et al.* related UST signal design to the problem of finding packings with larger minimum distance in the complex Grassmann space and reported a numerical optimization procedure for finding good packings in the complex Grassmann space. Based on the discovery of the space-time autocoding [11] where the space-time signals act as their own channel codes, a structured space-time autocoding constellation was proposed in [12] following the line of construction of the codes in [10].

For the continuously changing Rayleigh flat-fading channel, differential USTM was investigated in [14] and [16]. Both schemes employ $M \times M$ unitary complex matrices as the signals, however the former constructs the signals following the systematic approach in [10] while the latter is based on the design of group codes.

1.3 Bandwidth Efficient Coding for Unitary Space-Time Modulation

In single antenna communication system, trellis coded modulation (TCM) [32, 33] has been hailed over the past two decades as an important finding for its capability in realizing high data rate transmission without bandwidth expansion compared with its uncoded counterparts. TCM combines modulation and coding into one step by applying Ungerboeck's "mapping by set partitioning" to the two dimensional (2D) signal set, *e.g.*, *M*-ary phase-shift-keying (MPSK) and quadrature amplitude modulation (QAM). For its high spectrum efficiency, TCM has seen its many applications in the wide area of wired and wireless communication. As a big step forward, multiple trellis coded modulation (MTCM) [35, 36] and multi-dimensional trellis coded modulation [33, 57, 58] have been reported to achieve an even higher spectrum efficiency

over the TCM, where each trellis branch is assigned multiple and multi-dimensional (MD) symbols, respectively.

Naturally one would ask whether these bandwidth-efficient trellis coding techniques can be applied to the constellations for the non-coherent MIMO system, such as USTM. In this thesis, we have made efforts to address this problem and have come up with an affirmative answer. Intuitively, we can first consider a conventional modulation scheme (MPSK or QAM) operated in the additive white Gaussian noise (AWGN) channel. It is well known that the minimum Euclidean distance ($d_{\mathrm{E,min}}$) in the 2D signal set determines the overall error performance for the uncoded transmission. The larger is this metric, the smaller is the error probability. In TCM one achieves a coding gain by increasing the $d_{\mathrm{E,min}}$ through the trellis encoder. From the description of the signaling scheme for the non-coherent MIMO system in Section 1.2.2, one can also observe that each UST signal spans a distinct M-dimensional subspace in the T-dimensional vector space, where the *dissimilarity* between different subspaces determines the pairwise signal error probability. The larger is the dissimilarity, the lower is the pairwise error probability for mistaking one signal for another, and therefore a lower average bit error probability. Evidently, one can conjecture that through trellis coding for these UST signals, the minimum dissimilarity of a constellation can be effectively increased. This analogy between the conventional and the UST signaling schemes paves the way to a trellis coding scheme for the USTM. Hence one can apply a similar "mapping by set partitioning" strategy as that in [32] to the UST signal set to obtain a trellis coded USTM scheme, which possesses a much higher spectrum efficiency than its uncoded counterpart.

We will demonstrate by theoretical analysis in this thesis that through trellis

coding, one can observe that the diversity gain MN of the MIMO system can be increased to $MN\ell_{\min}$, where $\ell_{\min}$ is the length of the shortest error event. This observation suggests that through trellis coding, one can effectively obtain a MIMO system, whose number of transmit or receive antennas is $\ell_{\min}$ times greater than that of the real system. Hence the spatial complexity, in terms of the number of antennas, can now be transformed to temporal complexity, in terms of the encoding and decoding overhead, for a MIMO system.

Another advantage of trellis coding comes from the so-called *coding gain*, which further improves the error rate performance of the non-coherent MIMO system. Through careful design of the trellis encoder, one can make the *largest* dissimilarity in the UST signal set to be the minimum one (the *effective* minimum dissimilarity), and hence, the pairwise error probability can be reduced significantly. With the increase in $\ell_{\min}$, the coding gain increases accordingly.

1.4 Contributions

In this thesis, we have contributed mainly in the following areas.

- We proposed and investigated a bandwidth efficient trellis coding scheme, namely, the trellis coded USTM (TC-USTM), for the non-coherent MIMO system operated in the so-called piecewise constant Rayleigh flat-fading or rapid fading blockwise independent channel . Specifically, we focus on the systematically designed UST signal set and examine its dissimilarity structure. We derive the pairwise error event probability (PEP) as well as the bit error probability (BEP) for this trellis coding scheme, which leads to the optimal design criteria

for the TC-USTM. We also propose a systematic and universal "set partitioning" approach which applies to any UST signal set. This approach guarantees that all the design criteria can be satisfied and that a minimum BEP can be achieved by the resulting TC-USTM. We demonstrate that the coding gain is significant over the uncoded USTM. We also provide analytical PEP and BEP lower bounds for this trellis coding scheme, which agrees well with the computer simulation results.

- From our performance analysis of the TC-USTM, we are led to propose and investigate the multiple trellis-coded USTM (MTC-USTM) operated in the piecewise constant Rayleigh flat-fading channel, by assigning each trellis branch $k \geqslant 2$ UST signals. For this purpose, we propose an efficient set partitioning scheme for the k-fold Cartesian product of the UST signal set and formulate a systematic subset mapping strategy. Given the same information rate and number of trellis states, we demonstrate that MTC-USTM produces significant coding gain over the TC-USTM, especially at high SNR.

- We also address the trellis coding scheme for the non-coherent MIMO system, which operates in the continuously changing Rayleigh flat-fading channel. In this scheme, trellis coding is combined with the differential unitary space-time modulation, leading to the trellis coded differential USTM (TC-DUSTM). We employ a block interleaver to make the continuously changing channel to approximate the piecewise constant Rayleigh fading channel. We have derived the PEP and BEP formula, as well as the design criteria for the TC-DUSTM. We also apply Ungerboeck's "mapping by set partitioning" to the differential UST signal set. We also provide analytical lower bound and computer simulations,

which demonstrate that the TC-DUSTM can offer a much higher spectrum efficiency than the uncoded differential USTM.

1.5 Summary of Thesis

We first briefly introduce the concepts for a non-coherent MIMO system in Chapter 2. Then we divide the rest of this thesis into three major parts. In Chapter 3, we introduce the trellis coded USTM, which covers the performance analysis, design criteria and numerical results. In Chapter 4, we propose and investigate the MTC-USTM, including the performance analysis and the set partitioning scheme and numerical results. TC-DUSTM is introduced and investigated in Chapter 5. Chapter 6 contains our conclusion.

Chapter 2

Uncoded Unitary Space-Time Modulation

2.1 System Model

We consider a wireless communication system with M transmitter antennas and N receiver antennas, which operates in a Rayleigh flat-fading environment. Each receiver antenna responds to each transmitter antenna through a statistically independent fading coefficient that is constant for T symbol periods. The fading coefficients are not known by either the transmitter or the receiver. The received signals are corrupted by additive noise that is statistically independent among the N receivers and the T symbols periods.

The complex-valued signal $x_{t,n}$ that is measured at receiver antenna n, and discrete time t, is given by

$$x_{t,n} = \sqrt{\rho} \sum_{m=1}^{M} h_{m,n} s_{t,m} + w_{t,n}, \qquad t = 1, \cdots, T, \quad n = 1, \cdots, N. \tag{2.1}$$

Here $h_{m,n}$ is the complex-valued fading coefficient between the mth transmitter antenna and the nth receiver antenna. The fading coefficients are i.i.d. Gaussian random variables with zero mean and 0.5 variance in each real dimension, denoted as

$\mathcal{CN}(0,1)$, and are constant for $t = 1, \cdots, T$. The probability density function (pdf) is

$$p(h_{m,n}) = \frac{1}{\pi}\exp\left\{-|h_{m,n}|^2\right\}. \tag{2.2}$$

The complex-valued signal fed into transmitter antenna m at time t is denoted as $s_{t,m}$, and its average (over the M antennas) power is equal to one, i.e.,

$$\sum_{m=1}^{M} E\left|s_{t,m}\right|^2 = 1, \quad t = 1, \cdots, T \tag{2.3}$$

where E denotes expectation. $w_{t,n}$ is the additive white Gaussian noise at time t and receiver antenna n, and is also i.i.d. as $\mathcal{CN}(0,1)$. Due to the normalization in (2.3), ρ in (2.1) represents the expected SNR at each receiver antenna.

In matrix form, (2.1) can be re-written as

$$\mathbf{X} = \sqrt{\rho}\mathbf{S}\mathbf{H} + \mathbf{W}. \tag{2.4}$$

where $\mathbf{S} = [s_{t,m}]$ is the $T \times M$ transmitted signal matrix, $\mathbf{X} = [x_{t,n}]$ is the $T \times N$ received signal matrix, $\mathbf{H} = [h_{m,n}]$ is the $M \times N$ channel matrix and $\mathbf{W} = [w_{t,n}]$ is the $T \times N$ matrix of additive noise. $\mathbf{H}$ therefore has independent realizations for each $\mathcal{CN}(0,1)$ distributed entry every T-symbol period and remains constant during that interval. $\mathbf{H}$ is termed as piecewise constant Rayleigh fading channel in [4] or block fading channel in [15]. This channel model is an accurate representation of many TDMA, frequency hopping, or block-interleaved systems.

It is clear that $E\{\mathbf{X}|\mathbf{S}\}$=0 and each column in $\mathbf{X}$ has an identical covariance matrix $\mathbf{\Lambda} = I_T + \rho\mathbf{S}\mathbf{S}^\dagger$, where $\dagger$ denotes conjugate transpose and I_T denotes the $T \times T$ identity matrix. The received signal has a conditional probability density

$$p(\mathbf{X}|\mathbf{S}) = \frac{\exp\left(-\mathrm{tr}\left\{\mathbf{\Lambda}^{-1}\mathbf{X}\mathbf{X}^\dagger\right\}\right)}{\pi^{TN}\det{}^N\mathbf{\Lambda}} \tag{2.5}$$

where tr, det denote trace and determinant, respectively.

2.2 Unitary Space-Time Modulation

In [4], the capacity-attaining random signal matrix $\mathbf{S}$ may be constructed as a product $\mathbf{S} = \mathbf{\Phi V}$, where $\mathbf{\Phi}$ is an isotropically distributed $T \times M$ matrix whose columns are orthonormal, i.e., $\mathbf{\Phi}^\dagger \mathbf{\Phi} = I_M$, and $\mathbf{V} = \mathrm{diag}(v_1, \cdots, v_M)$ is an independent $M \times M$ real, nonnegative, diagonal matrix. When $\rho \gg 0$ or $T \gg M$, setting $v_1 = \cdots = v_M = \sqrt{T/M}$ attains capacity. Therefore in [9] a *unitary space-time modulation* is defined as $\mathbf{S} = \sqrt{T/M}\mathbf{\Phi}$, where $\mathbf{\Phi}^\dagger \mathbf{\Phi} = I_M$. Notice that it is the M-dimensional subspace spanned by the M columns of $\mathbf{S}$ in the T-dimensional vector space that delivers the information and distinguishes different signals. One can see that only $\mathbf{\Phi}$ in $\mathbf{S}$ contains information and therefore the signal set for USTM can be denoted simply by $\mathbf{\Phi}_L$, where the subscript L denotes the dimension (size) of the signal set. Given the information rate R in bits per channel use (symbol), $L = 2^{RT}$.

Suppose two unitary space-time (UST) signals $\Phi_l \neq \Phi_{l'} \in \mathbf{\Phi}_L$ are transmitted with equal probability and demodulated with a maximum likelihood (ML) algorithm, the pairwise block error probability (PBEP) of mistaking Φ_l for $\Phi_{l'}$, or vice versa, is [9]

$$\begin{aligned} P_e &= p(\Phi_l \to \Phi_{l'} | \Phi_l \text{ transmitted}) \\ &= p(\Phi_{l'} \to \Phi_l | \Phi_{l'} \text{ transmitted}) \\ &= \frac{1}{4\pi} \int_{-\infty}^{\infty} \frac{d\omega}{\omega^2 + 1/4} \prod_{m=1}^{M} \left[1 + \frac{(\rho T/M)^2 (1 - d_m^2)(\omega^2 + 1/4)}{1 + \rho T/M} \right]^{-N}, \end{aligned} \quad (2.6)$$

where d_m is the mth singular value of the *correlation matrix* $\Phi_l^\dagger \Phi_{l'}$. A Chernoff upper bound for the PBEP is [9]

$$P_e \leqslant \frac{1}{2} \prod_{m=1}^{M} \left[1 + \frac{(\rho T/M)^2 (1 - d_m^2)}{4(1 + \rho T/M)} \right]^{-N}. \quad (2.7)$$

For a good design of $\mathbf{\Phi}_L$, we should minimize the PBEP given in (2.6) or its upper bound in (2.7) for simplicity. At high SNR (as $\rho \to \infty$), the upper bound in inequality (2.7) is dictated by $\prod_{m=1}^{M}(1-d_m^2)$, whose geometric mean is defined as the *dissimilarity* between signal Φ_l and $\Phi_{l'}$

$$d(\Phi_l, \Phi_l') = \prod_{m=1, d_{l,l',m}<1}^{M} (1 - d_{l,l',m}^2)^{\frac{1}{2M}}. \tag{2.8}$$

where $d_{l,l',m}$ is the mth singular value of the correlation matrix $\Phi_l^\dagger \Phi_{l'}$. From the inequality in (2.7), we can see that the greater is the dissimilarity, the smaller is the PBEP. As the average block error probability of a signal set is determined by the minimum PBEP, we should construct $\mathbf{\Phi}_L$ such that for all $l \neq l'$, $0 \leqslant l, l' \leqslant L-1$, the minimum dissimilarity

$$d_{\min} = \min_{0 \leqslant l \neq l' \leqslant L-1} d(\Phi_l, \Phi_l') \tag{2.9}$$

is maximized.

A heuristic design method for $\mathbf{\Phi}_L$ was suggested in [9] through a random search to maximize $d_{\min}$. Later in [13], the search problem is recast into the problem of finding packings with the largest minimum dissimilarity in the complex Grassmann space.

In [10] a systematic construction approach for $\mathbf{\Phi}_L$ was proposed. The signals are formed by specifying a $T \times M$ unitary matrix, then rotated successively in the T-dimensional vector space to form the other $L-1$ signal matrices (subspaces). The initial matrix Φ_0 is usually formed by any $M \leqslant T$ columns in a $T \times T$ DFT matrix, scaled by a factor $\frac{1}{\sqrt{T}}$. Then signals can be systematically formed by

$$\Phi_l = \Theta^l \Phi_0, \quad l = 0, \cdots, L-1. \tag{2.10}$$

Here $\Theta = \mathrm{diag}(e^{j2\pi u_1/L}, \cdots, e^{j2\pi u_T/L})$, with $u_i \in \mathbb{Z}_L = \{0, \cdots, L-1\}, 1 \leqslant i \leqslant T$. Let $\boldsymbol{u} = [u_1, \cdots, u_T]$. Then $\boldsymbol{u}$ can be searched by maximizing $d_{\min}$. Taking into account

equation (2.9), the optimal $\boldsymbol{u}$, denoted as $\boldsymbol{u}_{\text{opt}}$ should be searched by

$$\boldsymbol{u}_{\text{opt}} = \arg\max_{\boldsymbol{u}} \min_{0 \leqslant l \neq l' \leqslant L-1} d(\Phi_l, \Phi_l'). \tag{2.11}$$

The systematically formed $\boldsymbol{\Phi}_L$ is attractive in the following aspects:

1) The design process is much simplified compared with that in [9] and [13].

2) All the signals form a *group code* that was initiated by Slepian for single-antenna communication in [31]. The group structure will reduce the memory needed both at the transmitter and the receiver for storing the alphabet. Only Φ_0 and Θ need to be stored while other signals can be formed through rotation.

3) The resulting signals have a regular dissimilarity structure which will be further investigated in the following chapters. The dissimilarity structure can be utilized for set partitioning of $\boldsymbol{\Phi}_L$, which plays an important role in trellis coding for the USTM.

2.3 Differential Unitary Space-Time Modulation

USTM is suitable for the piecewise constant Rayleigh fading channel, while for the continuously changing mobile radio Rayleigh flat fading channel, which is more realistic in a mobile environment, differential transmission and detection of the UST signals is a more natural choice. The differential USTM (DUSTM) constellation follows directly from the construction of UST signals in the previous section. The canonical representation of a differential UST signal is

$$\Phi_l = \frac{1}{\sqrt{2}} \begin{bmatrix} I_M \\ V_l \end{bmatrix}, \tag{2.12}$$

where V_l denotes a $M \times M$ unitary matrix, $l \in \mathbb{Z}_L$. In (2.12) it can be seen that only V_l delivers the information. The channel is used in blocks of $M = \frac{T}{2}$ symbols and $L = 2^{RM}$. The signal set is denoted as $\mathbf{V}_L = \{V_l \mid l \in \mathbb{Z}_L\}$.

Let t denote the time index for each signal and $z_t \in \mathbb{Z}_L$ denote the information data to be transmitted at time t. Usually a reference signal $\mathbf{S}_0 = I_M$ is first transmitted, followed by a signal $\mathbf{S}_1 = V_{z_1}$. In general the signal sequence transmitted is given as follows

$$\mathbf{S}_t = V_{z_t}\mathbf{S}_{t-1}, \quad t = 1, 2, \cdots \tag{2.13}$$

At the receiver the received signal is

$$\mathbf{X}_t = \sqrt{\rho}\mathbf{S}_t\mathbf{H} + \mathbf{W}_t. \tag{2.14}$$

where $\mathbf{H}$ takes the continuously changing Rayleigh fading channel model, such as the Clarke's model [61]. The ML demodulator is

$$(\hat{z}_t) = \arg\max_{l \in \mathbb{Z}_L} \left\| \mathbf{X}_{t-1} + V_l^{\dagger}\mathbf{X}_t \right\| \tag{2.15}$$

where $\|\cdot\|$ denotes the Frobenius norm, i.e., $\|A\|^2 = \mathrm{tr}(AA^{\dagger})$ for a matrix A. Substituting (2.12) into (2.8), one can obtain the *dissimilarity* between signals V_l and $V_{l'}, l \neq l'$, denoted as

$$\begin{aligned} \zeta(V_l, V_{l'}) &= \frac{1}{2}\prod_{m=1}^{M} \sigma_m(V_l - V_{l'})^{1/M} \\ &= \frac{1}{2}\left|\det(V_l - V_{l'})\right|^{1/M}. \end{aligned} \tag{2.16}$$

Here $\sigma_m(V_l - V_{l'})$ denotes the m-th singular value of the difference matrix $V_l - V_{l'}$.

$\mathbf{V}_L$ should be designed to maximize the minimum dissimilarity $\zeta_{\min} = \min_{l \neq l' \in \mathbb{Z}_L} \zeta(V_l, V_{l'})$ in $\mathbf{V}_L$, such that the average block error probability in $\mathbf{V}_L$ can be minimized.

Also $\mathbf{V}_L$ can be formed as a group under matrix multiplication as

$$V_l = V_1^l, \quad l = 0, \cdots, L-1 \tag{2.17}$$

where the initial matrix V_1 is an Lth root of unity. It is also desired that the signal matrices form an *Abelian* group, that is, the product of any two matrices commutes. For this purpose, V_1 should be a diagonal matrix $V_1 = \text{diag}(e^{i(2\pi/L)u_1}, \cdots, e^{i(2\pi/L)u_M})$, $u_m \in \mathbb{Z}_L$, $m = 1, \cdots, M$. Similar to (2.11), for DUSTM, the optimal set of u_m, denoted as $\boldsymbol{u}_{\text{opt}}$, can be derived as [14]

$$\boldsymbol{u}_{\text{opt}} = \arg\max_{\boldsymbol{u}} \min_{l=1,\cdots,L-1} \left| \prod_{m=1}^{M} \sin(\pi u_m l/L) \right|^{\frac{1}{M}}. \tag{2.18}$$

Signal sets formed by equation (2.17) and (2.18) are referred to as the systematically designed DUSTM.

2.4 Summary

In this chapter, we have briefly reviewed the system and the signal model for the non-coherent MIMO systems: the USTM and the DUSTM. These systems are considerably superior in error performance compared to the uncoded single antenna signaling scheme. However to achieve the promised MIMO channel capacity, coding techniques have to be combined with these modulations, which will be addressed in the following chapters.

Chapter 3

Trellis-Coded Unitary Space-Time Modulation

3.1 Background

In TCM [32], [33], we combine a convolutional encoder and a signal mapper. In one coding interval, the r information bits are divided into two parts: $m \leqslant r$ information bits are encoded with a rate $\frac{m}{m+1}$ convolutional encoder, with the output $m+1$ bits selecting a subset from a size-2^{r+1} constellation set, while the remaining $r-m$ information bits select the signal from the subset. The rate $\frac{r}{r+1}$ TCM combines coding and modulation into one step and coding gain is obtained by introducing redundancy into the subset selection procedure.

Let $\mathbb{C}$ denote the 2D size-2^{r+1} signal constellation, such as MPSK or QAM. Set partitioning of $\mathbb{C}$ plays an important role in TCM. Ungerboeck's "mapping by set partitioning" [32] presented a generic realization of the partitioning for $\mathbb{C}$ in a heuristic manner. Group theory and lattice theory are powerful tools for the partitioning of $\mathbb{C}$ of large size [53, 54, 63, 64]. There are two guidelines for the partitioning procedure:

1) The minimum Euclidean distance $d_{\mathrm{E,min}}$ in subsets of the same layer in the

partitioning tree is maximized and $d_{\mathrm{E,min}}$ increases as rapidly as possible after each partitioning of the subsets;

2) The distance structures in the subsets of the same layer are identical.

Rules for mapping the information bits to the signals are also given [32] which guarantee that the bit errors are minimized when signal errors occur at high SNR.

One can find similarities between the UST signal set $\mathbf{\Phi}_L$ and the 2D signal set $\mathbb{C}$, by making a comparison between the dissimilarity $d(\Phi_l, \Phi_{l'})$ for signals $\Phi_l, \Phi_{l'} \in \mathbf{\Phi}_L$ and the Euclidean distance $d_{\mathrm{E}}(s_l, s_{l'})$ for signals $s_l, s_{l'} \in \mathbb{C}$, $l \neq l'$. It is well known that a greater $d_{\mathrm{E,min}}$ gives rise to a smaller pairwise error probability of mistaking s_l for $s_{l'}$ and vice versa. Correspondingly, in Section 2.2, one also observes that a greater $d_{\min}$ leads to a smaller pairwise error probability of mistaking Φ_l for $\Phi_{l'}$ and vice versa. In most cases $d_{\min}$ in a subset of $\mathbf{\Phi}_L$ is greater than that in $\mathbf{\Phi}_L$. Hence one can partition $\mathbf{\Phi}_L$ successively into a series of subsets and obtain a series of $d_{\min}$, which increases after each partitioning of the subset. Accordingly, the average block error probability in the resulting subsets reduces. Therefore, intuitively, the aforementioned two guidelines for a 2D signal set $\mathbb{C}$ also applies to $\mathbf{\Phi}_L$, and "mapping by set partitioning" similar to that in [32] can be applied to these UST signal sets, leading to the bandwidth efficient trellis-coded USTM (TC-USTM).

In the following sections, we first introduce the properties of the systematically designed UST signal sets, then derive the PEP and BEP of the TC-USTM, which in turn leads to the design criteria for TC-USTM. To form the set partitioning of $\mathbf{\Phi}_L$, we propose a novel systematic approach through subset-pairing, which can be realized recursively. Through computer simulations as well as theoretical analysis, we demonstrate that the proposed TC-USTM produces significant coding gains over

its uncoded counterpart. And we also find that the derived lower bounds provide accurate estimates of the BEP error curves, especially at high SNR.

3.2 Properties of the UST Constellations

The systematically designed UST constellation [10] received much attention for its attractive properties explored in the following. Let the subscript l of $\Phi_l \in \mathbf{\Phi}_L$ be the *index* for the corresponding signal block Φ_l. Thus the *signal index difference* between signal $\Phi_l, \Phi_{l'} \in \mathbf{\Phi}_L, \Phi_l \neq \Phi_{l'}$ can be defined as

$$\Delta_{l,l'} = (l' - l) \text{ modulo} L = l' \oplus (-l) \tag{3.1}$$

where $\oplus$ denotes addition modulo-L. The set of the signal indices in $\mathbf{\Phi}_L$ form the integer set $\mathbb{Z}_L$, which is an integer group under $\oplus$. Equation (2.8) indicates that the metric $d(\Phi_l, \Phi_{l'})$ is a function of the singular values of the correlation matrix $\Phi_l^\dagger \Phi_{l'}$, and based on equation (2.10),

$$\Phi_l^\dagger \Phi_{l'} = \Phi_0^\dagger \Theta^{l' \oplus (-l)} \Phi_0, \tag{3.2}$$

we have

Property 1. $d(\Phi_l, \Phi_{l'})$ between distinct pair $\Phi_l, \Phi_{l'} \in \mathbf{\Phi}_L, l \neq l'$ is completely determined by $\Delta_{l,l'}$.

As a result, the dissimilarity can be expressed as $d(\Phi_l, \Phi_{l'}) = d_{\Delta_{l,l'}}$. It follows that any two signal pairs having the same index difference have the same dissimilarity.

The *dissimilarity profile* for a UST signal set $\mathbf{\Phi}_L$ is defined as the set $\mathcal{P}_{\mathbf{\Phi}_L}(l) = \{d_{\Delta_{l,l'}} \mid l', l \in \mathbb{Z}_L, l' \neq l\}$ with respect to a *reference signal* Φ_l. Note that the set of $\Delta_{l,l'}$ for $\mathbf{\Phi}_L$ with any reference $l \in \mathbb{Z}_L$ is $\{1, \cdots, L-1\}$, which is identical for any

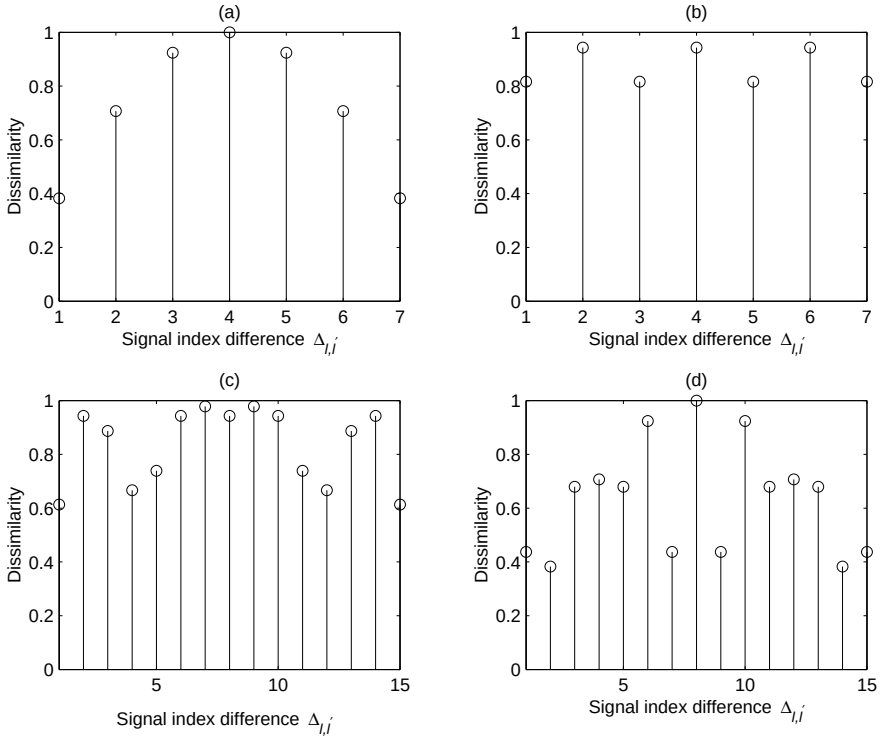

Figure 3.1: Dissimilarity profiles $\mathcal{P}_{\mathbf{\Phi}_L}$ for four UST signal sets. (a) $\mathbf{\Phi}_8(T = 2, M = 1, R = 1.5)$ (b) $\mathbf{\Phi}_8(T = 3, M = 1, R = 1)$ (c) $\mathbf{\Phi}_{16}(T = 3, M = 1, R = 1.33)$ (d) $\mathbf{\Phi}_{16}(T = 4, M = 2, R = 1)$.

reference l under $\oplus$ and can be denoted as $\mathbf{\Delta}_{\mathbb{Z}_L}$. Therefore the dissimilarity profile for the whole UST signal set is not a function of the reference signal, and can be simply denoted as $\mathcal{P}_{\mathbf{\Phi}_L}$. As examples, the dissimilarity profiles for four UST signal sets [1] are illustrated in Fig. 3.1. Recalling inequality (2.7) and (2.8), we note that at high SNR, the PBEP between Φ_l and $\Phi_{l'}$ is determined by the index difference $\Delta_{l,l'}$. Therefore we have the following property.

Property 2. The PBEP between Φ_l and $\Phi_{l'}$ is determined by the signal index

[1]The initial signal Φ_0 for signal set $\mathbf{\Phi}_{16}$ $(T = 4, M = 2, R = 1)$ is formed by the *first* and *third* columns of the 4×4 DFT matrix scaled by $\frac{1}{2}$, otherwise the dissimilarity profile will be different from the one illustrated in Fig. 3.1 (d).

difference $\Delta_{l,l'}$.

As a result, the PBEP between Φ_l and $\Phi_{l'}$ and that between $\Phi_{l\oplus\Delta}$ and $\Phi_{l'\oplus\Delta}$ are the same for any $\Delta \in \mathbb{Z}_L$.

Fig. 3.1 also exhibits another property of $\mathbf{\Phi}_L$ as follows.

Property 3. The dissimilarity profile $\mathcal{P}_{\mathbf{\Phi}_L}$ are symmetrical about the center point $\Delta_{l,l'} = \frac{L}{2}$, i.e., $d_{\Delta_{l,l'}} = d_{\Delta_{l',l}}$.

In fact, the correlation matrices $\Phi_l^\dagger \Phi_{l'}$ and $\Phi_{l'}^\dagger \Phi_l$ are complex conjugate of each other, and have the same set of singular values. Then based on equation (2.8), we have $d_{\Delta_{l,l'}} = d_{\Delta_{l',l}}$.

One also can observe from Fig. 3.1 that the maximum $d_{\Delta_{l,l'}}$ corresponds to an even $\Delta_{l,l'}$ as in Fig. 3.1 (a), (b), (d) or an odd $\Delta_{l,l'}$ as in Fig. 3.1 (c). Let the maximum dissimilarity in $\mathcal{P}_{\mathbf{\Phi}_L}$ be denoted as $d_{\max}$ and the corresponding $\Delta_{l,l'}$ be denoted as $\Delta_{\max}$. Then we have the following property, which is an important fact and will influence our proposed set partitioning scheme for the UST signal set in Section 3.5.

Property 4. $d_{\max}$ corresponds to an arbitrary (odd or even) $\Delta_{\max} \in \mathbf{\Delta}_{\mathbb{Z}_L}$ in distinct UST signal set $\mathbf{\Phi}_L$.

With Property 4, it is required that a good set partitioning scheme should be applicable to an arbitrary $\mathbf{\Phi}_L$, which may have distinct $\Delta_{\max}$.

These above properties will be exploited in Section 3.3, 3.4 and 3.5.

3.3 Performance Analysis for Trellis-Coded Unitary Space-Time Modulation

To propose a good trellis coding scheme for the USTM, it is necessary to find the key parameters that affect the BEP performance of the TC-USTM. Therefore in this section, we formulate the PEP as well as the BEP expression for TC-USTM.

Suppose a trellis coded sequence $\mathbf{\Phi}^K = \{\Phi_{l_t}, 1 \leqslant t \leqslant K\}$ of length K is transmitted, where t is the time index of each signal block and $l_t \in \mathbb{Z}_L$ is the data (in decimal form) transmitted at t. Each signal in the received sequence $\mathbf{X}^K = \{X_t, 1 \leqslant t \leqslant K\}$ is

$$X_t = \sqrt{\rho T/M}\Phi_{l_t} H_t + W_t, \tag{3.3}$$

where the channel matrix H_t has independent realizations in every other T-symbol period and remains constant during that time interval. This piecewise constant fading process mimics the behavior of a continuously changing fading process in a tractable manner. Furthermore, it is a very accurate representation of many TDMA, frequency hopping or fully block-interleaved systems [29, 30]. Entries in H_t are i.i.d as $\mathcal{CN}(0,1)$. W_t denotes the noise matrix and each entry in W_t is also $\mathcal{CN}(0,1)$ distributed. ρ is the SNR at each receiver antenna. Due to the independent realizations of H_t every T-symbol period, the received signals X_t are also statistically independent for different t's. Therefore based on (2.5), the conditional probability of the sequence $\mathbf{X}^K$ given the sequence $\mathbf{\Phi}^K$ is

$$\begin{aligned} p\left(\mathbf{X}^K|\mathbf{\Phi}^K\right) &= \prod_{t=1}^{K} p\left(X_t|\Phi_{l_t}\right) \\ &= \prod_{t=1}^{K} \frac{\exp\left(-\mathrm{tr}\left\{\Lambda_t^{-1} X_t X_t^{\dagger}\right\}\right)}{\pi^{TN}\det^N \Lambda_t}, \end{aligned} \tag{3.4}$$

where $\Lambda_t = I_T + \frac{\rho T}{M}\Phi_{l_t}\Phi_{l_t}^{\dagger}$. Hence the ML sequence decoder can be formulated as

$$\begin{aligned}
\mathbf{\Phi}_{ml}^{K} &= \arg\max_{\mathbf{\Phi}^K} p\left(\mathbf{X}^K|\mathbf{\Phi}^K\right) \\
&= \arg\max_{\Phi_{l_t}\in\mathbf{\Phi}_L, 1\leqslant t\leqslant K} \prod_{t=1}^{K} \frac{\exp\left(-\mathrm{tr}\left\{\Lambda_t^{-1}X_tX_t^{\dagger}\right\}\right)}{\pi^{TN}\det{}^{N}\Lambda_t} \\
&= \arg\max_{\Phi_{l_t}\in\mathbf{\Phi}_L, 1\leqslant t\leqslant K} \sum_{t=1}^{K} \mathrm{tr}\left\{X_t^{\dagger}\Phi_{l_t}\Phi_{l_t}^{\dagger}X_t\right\} \\
&= \arg\max_{\Phi_{l_t}\in\mathbf{\Phi}_L, 1\leqslant t\leqslant K} \sum_{t=1}^{K} \left\|X_t^{\dagger}\Phi_{l_t}\right\|^2 . \qquad (3.5)
\end{aligned}$$

The third equation in (3.5) takes into account the fact that the exponential function is monotonically increasing and omits the constant terms that do not affect the result. A Viterbi algorithm can efficiently implement the ML decoding procedure [59, 60].

Suppose the output of the ML decoder (3.5) at the receiver is another sequence $\hat{\mathbf{\Phi}}^K = \{\Phi_{\hat{l}_t}, 1 \leqslant t \leqslant K\}, \hat{l}_t \in \mathbb{Z}_L$, in place of $\mathbf{\Phi}^K$. In this thesis, we define $\hat{\mathbf{\Phi}}^K$ as an *error event* to the true signal sequence $\mathbf{\Phi}^K$ for $\hat{\mathbf{\Phi}}^K \neq \mathbf{\Phi}^K$. This definition is also adopted, for example, in [37]. The *length* of the error event is defined as the number of places for which the two coded sequences differ, i.e., the Hamming distance between $\mathbf{\Phi}^K$ and $\hat{\mathbf{\Phi}}^K$.

To design a TC-USTM which produces the minimal BEP performance, one should first find the BEP expression or its union bound, then reduce the BEP or its union bound. For this purpose, we set out to find the pairwise error-event probability (PEP) by considering two coded sequence $\mathbf{\Phi}^K$ and $\hat{\mathbf{\Phi}}^K$ which are transmitted with equal probability at the transmitter. The expression for BEP will be straightforward based on the PEP expression.

Based on equation (3.5), the PEP of mistaking $\mathbf{\Phi}^K$ for $\hat{\mathbf{\Phi}}^K$, or vice versa can be

derived in a integral form as

$$P_{\text{event}} = \frac{1}{2\pi}\int_{\omega=-\infty}^{\infty}\frac{d\omega}{\omega^2+1/4}\left\{\prod_{t\in\eta}\prod_{m=1,d_{m,t}<1}^{M}\left[1+\frac{(\rho T/M)^2(1-d_{m,t}^2)(\omega^2+1/4)}{1+\rho T/M}\right]^{-N}\right\}. \tag{3.6}$$

where $d_{m,t}$ denotes the mth singular value of the correlation matrix $\Phi_{l_t}^{\dagger}\Phi_{\hat{l}_t}$ and η is the set of t for which $\Phi_{l_t} \neq \Phi_{\hat{l}_t}$. The detailed derivation of equation (3.6) can be found in Appendix A. By setting ω in the bracket in (3.6) to be zero, we obtain an upper bound of the PEP as

$$P_{\text{event}} \leqslant \prod_{t\in\eta}\Gamma_t, \tag{3.7}$$

where

$$\Gamma_t = \frac{1}{2}\prod_{m=1,d_{m,t}<1}^{M}\left[1+\frac{(\rho T/M)^2(1-d_{m,t}^2)}{4(1+\rho T/M)}\right]^{-N} \tag{3.8}$$

is the Chernoff upper bound of the PBEP between Φ_{l_t} and $\Phi_{\hat{l}_t}$ in [9]. Suppose the size of η, i.e., the length of the error event is ℓ. Then the inequality (3.7) suggests that the error events with a long length ℓ can be neglected while the error events with the shortest length $\ell_{\min}$ play the main role when evaluating the PEP. When only taking the shortest error event into account, at sufficiently high SNR (as ρ approaches ∞), the PEP is upper bounded by

$$P_{\text{event}} \leqslant \left(\frac{1}{2^{\ell_{\min}}}\left(\frac{\rho T}{4M}\right)^{-MN\ell_{\min}}\right)\cdot\left(\prod_{t\in\eta_{\min}}\prod_{m=1,d_{m,t}<1}^{M}(1-d_{m,t}^2)^{-N}\right), \tag{3.9}$$

where $\eta_{\min}$ denotes the set of t for which $\Phi_{l_t} \neq \Phi_{\hat{l}_t}$ along the path of the shortest error event. The factor inside the first bracket of (3.9) suggests that the error curve of the PEP will vary as $\rho^{-MN\ell_{\min}}$. Thus not only a *diversity gain (order)* of MN results from the employed multiple antennas, but also a *coding gain* of $\ell_{\min}$ from the trellis-coding design ais obtained [2]. Alternatively, one can interpret it as that the maximum

[2]We can also view $MN\ell_{\min}$ as the total diversity gain. As $\ell_{\min}$ is introduced as well as controlled

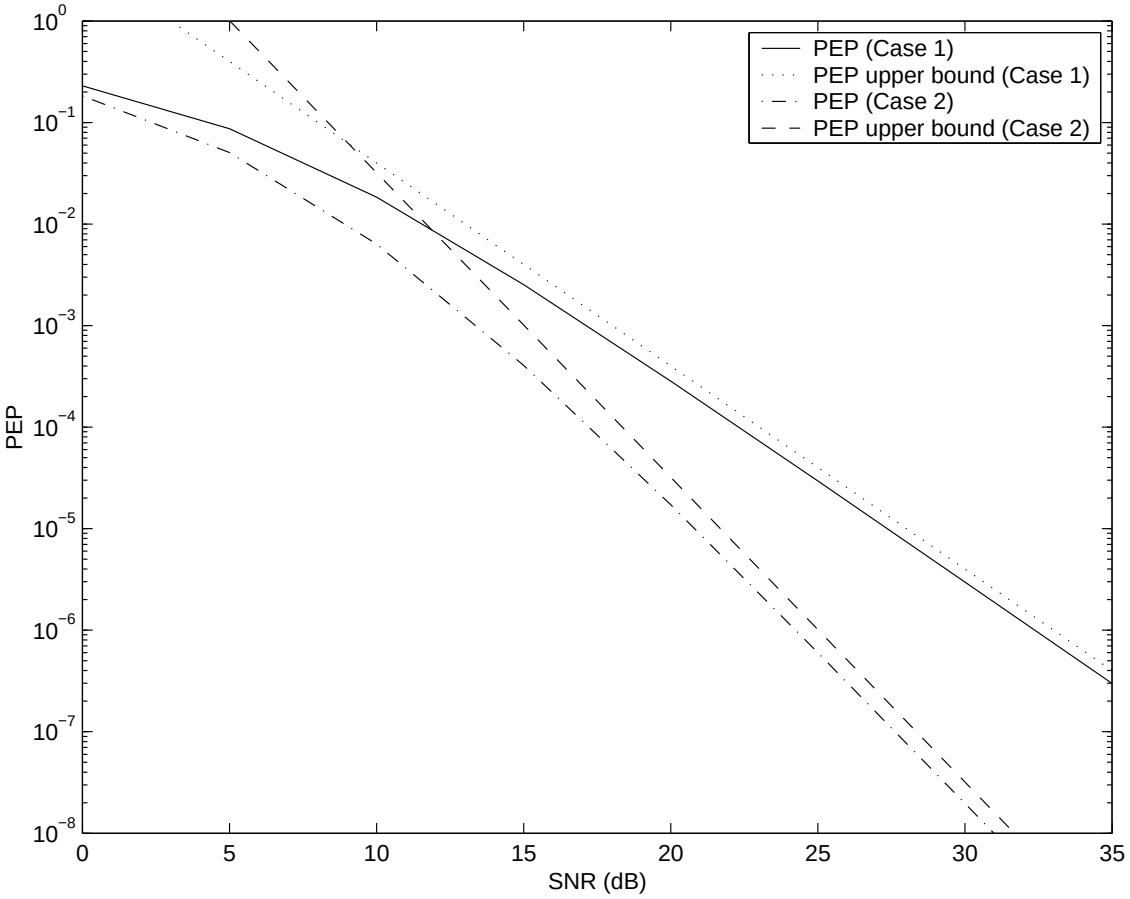

Figure 3.2: PEP and its upper bound. $\mathbf{\Phi}_8$ $(T = 2, M = 1, R = 1.5)$ is employed. Case 1: (Φ_0, Φ_0) and (Φ_2, Φ_6), $\ell_{\min} = 2$; Case 2: (Φ_0, Φ_0, Φ_0) and (Φ_1, Φ_3, Φ_6), $\ell_{\min} = 3$.

diversity gain of this non-coherent MIMO system has been increased to $MN\ell_{\min}$. Hence, the number of the transmit or receive antennas is effectively increased to $M\ell_{\min}$ or $N\ell_{\min}$. Therefore one can conclude that given the required diversity gain, the *spatial complexity* in terms of the number of antennas can be reduced, at the expense of *temporal complexity* in terms of the coding and decoding overhead from trellis coding. It suggests that one should choose a TC-USTM scheme with as large a

by trellis coding, in this thesis, we refer to it as coding gain.

value of $\ell_{\min}$ as computational complexity allows, as the decoding complexity usually increases exponentially with $\ell_{\min}$.

The PEP upper bound in inequality (3.9) and the exact PEP in equation (3.6) approach each other as SNR grows. This can be illustrated in Fig. 3.2. We use UST signal set $\mathbf{\Phi}_8(T = 2, M = 1, R = 1.5)$, and illustrate the PEP between (Φ_0, Φ_0) and (Φ_2, Φ_6), where $\ell_{\min} = 2$ and the PEP between (Φ_0, Φ_0, Φ_0) and (Φ_1, Φ_3, Φ_6) where $\ell_{\min} = 3$. Hence for simplicity, one can investigate the PEP upper bound in (3.9) for minimization of the PEP, instead of the exact PEP expression in (3.6) directly.

Additional coding gain comes from the factor inside the second bracket of (3.9). Recalling (2.8), we have

$$\prod_{t\in\eta_{\min}} \prod_{m=1,d_{m,t}<1}^{M} (1 - d_{m,t}^2)^{-N} = \prod_{t\in\eta_{\min}} d(\Phi_{l_t}, \Phi_{\hat{l}_t})^{-2MN}, \tag{3.10}$$

which suggests that the *product* of the dissimilarities along the path of the shortest error event should be maximized to minimize the upper bound in (3.9).

We note that these performance analysis are similar to those in [34] and [37] for TCM operated in the Rayleigh flat-fading channel for a single antenna system, where it is derived that the length of the shortest error event and the product of the Euclidean distance along the associated path determine the error performance. However, in this thesis it has now been generalized to a non-coherent MIMO system and it is the *dissimilarity* $d(\Phi_l, \Phi_{l'})$, instead of the *Euclidean distance* that is used as an index to evaluate the error rate performance.

Usually the BEP is a more useful performance measure. As the PEP has been derived in (3.6), an asymptotic BEP formula can be expressed as

$$P_b \approx \frac{1}{b} \sum_{\ell=\ell_{min}}^{\ell'} \sum_{j=1}^{J(\ell)} m_{\ell,j} p(\mathbf{\Phi}_{\ell,j}^K \to \hat{\mathbf{\Phi}}_{\ell,j}^K), \tag{3.11}$$

where $b = RT$ is the number of input information bits per signal block interval, $J(\ell)$ is the number of the possible error events having the same length ℓ. $J(\ell)$ is often referred to as the *multiplicity* of the error events of length ℓ. The metric $m_{\ell,j}$ is the number of bit errors associated with the jth error event of length ℓ and $p(\mathbf{\Phi}^K_{\ell,j} \rightarrow \hat{\mathbf{\Phi}}^K_{\ell,j})$ is the PEP associated with this error event and can be explicitly evaluated by equation (3.6). ℓ' is chosen so that most of the dominant error events are included. A BEP lower bound at sufficiently high SNR can be obtained by only taking the shortest error event into account, i.e., by setting $\ell' = \ell_{\min}$ in (3.11), we have

$$P_b \gtrsim \frac{1}{b} \sum_{j=1}^{J(\ell_{\min})} m_{\ell_{\min},j} p(\mathbf{\Phi}^K_{\ell_{min},j} \rightarrow \hat{\mathbf{\Phi}}^K_{\ell_{min},j}). \tag{3.12}$$

At sufficiently high SNR, the bound in (3.12) will give an accurate estimate of the BEP. As b and $m_{\ell_{\min},j}$ are constant once the trellis coding scheme is determined, the PEP's in (3.12) will determine the BEP curve. This lower bound can also be considered as a linear combination of the PEP's. Therefore one can conclude that the minimization of the PEP also leads to a lower BEP for TC-USTM.

3.4 Design Criteria for Set Partitioning

Through the inequality (3.9), one can see that $M, N, \ell_{\min}$ and the dissimilarity product $\prod_{t\in\eta} d(\Phi_{l_t}, \Phi_{\hat{l}_t})$ are four important factors that determine the upper bound of the PEP, among which, M and N are fixed once the MIMO channel model is determined, while $\ell_{\min}$ and $\prod_{t\in\eta} d(\Phi_{l_t}, \Phi_{\hat{l}_t})$ can be manipulated through designing the trellis encoder and the mapping strategy for TC-USTM.

There are two approaches known to us to increase the $\ell_{\min}$:

1) Avoid parallel paths between consecutive states in the trellis by increasing the

number of states 2^{ν}, where $\nu \geqslant 1$ is the constraint length in the trellis encoder. If every branch is assigned a *single* signal block, the $\ell_{\min}$ can be at least 2. More larger $\ell_{\min}$ is obtainable by introducing more memory ν, with the state number increasing exponentially.

2) Accommodate parallel branches between consecutive states in the trellis, however, every branch is assigned *multiple*, i.e., $k \geqslant 2$ signal blocks, which is defined as the k-tuple. $\ell_{\min}$ can then be increased by designing the k-tuples whose Hamming distance is k. In this way, the state number 2^{ν} remains unchanged while $\ell_{\min}$ increases.

The second approach involves a set partitioning of the k-fold Cartesian product of $\mathbf{\Phi}_L$, which will be addressed in Chapter 4. The first approach involves a set partitioning of the UST signal set $\mathbf{\Phi}_L$, following Ungerboeck's "mapping by set partitioning" for the 2D signal set $\mathbb{C}$ in [32]. This topic will be treated in detail in this chapter.

Usually increasing $\ell_{\min}$ can be realized by using more encoder memory ν. However, to derive the design criteria for TC-USTM, we proceed with a smaller $\ell_{\min}$, i.e., there are parallel paths between consecutive states. One reason is that for certain applications, we want to save the buffer size and to reduce the computational complexity and at the same time to achieve the required BEP performance. Therefore trellis coding with parallel paths is a tradeoff between decoding complexity and the coding gains. Another reason that we set out from trellis coding with parallel paths is that the coding gains obtained from the set partitioning of a signal set $\mathbf{\Phi}_L$ can be easily seen and demonstrated in the following.

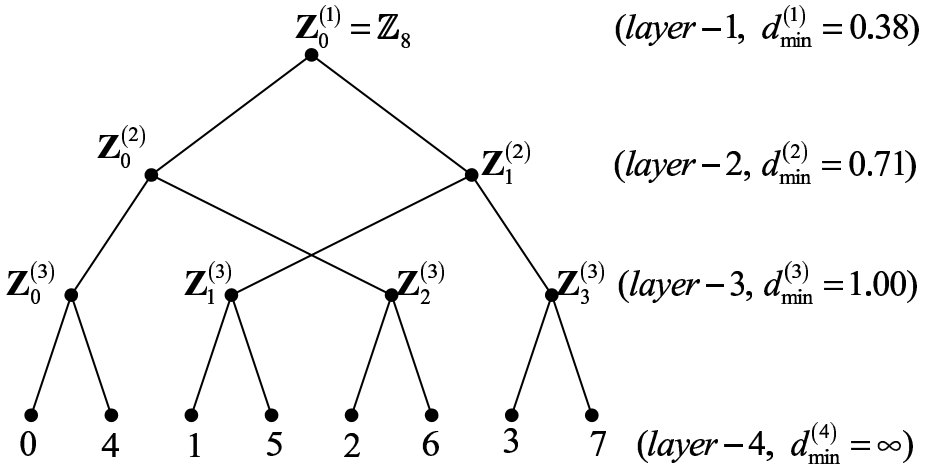

Figure 3.3: Set partitioning tree for $\mathbf{\Phi}_8$ $(T = 2, M = 1, R = 1.5)$.

3.4.1 Set Partitioning Tree

Since the signal size $L = 2^b$, $\mathbf{\Phi}_L$ can be two-branch partitioned until in the end the size-1 subsets (single signals) are obtained. Thus the partitioning tree has altogether $b+1$ layers, with $\mathbf{\Phi}_L$ in layer-1 and the single signals in layer-$(b+1)$. In layer-$j, 1 \leqslant j \leqslant b+1$, there are 2^{j-1} subsets, denoted as $\mathcal{G}_i^{(j)}, 0 \leqslant i \leqslant 2^{j-1}-1$, and each contains 2^{b-j+1} signals. For these subsets, we have $\bigcup_{i=0}^{2^{j-1}-1} \mathcal{G}_i^{(j)} = \mathbf{\Phi}_L$ and $\bigcap_{i=0}^{2^{j-1}-1} \mathcal{G}_i^{(j)} = \emptyset$, where $\emptyset$ denotes the empty set. Let $\mathbf{Z}_i^{(j)} = \{l \mid \Phi_l \in \mathcal{G}_i^{(j)}\}$ denote the *signal index set* for $\mathcal{G}_i^{(j)}$ and $\mathbf{\Delta}_i^{(j)}(l) = \{\Delta_{l,l'} \mid l', l \in \mathbf{Z}_i^{(j)}, l' \neq l\}$ the *signal index difference set* of $\mathbf{Z}_i^{(j)}$ with respect to any *reference index* $l \in \mathbf{Z}_i^{(j)}$. We define $d_{\min}(\mathcal{G}_i^{(j)}) = \min_{l,l' \in \mathbf{Z}_i^{(j)}, l \neq l'} d(\Phi_l, \Phi_{l'})$ as the *minimum dissimilarity* in $\mathcal{G}_i^{(j)}$. If for distinct i, $d_{\min}(\mathcal{G}_i^{(j)})$ are all the same, then $d_{\min}(\mathcal{G}_i^{(j)})$ can be denoted as $d_{\min}^{(j)}$. For example, we illustrate a set partitioning tree for $\mathbf{\Phi}_8$ $(T = 2, M = 1, R = 1)$ in Fig. 3.3. We can see that in layer-2, $\mathbf{Z}_0^{(2)} = \{0, 2, 4, 6\}$ and $\mathbf{\Delta}_0^{(2)} = \{2, 4, 6\}$, regardless of the reference index $l \in \mathbf{Z}_0^{(2)}$.

3.4.2 Design Criteria

Consider the case where there are $2^q, 1 \leqslant q \leqslant b$ parallel paths between two consecutive states in a TC-USTM trellis diagram ($\ell_{\min} = 1$). These parallel paths should be assigned signals from the same $\mathcal{G}_i^{(j)}$. We also require that $2^q = 2^{b-j+1}$, i.e., subsets in layer-$(b-q+1)$ of the set partitioning tree should be used. Minimization of the dissimilarity product in equation (3.10) is equivalent to maximizing $d_{\min}(\mathcal{G}_i^{(j)})$ for each i. Then we have the following design criterion :

Criterion 1. For subsets $\mathcal{G}_i^{(j)}, 0 \leqslant i \leqslant 2^{j-1}-1$ in $\mathbf{\Phi}_L$, $d_{\min}(\mathcal{G}_i^{(j)})$ should be maximized.

When a signal $\Phi_l \in \mathcal{G}_i^{(j)}$ is transmitted, it is most likely that Φ_l is decoded to be one of other $2^{b-j+1}-1$ signals in $\mathcal{G}_i^{(j)}$ if an error event happens. The error performance can be evaluated by the *average block error probability* (ABEP) in $\mathcal{G}_i^{(j)}$. It is desirable that the ABEP is identical for signal subsets formed by the 2^{b-j+1} signals assigned to the parallel paths emanating from or merging at *distinct* states, i.e., the ABEP in each signal subset $\mathcal{G}_i^{(j)}, 0 \leqslant i \leqslant 2^{j-1}-1$ is the same. This is because now the ABEP can be simply evaluated by only considering any one of the subsets $\mathcal{G}_i^{(j)}$. It is well known that at high SNR, the shortest error events dominate the error performance. So the overall block error probability of the TC-USTM can be approximated well by the ABEP. Therefore the error rate performance analysis for TC-USTM can be greatly simplified by assuming an all Φ_0's sequence is transmitted. For this purpose, the 2^{j-1} subsets should have the same "dissimilarity profile" such that the ABEP in

each size-2^{b-j+1} subset $\mathcal{G}_i^{(j)} \subseteq \mathbf{\Phi}_L, i = 0, \cdots, 2^{j-1}-1$

$$
\begin{aligned}
P_{\text{block}}(i) &= \sum_{l \in \mathbf{Z}_i^{(j)}} \sum_{l' \in \mathbf{Z}_i^{(j)}, l \neq l'} p(\Phi_l) p\left(\Phi_l \rightarrow \Phi_{l'} \mid \Phi_l\right) \\
&= \frac{1}{2^{b-j+1}} \sum_{l \in \mathbf{Z}_i^{(j)}} \sum_{l' \in \mathbf{Z}_i^{(j)}, l \neq l'} p(\Phi_l \rightarrow \Phi_{l'} \mid \Phi_l) \\
&= \frac{1}{2^{b-j+1}} \sum_{l \in \mathbf{Z}_i^{(j)}} \sum_{\Delta_{l,l'} \in \mathbf{\Delta}_{\mathbf{Z}_i^{(j)}}(l)} p(\Phi_l \rightarrow \Phi_{l \oplus \Delta_{l,l'}} \mid \Phi_l) \\
&= \frac{1}{2^{b-j+1}} \left\{ \sum_{\Delta_{l,l'} \in \mathbf{\Delta}_{\mathbf{Z}_i^{(j)}}(l)} p(\Phi_l \rightarrow \Phi_{l \oplus \Delta_{l,l'}} \mid \Phi_l) + \right. \\
&\qquad \left. \sum_{\Delta_{l,l''} \in \mathbf{\Delta}_{\mathbf{Z}_i^{(j)}}(l)} \sum_{\Delta_{l,l'} \in \mathbf{\Delta}_{\mathbf{Z}_i^{(j)}}(l)} p(\Phi_{l \oplus \Delta_{l,l''}} \rightarrow \Phi_{l \oplus \Delta_{l,l'}} \mid \Phi_l) \right\} \qquad (3.13)
\end{aligned}
$$

are identical for distinct i's. From equation (3.13), we can see that any signal $\Phi_l \in \mathcal{G}_i^{(j)}$ and its associated signal index difference set $\mathbf{\Delta}_{\mathbf{Z}_i^{(j)}}(l)$ fully characterize the subset $\mathcal{G}_i^{(j)}$ and determine the $P_{\text{block}}(i)$ in $\mathcal{G}_i^{(j)}$. In fact, we can reconstruct $\mathcal{G}_i^{(j)}$ from $\mathbf{\Delta}_{\mathbf{Z}_i^{(j)}}(l)$. For example, suppose $\mathbf{\Delta}_{\mathbf{Z}_i^{(j)}}(2) = \{1, 3, 6\}$, then $\mathcal{G}_i^{(j)} = \{\Phi_2,\ \Phi_{2\oplus 1=3},\ \Phi_{2\oplus 3=5},\ \Phi_{2\oplus 6=0}\} \subseteq \mathbf{\Phi}_8$. The second step of (3.13) also assumes that every signal in $\mathcal{G}_i^{(j)}$ is transmitted with equal probability.

To ensure $P_{\text{block}}(i) = P_{\text{block}}(i'), i \neq i'$, from (3.13) and recalling that the PBEP is a function of the index difference at high SNR (*Property* 2), i.e., $p(\Phi_l \rightarrow \Phi_{l \oplus \Delta}) = p(\Phi_{l'} \rightarrow \Phi_{l' \oplus \Delta})$ for $l \neq l'$ and $\Delta \in \{1, \cdots, L-1\}$, we require that there exist $l \in \mathbf{Z}_i^{(j)}$ and $l' \in \mathbf{Z}_{i'}^{(j)}$ such that $\mathbf{\Delta}_{\mathbf{Z}_i^{(j)}}(l) = \mathbf{\Delta}_{\mathbf{Z}_{i'}^{(j)}}(l')$. $\mathcal{G}_i^{(j)}$ and $\mathcal{G}_{i'}^{(j)}$ satisfying this requirement are defined as *congruent subsets*, denoted as $\mathcal{G}_i^{(j)} \cong \mathcal{G}_{i'}^{(j)}$. Correspondingly, the associated index subsets $\mathbf{Z}_i^{(j)}$ and $\mathbf{Z}_j^{(j)}$ are also defined as *congruent integer subsets*, denoted as $\mathbf{Z}_i^{(j)} \cong \mathbf{Z}_{i'}^{(j)}$.

Accordingly, we have the following criterion:

Criterion 2. In layer-$j, 1 \leqslant j \leqslant b+1$ of the set partitioning tree, all subsets should be congruent, i.e., $\mathcal{G}_0^{(j)} \cong \cdots \cong \mathcal{G}_{2^{j-1}-1}^{(j)}$.

Equivalently, Criterion 2 requires that in each layer, $\mathbf{Z}_0^{(j)} \cong \cdots \cong \mathbf{Z}_{2^{j-1}-1}^{(j)}$. Therefore only the integer subsets $\mathbf{Z}_i^{(j)}$ in $\mathbb{Z}_L$ need to be considered to satisfy Criterion 2.

Based on Criterion 2, the $d_{\min}(\mathcal{G}_i^{(j)})$ in Criterion 1 are identical for $i = 0, \cdots, 2^{j-1}-1$ and can be simply denoted as $d_{\min}^{(j)}$.

In this thesis, set partitioning of $\mathbf{\Phi}_L$ is defined as *optimal set partitioning* if both Criterion 1 and Criterion 2 are satisfied. In the following sections of this chapter we have formulated a *universal* optimal set partitioning approach, in the sense that the it is applicable for an arbitrary UST signal set $\mathbf{\Phi}_L$. This approach should also be *systematic* in the sense that every step in the set partitioning is given explicitly, and optimal set partitioning can be obtained following these steps. Thus a systematic partitioning renders the set partitioning for large-size signal set realizable.

3.5 A Systematic and Universal Set Partitioning for UST Signal Sets

In this section we shall formulate a systematic and universal set partitioning scheme for $\mathbf{\Phi}_L$. Instead of making successive *set partitioning* of a UST signal set as that in [32, 33], we employ successive *subset-pairing* in forming the set partitioning tree. That is, subsets in the same layer of the partitioning tree are paired to form a larger subset in the immediately higher layer. Therefore one should start with the *single* signals from the bottom layer (layer-$(b+1)$). We first present a framework to produce

all the possible realizations of the set partitioning tree which guarantees congruent subsets in each layer to satisfy Criterion 2. Then from these *candidate* partitioning trees, we select the one which satisfies Criterion 1 as the optimal set partitioning.

To form congruent subsets, from arguments in Section 3.4, we only need to consider the integer subsets $\mathbf{Z}_i^{(j)}, 0 \leqslant i \leqslant 2^{j-1}-1$ in $\mathbb{Z}_L$. Therefore we proceed with congruent set partitioning in $\mathbb{Z}_L$.

3.5.1 Congruent Partitioning in An Integer Group $\mathcal{S}$

By *congruent partitioning*, we mean that the partitioned subsets are all congruent. We first consider a generic integer group, defined as $\mathcal{S} = \{0, 2^p, 2^p \cdot 2, \cdots, 2^p \cdot (2^{B-p}-1)\} = 2^p\mathbb{Z}_{2^{B-p}}$, where the integers p and B are constrained to satisfy $0 \leqslant p \leqslant B-1$. By choosing an appropriate set of p and B, any integer group with a size given as a power of 2 can be expressed as $\mathcal{S}$. The group operation is addition modulo-2^B, denoted as $\oplus_B$. The integer difference set for $\mathcal{S}$ can be denoted as $\mathbf{\Delta}_\mathcal{S} = \{2^p, \cdots, 2^p \cdot (2^{B-p}-1)\}$, regardless of the reference integer $s \in \mathcal{S}$. For example, the integer group $\{0, 2, 4, 6\}$ can be expressed by $\mathcal{S} = 2\mathbb{Z}_4$, with $p = 1, B = 3$ and $\mathbf{\Delta}_\mathcal{S} = \{2, 4, 6\}$. We now present a systematic approach to form the size-2 congruent subsets in $\mathcal{S}$, with an *arbitrary* integer $\Delta \in \mathbf{\Delta}_\mathcal{S}$ as the identical difference for these size-2 subsets. We stress the *arbitrariness* of Δ in our optimal set partitioning, to be elaborated later in Section 3.5.4. Let $\delta = \frac{\Delta}{2^p} \in \mathbb{Z}_{2^{B-p}}$ be the *normalized difference*, in the sense that δ is an element in the *continuous* integer group $\mathbb{Z}_{2^{B-p}}$.

Lemma 1.1 For an odd integer δ, $\{2^{p+1}i, 2^{p+1}i \oplus_B \Delta\}, i \in \mathbb{Z}_{2^{B-p-1}}$ forms the congruent size-2 subsets in $\mathcal{S}$;

Lemma 1.2 For an even integer δ, $\{2^{p+p'+1}i \oplus_B m, 2^{p+p'+1}i \oplus_B \Delta \oplus_B m\}, i \in \mathbb{Z}_{2^{B-p-p'-1}}, m \in 2^p\mathbb{Z}_{2^{p'}}$ forms the congruent size-2 subsets in $\mathcal{S}$, where $p', 1 \leqslant p' \leqslant B-p-1$, is chosen such that $\frac{\delta}{2^{p'}}$ is an odd integer.

Lemma 1.1 and Lemma 1.2 can be easily proved from the definition of congruent subsets. When δ is an odd integer, $\forall s \in \mathcal{S}$, we define a one-to-one and onto mapping function $f : s \rightarrow \frac{s}{2^p}$, then $\mathcal{S}$ is isomorphic to $\mathbb{Z}_{2^{B-p}}$, denoted as $\mathcal{S} \sim \mathbb{Z}_{2^{B-p}}$. As $\{2i \mid i \in \mathbb{Z}_{2^{B-p-1}}\}$ is the even integer set in $\mathbb{Z}_{2^{B-p}}$ and $\{2i \oplus_{B-p} \delta \mid i \in \mathbb{Z}_{2^{B-p-1}}\}$ is the complementary odd integer set, the pairing of the corresponding elements in each set forms the congruent size-2 subsets $\{2i, 2i \oplus_{B-p} \delta\}, i \in \mathbb{Z}_{2^{B-p-1}}$ in $\mathbb{Z}_{2^{B-p}}$. This is because the difference sets $\{\delta\}$ are identical with references $2i$. Now using the inverse mapping function f^{-1}, that is, by multiplying 2^p back to the congruent size-2 subsets in $\mathbb{Z}_{2^{B-p}}$, $2^p\{2i, 2i \oplus_{B-p} \delta\} = \{2^{p+1}i, 2^{p+1}i \oplus_B \Delta\}, i \in \mathbb{Z}_{2^{B-p-1}}$, we form congruent size-2 subsets in $\mathcal{S}$. The difference sets $\{\Delta\}$ are now identical with references $2^{p+1}i$. We define $\mathcal{R} = \{2^{p+1}i \mid i \in \mathbb{Z}_{2^{B-p-1}}\} = 2^{p+1}\mathbb{Z}_{2^{B-p-1}}$ as the *reference set*. Each reference $r \in \mathcal{R}$ *represents* the size-2 subset $\{r, r \oplus_B \Delta\}$ that it belongs to. The operation involved in forming $\mathcal{R}$ from $\mathcal{S}$ in Lemma 1.1 is defined as *Operation I*, by which elements in $\mathcal{S}$ are directly paired to form $\mathcal{R}$. For example, we illustrate the procedure of Operation I in Fig. 3.4, where $\mathcal{S} = 2\mathbb{Z}_8$ is denoted by a set of elements evenly distributed on a circle. Given a $\Delta = 2$, the corresponding $\delta = \frac{\Delta}{2^p} = 1$ is an odd integer, hence Operation I can be used and as a result we have $\mathcal{R} = 4\mathbb{Z}_4$. The solid lines in Fig. 3.4 denote that the two connected integers form the size-2 subsets.

In Lemma 1.2 where δ is an even integer, we need to introduce an intermediate step to form a subgroup $\mathcal{S}_{\text{in}} = 2^{p+p'}\mathbb{Z}_{2^{B-p-p'}} \subset \mathcal{S}$ such that $\frac{\delta}{2^{p'}}$ is an odd integer for $p' \geqslant 1$. The integer p' is always available. In fact, any even integer δ can be factored

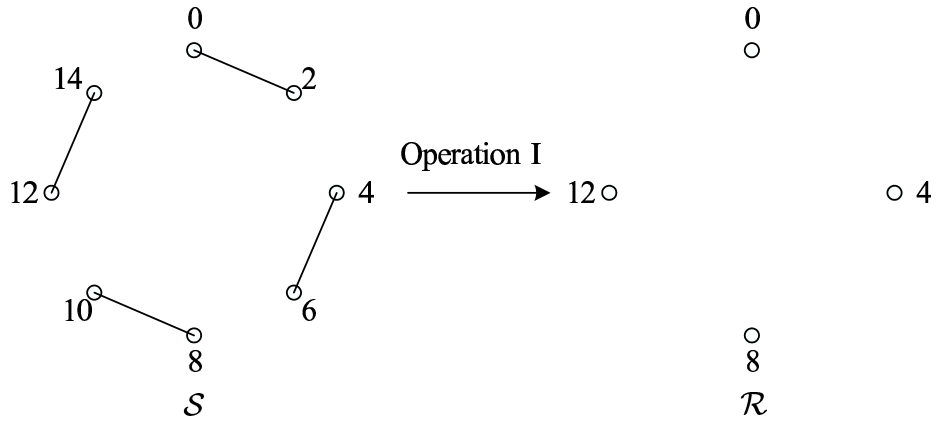

Figure 3.4: Illustration for Operation I. $\mathcal{S} = 2\mathbb{Z}_8, \Delta = 2$ ($\delta = \frac{\Delta}{2} = 1$ is an odd integer) and $\mathcal{R} = 4\mathbb{Z}_4$.

into the product of the powers of prime numbers as

$$\delta = 2^{n_1}3^{n_2}5^{n_3}\cdots, n_1 \geqslant 1, n_k \geqslant 0, k = 2, 3, \cdots \tag{3.14}$$

In (3.14), we see that 2^{n_1} is an even integer and the remaining factor $3^{n_2}5^{n_3}\cdots$ is an odd integer. We can cancel the even integer by dividing δ by 2^{n_1}. Therefore we always have $p' = n_1$. As $\frac{\delta}{2^{p'}} \geqslant 1$ and $\delta \leqslant 2^{B-p} - 2$, we have $p' \leqslant \log_2(2^{B-p} - 2) < \log_2(2^{B-p}) = B - p$, i.e., $p' \leqslant B - p - 1$.

The cosets[3] of $\mathcal{S}_{\text{in}}$ in $\mathcal{S}$ can be expressed as $\mathcal{S}_{\text{in}} \oplus_B m, m \in 2^p\mathbb{Z}_{2^{p'}}$. As $\frac{\delta}{2^{p'}}$ is now an odd integer and $\mathcal{S}_{\text{in}} \sim \mathbb{Z}_{2^{B-p-p'}}$, from Lemma 1.1, the congruent size-2 subsets in $\mathcal{S}_{\text{in}}$ are $\{2^{p+p'+1}i, 2^{p+p'+1}i \oplus_B \Delta\}, i \in \mathbb{Z}_{2^{B-p-p'-1}}$. Then the congruent size-2 subsets in $\mathcal{S}_{\text{in}} \oplus_B m$ are

$$\left\{2^{p+p'+1}i \oplus_B m, 2^{p+p'+1}i \oplus_B \Delta \oplus_B m\right\}.$$

This shows that by rotating the congruent size-2 subsets in $\mathcal{S}_{\text{in}}$ by an integer m, we can form congruent size-2 subsets in its cosets. Therefore it suffices to only consider

[3]Here the term coset has the standard meaning as in an additive group.

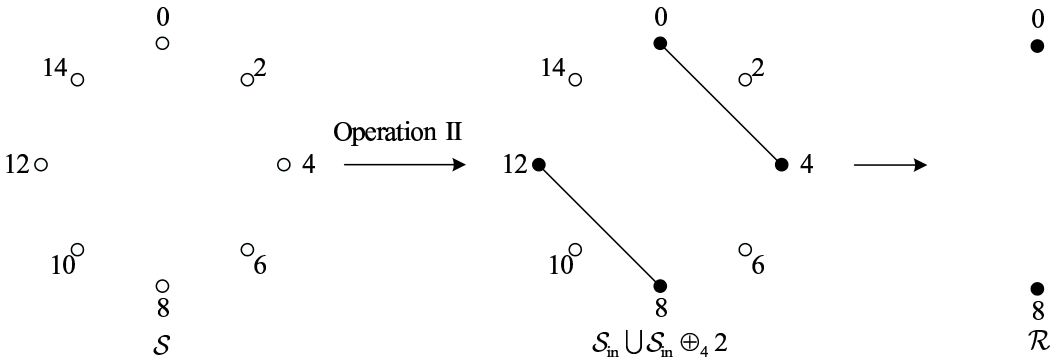

Figure 3.5: Illustration for Operation II. $\mathcal{S} = 2\mathbb{Z}_8, \Delta = 4$ ($\delta = \frac{\Delta}{2} = 2$ is an even integer), $\mathcal{S}_{\text{in}} = 4\mathbb{Z}_4, \mathcal{R} = 8\mathbb{Z}_2$.

$\mathcal{S}_{\text{in}}$ when partitioning $\mathcal{S}$ with an even δ. Accordingly the reference set should be defined over $\mathcal{S}_{\text{in}}$ as $\mathcal{R} = \{2^{p+p'+1}i \mid i \in \mathbb{Z}_{2^{B-p-p'-1}}\} = 2^{p+p'+1}\mathbb{Z}_{2^{B-p-p'-1}}$. We define the operation involved in Lemma 1.2 in forming $\mathcal{R}$ from $\mathcal{S}$ as *Operation II*. This process is illustrated in Fig. 3.5. Given $\mathcal{S} = 2\mathbb{Z}_8$ and $\Delta = 4$, as $\frac{\Delta}{2^p} = 2$ is an even integer, we select $p' = 1$ such that $\frac{\delta}{2^{p'}} = 1$ is an odd integer. Therefore we have an intermediate group $\mathcal{S}_{\text{in}} = 4\mathbb{Z}_4$ (denoted in the figure by the shaded circles) and its coset $\mathcal{S}_{\text{in}} \oplus_4 2$. Accordingly, $\mathcal{R} = 8\mathbb{Z}_2$.

3.5.2 Recursive Subset-Pairing in $\mathcal{S}$

Note that the reference set $\mathcal{R} = 2^{p+1}\mathbb{Z}_{2^{B-p-1}}$ resulting from Lemma 1.1 or $2^{p+p'+1}\mathbb{Z}_{2^{B-p-p'-1}}$ resulting from Lemma 1.2 is still in the generic form. Therefore we can set $\mathcal{S}^{(1)} \leftarrow \mathcal{R}$, i.e., set $p \leftarrow p + 1$ or $p \leftarrow p + p' + 1$. The superscript in $\mathcal{S}^{(1)}$ simply distinguish $\mathcal{S}^{(1)}$ from the original $\mathcal{S}$, which may also be denoted as $\mathcal{S}^{(0)}$. Then Operation I and II designed to partition $\mathcal{S}$ can be used to partition $\mathcal{S}^{(1)}$ into congruent size-2 subsets with an arbitrary $\Delta \in \mathbf{\Delta}_{\mathcal{S}^{(1)}}$. To distinguish from the previously defined $\mathcal{R}$ (which may also be denoted as $\mathcal{R}^{(0)}$), we denote the reference set for these new size-2 subsets

by $\mathcal{R}^{(1)}$. By setting $\mathcal{S}^{(2)} \leftarrow \mathcal{R}^{(1)}$, we can use Operation I or II to partition $\mathcal{R}^{(1)}$. As this process continues, we have *recursively* formed a new reference set $\mathcal{R}^{(k+1)}$ from the *preceding* $\mathcal{R}^{(k)}, k \geqslant 1$ by setting $\mathcal{S}^{(k+1)} \leftarrow \mathcal{R}^{(k)}$ and a chain of reference sets $\mathcal{R}^{(0)}, \mathcal{R}^{(1)}, \cdots, \mathcal{R}^{(k+1)}$ is generated.

For example, given $\mathcal{S} = 2\mathbb{Z}_8$ and $\mathcal{R} = 4\mathbb{Z}_4$ (the outcome of Operation I on $\mathcal{S}$, see Fig. 3.4), we can set $\mathcal{S}^{(1)} \leftarrow \mathcal{R}$ for the purpose of partitioning $\mathcal{R}$. Suppose that the $\Delta \in \mathbf{\Delta}_{\mathcal{S}^{(1)}}$ is 4. Then as the normalized $\delta = \frac{4}{4} = 1$ is an odd integer, we use Operation I on $\mathcal{S}^{(1)}$, giving rise to $\mathcal{R}^{(1)} = 8\mathbb{Z}_2$. Note that the reference integers 0 and 8 represent the size-4 subsets $\{0, 2, 4, 6\}$ and $\{8, 10, 12, 14\}$, respectively. To further pair 0 and 8, as a trivial step, we set $\mathcal{S}^{(2)} \leftarrow \mathcal{R}^{(1)} = \{0, 8\}$. Now the only possible $\Delta \in \mathbf{\Delta}_{\mathcal{S}^{(2)}}$ is 8, and the normalized integer difference $\delta = \frac{8}{8} = 1$ is an odd integer. So applying Operation I on $\mathcal{S}^{(2)}$ once again, we pair 0 and 8 (correspondingly, their associated size-4 subsets) to obtain a new $\mathcal{R}^{(2)} = \{0\}$. Thus, we have formed a chain of the reference sets as $4\mathbb{Z}_4, 8\mathbb{Z}_2, \{0\}$.

From the above example, we can see that when we achieve $\mathcal{R}^{(k)} = \{0\}$ for $k \geqslant 1$, subset pairing in $\mathcal{S}$ is completed. However, this statement is valid only for the case where Operation I is used all along. If Operation II is applied once, the situation will be different and a procedure called *redefinition of reference set*, to be elaborated in the following, must be carried out.

Suppose Operation II is applied on $\mathcal{S}$, giving rise to the cosets $\mathcal{S}_{\text{in}} \oplus_B m, m \in 2^p\mathbb{Z}_{2^{p'}}$ and the reference set $\mathcal{R} = 2^{p+p'+1}\mathbb{Z}_{2^{B-p-p'-1}}$. Assume Operation I is used all along to partition this $\mathcal{R}$ and all its successive reference sets. In this process, we need to set $\mathcal{S}^{(k)} \leftarrow \mathcal{R}^{(k-1)}$ for $1 \leqslant k \leqslant K$ where $K = B - p - p' - 1$ and apply Operation I individually. When we obtain $\mathcal{R}^{(K)} = \{0\}$, we know that the subset-pairing in

$\mathcal{S}_{\text{in}}$ is completed. At this stage, however, we find that the cosets themselves, i.e., $\mathcal{S}_{\text{in}}, \mathcal{S}_{\text{in}} \oplus_B 2^p, \cdots, \mathcal{S}_{\text{in}} \oplus_B (2^{p+p'} - 2^p)$, need to be paired further for a complete subset-pairing in $\mathcal{S}$. For this purpose, $\mathcal{R}^{(K)} = \{0\}$ must be *redefined* to represent these cosets. A natural way is to let m to be the reference for $\mathcal{S}_{\text{in}} \oplus_B m$, because the difference set of $\mathcal{S}_{\text{in}} \oplus_B m$ with respect to m, $\mathbf{\Delta}_{\mathcal{S}_{\text{in}} \oplus_B m}$, is identical for distinct m. Then $\mathcal{R}^{(K)}$ is redefined to be $\mathcal{R}^{(K)} = 2^p \mathbb{Z}_{2^{p'}} = 2^p \mathbb{Z}_{2^{B'-p}}$ where $B' = p+p'$. We find that the redefined $\mathcal{R}^{(K)}$ is still in the generic form. Therefore if we set $\mathcal{S}^{(K+1)} \leftarrow \mathcal{R}^{(K)}$, Operation I or II is still applicable, with addition $\oplus_{B'}$ instead of $\oplus_B$. By induction, one can conclude that every time Operation II is applied, an accompanying redefinition of the reference set is necessary. For example, we still consider subset-pairing in $\mathcal{S} = 2\mathbb{Z}_8$. We can see from Fig. 3.5 that given $\Delta = 4$, we can obtain $\mathcal{S}_{\text{in}} = 4\mathbb{Z}_4$ and $\mathcal{R} = 8\mathbb{Z}_2$ by applying Operation II. Then we set $\mathcal{S}^{(1)} \leftarrow \mathcal{R}$. Now Δ has only one value 8 and $\delta = \frac{8}{8} = 1$ is an odd integer, hence we use Operation I on $\mathcal{S}^{(1)}$ and obtain $\mathcal{R}^{(1)} = \{0\}$. At this stage, $\mathcal{R}^{(1)} = \{0\}$ only means that subset-pairing in $\mathcal{S}_{\text{in}} = 4\mathbb{Z}_4$ is completed. However, $\mathcal{S}_{\text{in}}$ and $\mathcal{S}_{\text{in}} \oplus_4 2$ need to be paired further for a complete subset-pairing in $\mathcal{S}$. Therefore we redefine $\mathcal{R}^{(1)}$ as $\mathcal{R}^{(1)} = 2\mathbb{Z}_2$, which is shown in Fig. 3.6. Then we set $\mathcal{S}^{(2)} \leftarrow \mathcal{R}^{(1)}$ and employ Operation I (as the only possible Δ is 2 and $\delta = \frac{2}{2} = 1$ is and odd integer) to form integer-pairing in $\mathcal{S}^{(2)}$, leading to $\mathcal{R}^{(2)} = \{0\}$. Then subset-pairing in $\mathcal{S}$ is completed.

To justify the above proposed subset-pairing strategy in $\mathcal{S}$, it is critical to prove that congruent integer-subsets in $\mathcal{S}^{(k)}, k \geqslant 1$ will lead to congruent integer subsets in $\mathcal{S}$. For this purpose, we first present the following two lemmas.

Lemma 2. Given $\mathcal{S}^{(k)}, k \geqslant 0$ and the resulting $\mathcal{R}^{(k)}$ by Operation I, with a $\Delta \in \mathbf{\Delta}_{\mathcal{S}^{(k)}}$. Set $\mathcal{S}^{(k+1)} \leftarrow \mathcal{R}^{(k)}$. Then the congruent size-2^n (generally $n \geqslant 1$) subsets

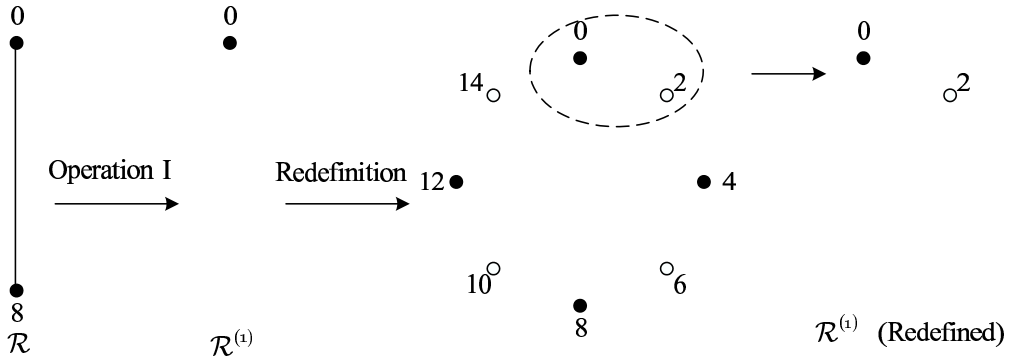

Figure 3.6: Illustration for Redefinition. $\mathcal{R}^{(1)} = \{0\}$ is redefined to be $\mathcal{R}^{(1)} = 2\mathbb{Z}_2$.

in $\mathcal{S}^{(k+1)}$ give rise to congruent size-2^{n+1} subsets in $\mathcal{S}^{(k)}$.

Proof. We know that $\mathcal{S}^{(k+1)}$ can be expressed as a generic form as $= 2^q\mathbb{Z}_{2Q-q}$ for $0 \leqslant q \leqslant Q-1, Q \leqslant B$. For the congruent size-2^n subsets in $\mathcal{S}^{(k+1)}$, let the identical difference set be denoted as $\mathbf{\Delta} = \{\Delta_1, \cdots, \Delta_{2^n-1}\}$, $\Delta_m \in \mathbf{\Delta}_{\mathcal{S}^{(k+1)}}$ for $1 \leqslant m \leqslant 2^n - 1$. So for an $s \in \mathcal{S}^{(k+1)}$, $\{s\} \bigcup \{s \oplus_Q \mathbf{\Delta}\}$ is one of the congruent size-2^n subsets in $\mathcal{S}^{(k+1)}$. By the definition of *reference*, s and $s \oplus_Q \Delta_m$ are the references for the size-2 subsets $\mathbf{G}_0 = \{s, s \oplus_Q \Delta\}$ and $\mathbf{G}_m = \{s \oplus_Q \Delta_m, s \oplus_Q \Delta_m \oplus_Q \Delta\}$ in $\mathcal{S}^{(k)}$. Then the size-2^{n+1} subset in $\mathcal{S}^{(k)}$ is $\mathbf{G}_0 \bigcup \mathbf{G}_1 \bigcup \cdots \bigcup \mathbf{G}_{2^n-1}$ and the difference set with respect to s is $\mathbf{\Delta}_{\mathbf{G}_0 \bigcup \mathbf{G}_1 \bigcup \cdots \bigcup \mathbf{G}_{2^n-1}} = \{\Delta\} \bigcup \{\Delta_1, \Delta_1 \oplus_Q \Delta\} \bigcup \cdots \bigcup \{\Delta_{2^n-1}, \Delta_{2^n-1} \oplus_Q \Delta\}$, which is not a function of s. This means that all the size-2^{n+1} subsets have the identical difference set and therefore are congruent. Note that all additions are under $\oplus_Q$. ■

As a special case of Lemma 2, letting $n = 1$, we can see that congruent size-2 subsets in $\mathcal{S}^{(k+1)}$ give rise to congruent size-4 subsets in $\mathcal{S}^{(k)}$.

Using a similar method, we can prove:

Lemma 3. Given $\mathcal{S}^{(k)}, k \geqslant 0$ and the resulting $\mathcal{R}^{(k)}$ by Operation II, with a

$\Delta \in \mathbf{\Delta}_{\mathcal{S}^{(k)}}$. Suppose K operations have been applied in subsequent subset-pairing in $\mathcal{S}^{(k+1)} \leftarrow \mathcal{R}^{(k)}$ and $\mathcal{R}^{(k+K)}$ is the *redefinition* corresponding to this Operation II. Set $\mathcal{S}^{(k+K+1)} \leftarrow \mathcal{R}^{(k+K)}$. Then congruent size-$2^n$ (generally $n \geqslant 1$) subsets in $\mathcal{S}^{(k+K+1)}$ give rise to congruent size-2^{K+n+1} subsets in $\mathcal{S}^{(k)}$.

Based on these two lemmas, we have the following theorem.

Theorem 1. Given $\mathcal{S}$ and $\mathcal{S}^{(1)}, \mathcal{S}^{(2)}, \cdots, \mathcal{S}^{(k)}, k \geqslant 1$, which is a series of the generic forms on which Operation I or II has been applied. Then congruent size-2 subsets in $\mathcal{S}^{(k)}$ leads to congruent subsets in $\mathcal{S}$.

Proof. From Lemma 2 and 3, congruent size-2 subsets in $\mathcal{S}^{(k)}$ will lead to congruent subsets in a $\mathcal{S}^{(k')}, k' \leqslant k-1$. For $\mathcal{S}^{(k')}$, we can still apply Lemma 2 or 3 and conclude that the congruent subsets in $\mathcal{S}^{(k')}$ will lead to congruent subsets in $\mathcal{S}^{(k'')}, k'' \leqslant k'-1$. We can repeatedly use Lemma 2 or 3 and eventually get the conclusion that the resulting subsets in $\mathcal{S}^{(0)}$ are congruent. ■

Theorem 1 justifies the recursive subset-pairing strategy: at time k, one only needs to form congruent size-2 subsets in the current $\mathcal{R}^{(k)}$ by setting $\mathcal{S}^{(k+1)} \leftarrow \mathcal{R}^{(k)}$ and applying Operation I or II, regardless of the previously used reference sets ($\mathcal{R}^{(t)}, t \leqslant k-1$) and the original $\mathcal{S}$, and we always have that the integer subsets in $\mathcal{S}$ at time k are congruent. In this sense, we can say that the reference set $\mathcal{R}^{(k)}$ contains *sufficient* information for a congruent subset-pairing in $\mathcal{S}$.

3.5.3 Congruent Subset-Pairing in $\mathbb{Z}_L$

By setting $\mathcal{S} \leftarrow \mathbb{Z}_L$ (i.e., $B \leftarrow b, p \leftarrow 0$), we can see that the recursive subset-pairing strategy proposed in Section **??** can be applied for a complete subset-pairing

in $\mathbb{Z}_L$ under $\oplus_b$. The size-2 subsets in $\mathcal{S}$ will form $\mathbf{Z}_0^b, \cdots, \mathbf{Z}_{2^{b-1}-1}^b$ (correspondingly, $\mathcal{G}_0^b, \cdots, \mathcal{G}_{2^{b-1}-1}^b$) in layer-$b$ of the partitioning tree. By definition, we can form the reference set $\mathcal{R}$ of size $\frac{L}{2}$ for these size-2 subsets. Then by setting $\mathcal{S}^{(1)} \leftarrow \mathcal{R}$, we can use Operation I or II to form size-2 subsets in $\mathcal{S}^{(1)}$, thus resulting in the congruent size-4 subsets in $\mathbb{Z}_L$. Then we form $\mathbf{Z}_0^{b-1}, \cdots, \mathbf{Z}_{2^{b-2}-1}^{b-1}$ (correspondingly, $\mathcal{G}_0^{b-1}, \cdots, \mathcal{G}_{2^{b-2}-1}^{b-1}$) in layer-$(b-1)$ of the partitioning tree. This process continues until finally we reach layer-1.

Note that when forming the partitioning tree, the Δ from the corresponding difference set $\mathbf{\Delta}_{\mathcal{S}^{(k)}}$ is selected arbitrarily. In the next section, we will choose the optimal Δ to satisfy Criterion 1, i.e., to form an optimal partitioning.

3.5.4 Optimal Subset-Pairing in $\mathbf{\Phi}_L$

Based on the framework proposed in Section 3.5.1, to satisfy Criterion 1, one should further determine an optimal $\Delta \in \mathbf{\Delta}_{\mathcal{R}^{(k)}}$, denoted as Δ^*, for the integer-pairing in $\mathcal{R}^{(k)}$. For a reference $r \in \mathcal{R}^{(k)}$, let $\mathcal{G}(r)$ denote the associated signal subset. Suppose the addition is $\oplus_Q$ in $\mathcal{R}^{(k)}$. To satisfy Criterion 1, we can see that Δ^* should be searched by

$$\Delta^* = \arg \max_{r \in \mathcal{R}^{(k)}, \Delta \in \mathbf{\Delta}_{\mathcal{R}^{(k)}}} d_{\min} \left(\mathcal{G}(r) \bigcup \mathcal{G}(r \oplus_Q \Delta) \right). \tag{3.15}$$

As $\{0, \Delta\}$ and $\{0 \oplus_Q r, \Delta \oplus_Q r\}$ are congruent size-2 subsets in $\mathcal{R}^{(k)}$, we have $\mathcal{G}(0) \bigcup \mathcal{G}(\Delta) \cong \mathcal{G}(r) \bigcup \mathcal{G}(r \oplus_Q \Delta)$ for $r \in \mathcal{R}^{(k)}, r \neq 0$. Therefore $d_{\min}\left(\mathcal{G}(0) \bigcup \mathcal{G}(\Delta)\right) = d_{\min}\left(\mathcal{G}(r) \bigcup \mathcal{G}(r \oplus_Q \Delta)\right)$, and it suffices to only consider $\mathcal{G}(0) \bigcup \mathcal{G}(\Delta)$ to obtain the optimal Δ^*. Therefore (4.16) can be simplified into

$$\Delta^* = \arg \max_{\Delta \in \mathbf{\Delta}_{\mathcal{R}^{(k)}}} d_{\min} \left(\mathcal{G}(0) \bigcup \mathcal{G}(\Delta) \right). \tag{3.16}$$

Once Δ^* is determined, one can obtain the corresponding normalized difference δ. Note that Δ^* can be an arbitrary integer in $\mathbf{\Delta}_{\mathcal{R}^{(k)}}$. For instance, in Fig. 3.1(a), (b) and (d), Δ^* for size-2 subsets in $\mathbb{Z}_L$ are even integers while in (c), Δ^* is an odd integer. From this observation, we can justify that Δ^* should be taken as an arbitrary integer in $\mathbf{\Delta}_{\mathcal{R}^{(k)}}$ for a congruent subset-pairing.

Based on the above arguments, we have the following proposition for a complete subset-pairing.

Proposition. The subset-pairing for an arbitrary UST signal set $\mathbf{\Phi}_L$ can be formulated as follows:

1) (*Initialization*) Set $k \leftarrow 0$, $\mathcal{S}^{(k)} \leftarrow \mathbb{Z}_L$ and $\oplus \leftarrow \oplus_b$;

2) (*Subset-pairing*) Obtain $\Delta^* \in \mathbf{\Delta}_{\mathcal{S}^{(k)}}$ through (3.16) and determine the corresponding δ. Depending on δ, employ Operation I or Operation II based on $\oplus$ to form congruent size-2 subsets in $\mathcal{S}^{(k)}$, resulting in $\mathcal{R}^{(k)}$;

3) If $\mathcal{R}^{(k)} = \{0\}$, go to step 4); otherwise set $k \leftarrow k+1$, $\mathcal{S}^{(k)} \leftarrow \mathcal{R}^{(k-1)}$ and go to step 2);

4) (*Redefinition*) If $|\mathcal{G}(0)| = L$, go to step 5); otherwise redefine $\mathcal{R}^{(k)}$ and determine Q for $\oplus_Q$ in the redefined $\mathcal{R}^{(k)}$. Set $k \leftarrow k+1$, $\mathcal{S}^{(k)} \leftarrow \mathcal{R}^{(k-1)}$, $\oplus \leftarrow \oplus_Q$, then go to step 2);

5) (*Termination*) The subset-pairing procedure terminates.

Set partitioning examples for $\mathbf{\Phi}_L$ using the Proposition will be given in Section 3.6.

A two-branch set partitioning tree is obtained following the Proposition. Similar to Ungerboeck's mapping strategy, one can map binary bits 0 and 1 to the left and right branch in the partitioning tree, respectively to obtain the so-called "mapping by set partitioning" for TC-USTM.

3.5.5 General Extension to Other Constellations

This recursive subset-pairing strategy can be generalized to any constellation $\mathcal{C}$, that has the following property:

1) The *distance profile* $\mathcal{P}_{\mathcal{C}}(l)$, defined as the set of the distances between any $c_l \in \mathcal{C}$ and all other signals $c_{l'} \in \mathcal{C}, c_{l'} \neq c_l$, is the same for all the different l's; in other words, $\mathcal{P}_{\mathcal{C}}(l)$ is not a function of l.

2) The set of all signal indices forms an integer group of dimension as a power of 2.

For example, an M-ary phase-shift-keying (MPSK) signal set satisfies the above two conditions. Consider 8PSK, whose Euclidean distance profile is similar to that in Fig. 3.1(a) ($\mathcal{P}_{\mathcal{C}} = \{0.77, 1.41, 1.93, 2, 1.93, 1.41, 0.77\}$, regardless of reference l). Let $\mathbb{Z}_8$ denote the signal index set. Then Proposition in Section 3.5.4 is still applicable for $\mathcal{C}$, through the so-called recursive subset-pairing. The procedure is recorded in Table 3.1, where the subset-pairing procedure is first recorded in the bottom row, then the second row from the bottom, and so on. In each row, the layer number, the size of the subset $\mathcal{G}_i^{(j)}$, denoted as $|\mathcal{G}_i^{(j)}|$, the minimum distance $d_{\min}^{(j)}$, the optimal index difference Δ^* and its normalized counterpart δ, the generic form $\mathcal{S}^{(k)}$, the operation type and the resulting $\mathcal{R}^{(k)}$ for the current subsets, are all listed (we use the same set of symbols as those for UST signal sets). In detail, we initiate this process by letting

Table 3.1: Subset-pairing for 8PSK.

Layer-j	$\lvert\mathcal{G}_i^{(j)}\rvert$	$d_{\min}^{(j)}$	Δ^*	δ	k	$\mathcal{S}^{(k)}$	–	Operation	$\rightarrow$	$\mathcal{R}^{(k)}$
1	8	0.77	$\sim$	$\sim$	3	$\sim$		$\sim$		$\sim$
2	4	1.41	1	1	2	$\mathbb{Z}_2$		I		$2\mathbb{Z}_1$
3	2	2.00	2	2	1	$\mathbb{Z}_4$		II		$\mathbb{Z}_2$
4	1	∞	4	4	0	$\mathbb{Z}_8$		II		$\mathbb{Z}_4$

$\mathcal{S}^{(0)} \leftarrow \mathbb{Z}_8$. As $\Delta^* = \delta = 4$ (as the resulting $d_{\min}^3 = 2$ will be maximized) is an even integer, then letting $p' = 2$ so that $\frac{4}{2^2} = 1$ is an odd integer, and have $\mathcal{S}_{\text{in}}^{(0)} = \{0, 4\}$ and its cosets $\mathcal{S}_{\text{in}}^{(0)} \oplus_3 m, m \in \mathbb{Z}_4$. Thus, by Operation II, we have $\mathcal{R} = \{0\}$, then $\mathcal{R}$ is redefined to be $\mathcal{R} = \mathbb{Z}_4$. Then setting $\mathcal{S}^{(1)} \leftarrow \mathcal{R}$ we obtain that $\Delta^* = \delta = 2$ (as the resulting $d_{\min}^{(2)} = 1.41$ will be maximized). Letting $p' = 1$, we have $\frac{2}{2} = 1$, an odd integer. Then $\mathcal{S}_{\text{in}}^{(1)} = \{0, 2\}$ and its coset $\mathcal{S}_{\text{in}}^{(1)} \oplus_2 1$. As a result, $\mathcal{R}^{(1)} = \{0\}$ and redefined to be $\mathcal{R}^{(1)} = \mathbb{Z}_2$. The last integer-pairing in $\mathcal{R}$ is straightforward.

The resulting set partitioning tree is identical to that proposed in [32], where the two-branch partition can be formulated as 8PSK / 4PSK / 2PSK / 1PSK (see also in [53, 54]), where / denotes the quotient group operation. However we note that this simple partitioning strategy only suits the MPSK signal set which has an inherent regular distance profile, *i.e.*, the Euclidean distance is symmetrical, has a maximum at the center and is monotonically increasing (decreasing) for the first (second) half of the profiles (similar to the distance profile shown in Fig. 3.1(a)). Our proposed Proposition, however, can handle more complicated constellations where the distance profile has not much regularities, as that in Fig. 3.1(b),(c) and (d).

Table 3.2: Subset-pairing for $\mathbf{\Phi}_{16}$ $(T = 4, M = 2, R = 1)$.

Layer-j	$\lvert\mathcal{G}_i^{(j)}\rvert$	$d_{\min}^{(j)}$	Δ^*	δ	k	$\mathcal{S}^{(k)}$	$-$	Operation	$\rightarrow$	$\mathcal{R}^{(k)}$
1	16	0.38	$\sim$	$\sim$	4	$\sim$		$\sim$		$\sim$
2	8	0.44	1	1	3	$2\mathbb{Z}_2$		I		$4\mathbb{Z}_1$
3	4	0.71	1	1	2	$\mathbb{Z}_4$		I		$2\mathbb{Z}_2$
4	2	1.00	4	4	1	$\mathbb{Z}_8$		II		$\mathbb{Z}_4$
5	1	∞	8	8	0	$\mathbb{Z}_{16}$		II		$\mathbb{Z}_8$

3.6 Examples and Numerical Results

In this section, we perform the optimal set partitioning for the UST constellation $\mathbf{\Phi}_L$ and evaluate the BEP performance for the resulting TC-USTM. In all cases of the simulations, we assume that there is a single receive antenna ($N = 1$) and that the channel is a piecewise constant Rayleigh flat-fading channel.

3.6.1 TC-USTM with $\mathbf{\Phi}_{16}$ $(T = 4, M = 2, R = 1)$

The set partitioning tree for $\mathbf{\Phi}_{16}$ $(T = 4, M = 2, R = 1)$, whose intra-distance profile is given in Fig. 3.1(d), is illustrated in Fig. 3.7. As $b = R \cdot T = 4$, the tree has 5 layers and the j-th layer contains 2^{5-j} subsets of size-2^{j-1}, $1 \leqslant j \leqslant 5$. The integer beside each node in the tree denotes the reference for the subset in each layer. On the left hand side in Fig. 3.7, we also illustrate the subset-pairing process. The pertinent parameters in the subset-pairing are recorded in Table 3.2. Note that in Table 3.2, we first record the parameters associated with the first operation in the bottom row, then the parameters associated with the second operation in the second row from the bottom, and so on.

Following the Proposition in Section 3.5.4, we proceed with setting $\mathcal{S}^{(0)} \leftarrow \mathbb{Z}_{16}$. By (3.16), $\Delta^* = 8$ and accordingly $\delta = \Delta^* = 8$, an even integer. Let $p' = 3$ such

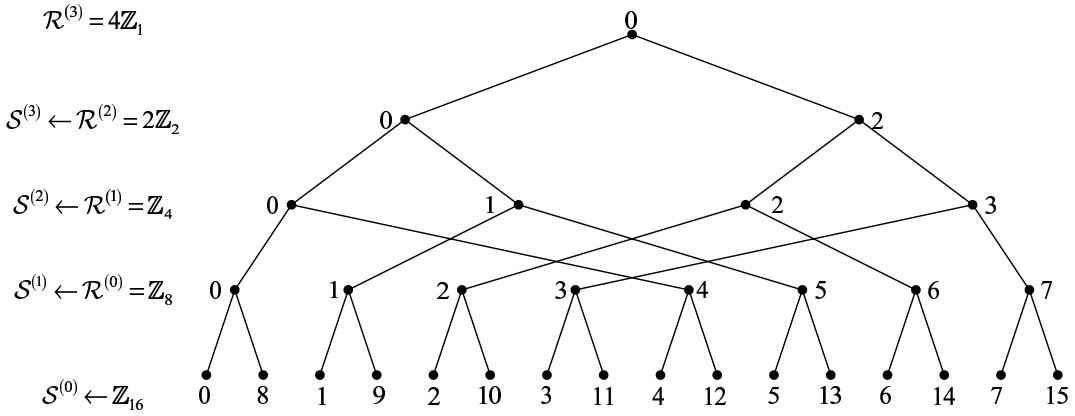

Figure 3.7: Set partitioning for $\mathbf{\Phi}_{16}$ $(T = 4, M = 2, R = 1)$.

that $\frac{\delta}{2^{p'}} = 1$, an odd integer. Therefore applying Operation II on $\mathcal{S}^{(0)}$, one obtains $\mathcal{S}_{\text{in}}^{(0)} = 8\mathbb{Z}_2 = \{0, 8\}$ and its cosets $\mathcal{S}_{\text{in}}^{(0)} \oplus_4 m, m \in \mathbb{Z}_8$ in $\mathcal{S}^{(0)}$. Note that $\mathcal{S}_{\text{in}}^{(0)}$ itself is already a size-2 subset and the subset-pairing in it is straightforward. The resulting reference set is $\mathcal{R}^{(0)} = \{0\}$. So at this stage, one needs to redefine $\mathcal{R}^{(0)} = \mathbb{Z}_8$ and set $Q = 3$ according to the Proposition. Then set $\mathcal{S}^{(1)} \leftarrow \mathbb{Z}_8$. By (3.16), one can find that $\Delta^* = 4$ and accordingly $\delta = 4$, an even integer. Therefore Operation II should be used once again on $\mathcal{S}^{(1)}$. Let $p' = 2$ such that $\frac{\delta}{2^{p'}} = 1$, an odd integer. One obtains $\mathcal{S}_{\text{in}}^{(1)} = \{0, 4\}$ and its cosets $\mathcal{S}_{\text{in}}^{(1)} \oplus_3 m, m \in \mathbb{Z}_4$ in $\mathcal{S}^{(1)}$. As $\mathcal{S}_{\text{in}}^{(1)}$ is a size-2 set, readily we have $\mathcal{R}^{(1)} = \{0\}$ and once again $\mathcal{R}^{(1)}$ is redefined to be $\mathcal{R}^{(1)} = \mathbb{Z}_4$, and $Q = 2$. Set $\mathcal{S}^{(2)} \leftarrow \mathcal{R}^{(1)}$. By (3.16), $\delta = \Delta^* = 1$, which is an odd integer. Thus Operation I should be employed to partition $\mathcal{S}^{(2)}$ into $\{0, 1\}$ and $\{2, 3\}$ resulting in $\mathcal{R}^{(2)} = \{0, 2\}$. The last pairing of 0 and 2 is straightforward.

We employ a rate $\frac{b}{b+1}$ TC-USTM encoder. The above partitioning scheme can be used for the TC-USTM of $T = 4, M = 2, R = \frac{3}{4}$ and the trellis diagram is illustrated in Fig. 3.8 (a). For comparison, we also consider two non-optimal set partitioning

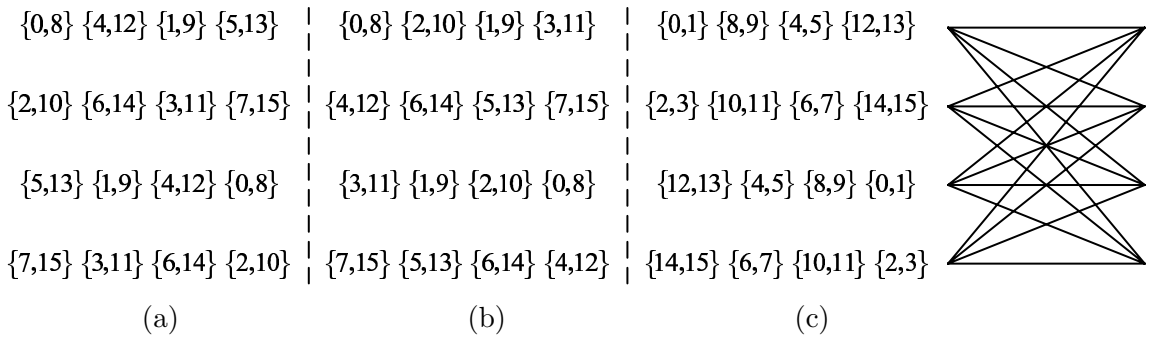

Figure 3.8: 4-state trellis diagrams for TC-USTM employing $\mathbf{\Phi}_{16}(T = 4, M = 2, R = 1)$. Mapping is based on (a) optimal set partitioning; (b) non-optimal set partitioning (Case 1); (c) non-optimal set partitioning (Case 2).

schemes. The first one is referred to as *Case* 1, in which signals in layer-5 are paired optimally ($\Delta^* = 8$), however subsets in layer-4 are non-optimally paired by letting $\Delta = 2 \neq \Delta^* = 4$. The subsequent subset-pairing follows the Proposition. The trellis diagram that results from Case 1 is illustrated in Fig. 3.8(b). Another non-optimal set partitioning is referred to as *Case* 2, in which $\Delta = 1 \neq \Delta^* = 8$ for integers in layer-1. The remaining subset-pairing in Case 2 follows the Proposition. The trellis diagram is illustrated in Fig. 3.8(c).

In Fig. 3.9 we show that TC-USTM with the optimal set partitioning has a significant coding gain ($\geqslant$ 7 dB) over Case 2 in the high SNR region. However, compared with Case 1, it has a slight coding gain ($\leqslant$ 1 dB) in the moderate SNR region and has almost the same performance at high SNR. Here we see that $d^{(4)}_{\min}$ for size-2 subsets plays a more important role than $d^{(j)}_{\min}, j \leqslant 3$ for larger size subsets when there are 2 parallel paths in the trellis diagram. This justifies that the two signals with the largest distance should be paired to form the size-2 subsets. It can be easily deduced that if there are $2^\kappa, \kappa \geqslant 2$ parallel paths between consecutive states, then the minimum distance in the size-2^κ subsets is more important than that in the

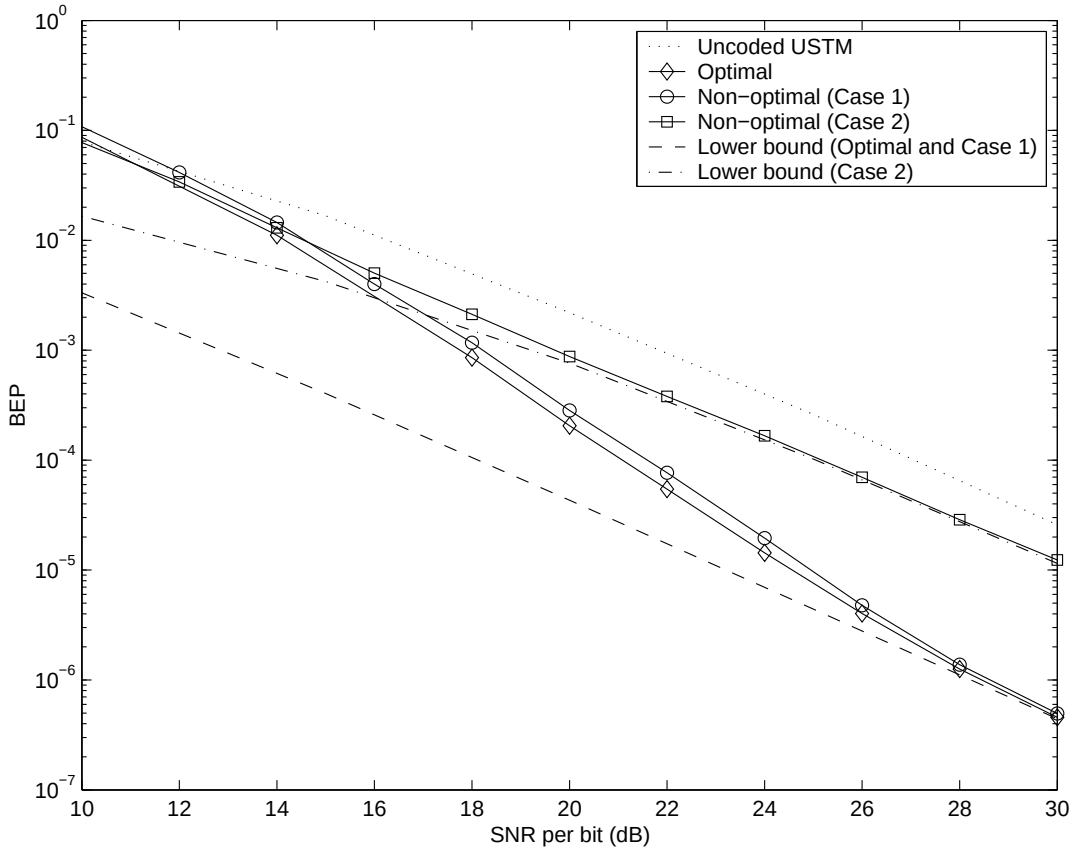

Figure 3.9: BEP comparison between TC-USTM ($T = 4, M = 2, R = 0.75$) with optimal set partitioning and non-optimal set partitioning.

larger subsets.

The BEP lower bound can be evaluated by following the formula given in Section 3.3. Due to that now the size-2 subsets are all congruent, and the associated number of bit error is 1 for the "mapping by set partitioning", the analytical BEP performance can be evaluated by simply assuming that the all Φ_0 sequence is transmitted and the shortest error event with length 1 is $\{\Phi_8, \Phi_0, \Phi_0, \cdots\}$. At high SNR, the BEP associated with the shortest error event dominates the overall error performance. We

Table 3.3: Subset-pairing for $\mathbf{\Phi}_{16}$ $(T = 3, M = 1, R = 1.33)$.

Layer-j	$\lvert\mathcal{G}_i^{(j)}\rvert$	$d_{\min}^{(j)}$	Δ^*	δ	k	$\mathcal{S}^{(k)}$	$-$	Operation	$\rightarrow$	$\mathcal{R}^{(k)}$
1	16	0.61	$\sim$	$\sim$	4	$\sim$		$\sim$		$\sim$
2	8	0.61	8	1	3	$8\mathbb{Z}_2$		I		$16\mathbb{Z}_1$
3	4	0.74	4	1	2	$4\mathbb{Z}_4$		I		$8\mathbb{Z}_2$
4	2	0.98	2	1	1	$2\mathbb{Z}_8$		I		$4\mathbb{Z}_4$
5	1	∞	7	7	0	$\mathbb{Z}_{16}$		I		$2\mathbb{Z}_8$

find that the simulation and the analytical results agree well at high SNR. As TC-USTM with the optimal set partitioning and that in Case 1 have the same shortest error events, the lower bounds for both cases are identical.

3.6.2 TC-USTM with $\mathbf{\Phi}_{16}$ $(T = 3, M = 1, R = 1.33)$

Set partitioning for $\mathbf{\Phi}_{16}$ $(T = 3, M = 1, R = 1.33)$, whose distance profile is given in Fig. 3.1(c), is illustrated in Fig. 3.10. The subset-pairing procedure is shown on the left hand side of the figure. We follow the Proposition in Section 3.5.4 and initiate the subset-pairing by setting $\mathcal{S}^{(0)} \leftarrow \mathbb{Z}_{16}$. The detailed parameters in this process are recorded in Table 3.3.

For comparison, we employ a non-optimal set partitioning of $\mathbf{\Phi}_{16}$ by letting $\Delta = 5 \neq \Delta^* = 7$ for the first layer while the subsequent subset-pairing follows the Proposition. In this example, we employ a 4-state and a 16-state trellis diagrams to investigate the BEP of the TC-USTM with and without the optimal set partitioning. In Fig. 3.11 we show for TC-USTM of 4-state, around 2 dB coding gain can be obtained at high SNR by TC-USTM with the optimal set partitioning over the one with non-optimal partitioning. For 16-state trellis, one can see that the coding gain is not that significant and the lower bounds are quite loose compared with the 4-state

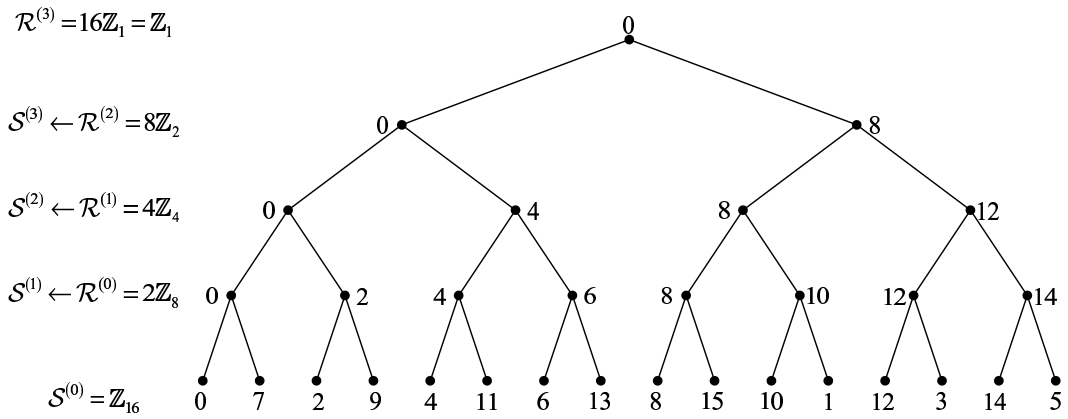

Figure 3.10: Set partitioning for $\mathbf{\Phi}_{16}$ $(T = 3, M = 1, R = 1.33)$.

Table 3.4: Subset-pairing for $\mathbf{\Phi}_8$ $(T = 2, M = 1, R = 1.5)$.

Layer-j	$\lvert\mathcal{G}_i^{(j)}\rvert$	$d_{\min}^{(j)}$	Δ^*	δ	k	$\mathcal{S}^{(k)}$	– Operation →	$\mathcal{R}^{(k)}$
1	8	0.38	$\sim$	$\sim$	3	$\sim$	$\sim$	$\sim$
2	4	0.71	1	1	2	$\mathbb{Z}_2$	I	$2\mathbb{Z}_1$
3	2	1.00	2	2	1	$\mathbb{Z}_4$	II	$\mathbb{Z}_2$
4	1	∞	4	4	0	$\mathbb{Z}_8$	II	$\mathbb{Z}_4$

case. However, the value of coding gain demonstrated by the lower bounds and the simulation results agree well.

3.6.3 TC-USTM with $\mathbf{\Phi}_8$ $(T = 2, M = 1, R = 1.5)$

In this example, we perform the optimal set partitioning for the signal set $\mathbf{\Phi}_8$ $(T = 2, M = 1, R = 1.5)$, which is used for the TC-USTM of $T = 2, M = 1, R = 1$. In Table 3.4, we recorded the pertinent parameters in the subset-pairing procedure. The set partitioning tree has the same structure as the one in Fig. 3.3.

In this section, we mainly compare the BEP performance between the resulting TC-USTM $(T = 2, M = 1, R = 1)$ using $\mathbf{\Phi}_8$ and the TC-USTM $(T = 4, M =$

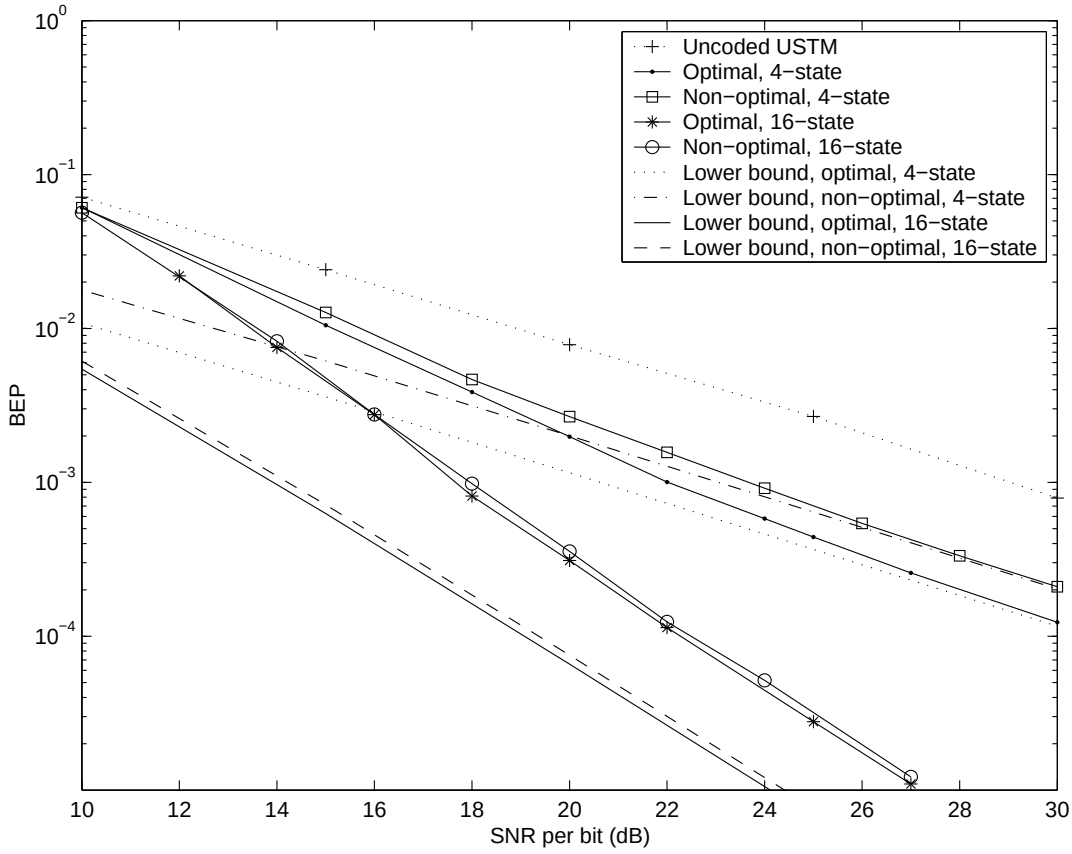

Figure 3.11: BEP comparison between TC-USTM ($T = 3, M = 1, R = 1$) with optimal set partitioning and non-optimal set partitioning.

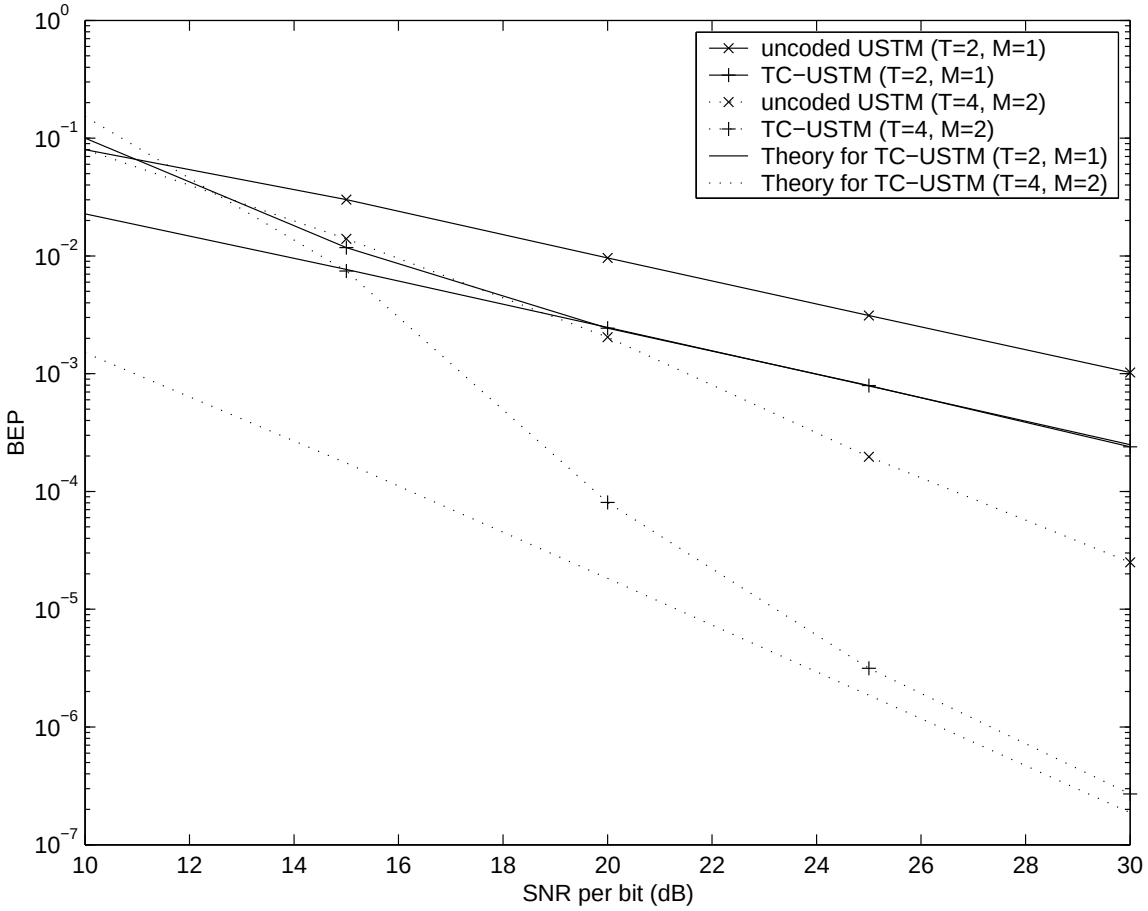

Figure 3.12: BEP comparisons between TC-USTM ($T = 2, M = 1, R = 1$) and TC-USTM ($T = 4, M = 2, R = 1$), with optimal set partitioning. $\ell_{\min} = 1$.

$2, R = 1$) with $\Phi_{32}(T = 4, M = 2, R = 1.25)$. We examine two cases: $\ell_{\min} = 1$ and $\ell_{\min} = 2$. In the first case, we use a 2-state trellis for TC-USTM with $\mathbf{\Phi}_8$ and a 16-state trellis for the one with $\mathbf{\Phi}_{32}$. In the second case, we use an 8-state trellis and a 32-state trellis, respectively for the two TC-USTM schemes. The error performance is given in Fig. 3.12 and Fig. 3.13. Both TC-USTM schemes have significant coding gains over the uncoded USTM. We know that the TC-USTM with $T = 4, M = 2$ has diversity gain (order) $MN = 2$, while the TC-USTM with $T = 2, M = 1$ has diversity

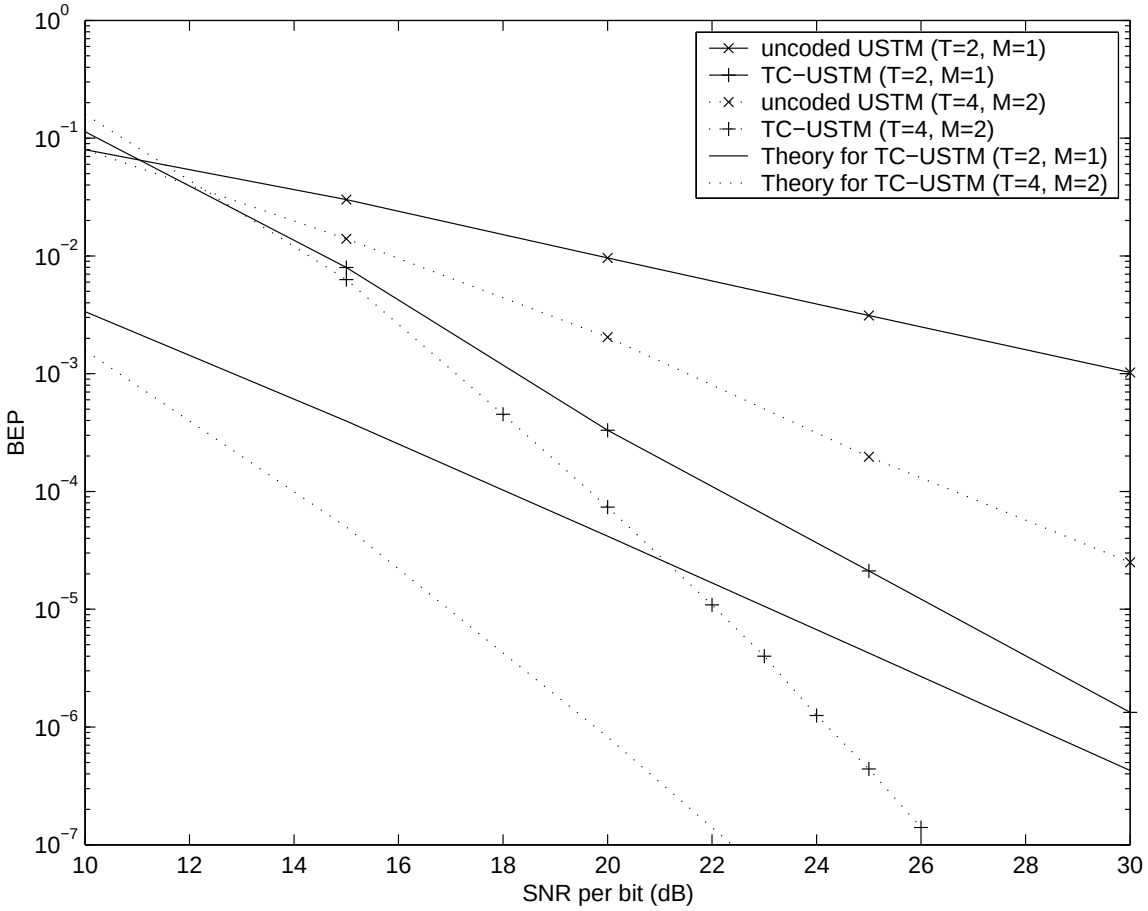

Figure 3.13: BEP comparisons between TC-USTM ($T = 2, M = 1, R = 1$) and TC-USTM ($T = 4, M = 2, R = 1$), with optimal set partitioning. $\ell_{\min} = 2$.

gain $MN = 1$. Therefore though both schemes have the same coding gain $\ell_{\min} = 1$, the TC-USTM using larger number antennas performs much better than the former, which is shown in both figures. One can also observe that the slope of the error rate curves in Fig. 3.13 where $\ell_{\min} = 2$ is much more sharper than their counterparts in Fig. 3.12 where $\ell_{\min} = 1$. This is because for the former, the coding gain in terms of $\ell_{\min}$ is increased to 2. One can also observe that the BEP lower bounds in Fig. 3.13 are not as tight as those in Fig. 3.12.

3.7 Summary

We have performed the PEP and BEP analysis of the TC-USTM in Rayleigh flat fading channel in this section. Based on these analysis, the design criteria for a good TC-USTM have been proposed, and lead to the so-called optimal set partitioning. A systematic as well as universal set partitioning strategy is proposed for an arbitrary UST signal set. This approach is based on a procedure called subset-pairing, and this procedure can be implemented in the recursive manner through the definition of the reference set $\mathcal{R}$. The BEP performance of the TC-USTM is investigated in terms of computer simulations and theoretical analysis. It is demonstrated that TC-USTM outperforms its uncoded counterparts and in most cases the BEP lower bounds agree well with the simulation results. Due to the assumption of piecewise constant Rayleigh fading channel, we should point out that in practice TC-USTM is especially catered for a rapid fading channel, or for a frequency hopping or fully block-interleaved communication system.

Chapter 4

Multiple Trellis-Coded Unitary Space-Time Modulation

4.1 Background

In the classical work by Divsalar and Simon [34]-[36], multiple trellis coded modulation (MTCM) was proposed for a single antenna communication system, where $k \geqslant 2$ MPSK signals are assigned to a trellis branch. The accompanying set partitioning scheme for MTCM employing k-fold *Cartesian products* of the MPSK signal set was proposed in [36]. Significant coding gain can be obtained by MTCM over the *conventional* (single signal per trellis branch) TCM, when both have the same number of trellis states and information rates. Most recently we have noticed that MTCM has been combined with space-time trellis codes [17, 43] and a concatenated space-time block codes with trellis codes [26] to obtain a better BEP performance. However, in [17], [43], [26], the CSI is assumed to be known *a priori* or has to be estimated and tracked through training.

In this chapter, we extend the TC-USTM scheme to the *multiple* trellis-coded USTM (MTC-USTM) by combining USTM and MTCM, where $k \geqslant 2$ UST signal blocks are assigned to a single trellis branch. As in previous works [4, 9, 10, 15], we

assume the so-called piecewise constant Rayleigh flat fading channel where CSI is not known both at the transmitter and receiver. We propose design criteria which are aimed at minimizing the PEP, which also leads to a lower BEP for the MTC-USTM. We also designed a partitioning approach for the k-fold Cartesian product of the UST signal set. Through analysis and computer simulations, we shall demonstrate that MTC-USTM can produce superior BEP performance over the TC-USTM of the same information rate and number of trellis states.

This chapter is organized as follows. Design criteria minimizing the PEP are presented in Section 4.2. A systematic code design approach and the numerical results are presented in Section 4.3 and 4.4 respectively. We summarize this chapter in Section 4.5.

4.2 Performance Analysis and Design Criteria for MTC-USTM

In this section, we are concerned with a rate $\frac{bk}{(b+1)k} = \frac{b}{(b+1)}, k \geqslant 2$ MTC-USTM in which a k-tuple $\boldsymbol{c} = (\Phi_{d_1}, \cdots, \Phi_{d_k})$ is assigned to a single trellis branch, where $d_r \in \mathbb{Z}_L$ for $r = 1, \cdots, k$ and $L = 2^{b+1}$. Let $\boldsymbol{c}^r$ denote the r-th signal in $\boldsymbol{c}$. Suppose a multiple trellis coded sequence $\boldsymbol{\Phi}^K = \{\Phi_{l_t}, 1 \leqslant t \leqslant K\}$ is transmitted, where t is the time index of each signal block and $l_t \in \mathbb{Z}_L$ is the data transmitted at t. Note that the sequential signal blocks of length k belong to the same k-tuple and K is a multiple of k. The received signal X_t can be expressed as

$$X_t = \sqrt{\rho T/M}\Phi_{l_t} H_t + W_t. \tag{4.1}$$

In equation (4.1), H_t and W_t follow the same definitions as those for equation (3.3). ρ is the signal-to-noise ratio (SNR) at each receive antenna. An error event happens

when the decoder selects another sequence $\hat{\mathbf{\Phi}}^K = \{\Phi_{\hat{l}_t}, 1 \leqslant t \leqslant K\}, \hat{l}_t \in \mathbb{Z}_L$ in place of $\mathbf{\Phi}^K$. The *length* of the error event is defined as the number of places in which the two coded sequences differ, i.e., the Hamming distance between $\mathbf{\Phi}^K$ and $\hat{\mathbf{\Phi}}^K$.

As $X_t, 1 \leqslant t \leqslant K$ are independent due to the independent realizations of H_t, the PEP for MTC-USTM can be derived using the same method as that for TC-USTM in Section 3. The PEP $p(\mathbf{\Phi}^K \to \hat{\mathbf{\Phi}}^K)$ of mistaking $\mathbf{\Phi}^K$ for $\hat{\mathbf{\Phi}}^K$, or vice versa, is

$$p(\mathbf{\Phi}^K \to \hat{\mathbf{\Phi}}^K) = \frac{1}{4\pi} \int_{-\infty}^{\infty} \frac{dx}{x^2 + 1/4} \prod_{t \in \eta} \prod_{m=1}^{M} \left[1 + \frac{(\rho T/M)^2 (1 - d_{m,t}^2)(x^2 + 1/4)}{1 + \rho T/M} \right]^{-N}, \tag{4.2}$$

where η denotes the set of t for which $\Phi_{l_t} \neq \Phi_{\hat{l}_t}$ along the path of the error event and $d_{m,t}$ is the mth singular value of the correlation matrix $\Phi_{l_t}^{\dagger} \Phi_{\hat{l}_t}$. By letting ρ approach ∞, i.e., in the region of sufficiently high SNR, we have

$$p(\mathbf{\Phi}^K \to \hat{\mathbf{\Phi}}^K) \leqslant \frac{1}{2^{\ell_{\min}}} \left(\frac{\rho T}{4M} \right)^{-MN\ell_{\min}} \prod_{t \in \eta_{\min}} \zeta(\Phi_{l_t}, \Phi_{\hat{l}_t})^{-2MN}, \tag{4.3}$$

where $\eta_{\min}$ denotes the set of t along the path of the shortest error event of length $\ell_{\min}$. In this chapter, we shall employ d to denote the Hamming distance between two k-tuples. So in the sequel, the dissimilarity between Φ_l and $\Phi_{l'}$ is denoted as $\zeta(\Phi_l, \Phi_{l'})$ (instead of $d(\Phi_l, \Phi_{l'})$) and we also refer to $\prod_{t \in \eta_{\min}} \zeta(\Phi_{l_t}, \Phi_{\hat{l}_t})$ as the *dissimilarity product* along the path of the shortest error event. The upper bound in (4.3) gives an approximate estimate of the exact PEP given by equation (4.2), which has been demonstrated in Section 3.3 in Chapter 3. Therefore for simplicity, we can investigate (4.3) instead of (4.2) to minimize the PEP. It follows that $\ell_{\min}$ plays a more important role than the dissimilarity product, because the PEP bound (4.3) is inversely proportional to the $(MN\ell_{\min})$-th power of the SNR. Therefore the prime objective of a good MTC-USTM design is to maximize $\ell_{\min}$ while the second objective

is to maximize the dissimilarity product along the path of the shortest error event.

There are bk information bits per encoding interval (T-symbol period), where $b = RT$. Therefore there are 2^{bk} paths emanating from each state. The number of parallel paths between two consecutive states depends on the connectivity of the trellis. For example, if the trellis is *fully* connected (all the 2^{ν} states are mutually connected), there are $2^{bk-\nu}$ parallel paths between any two states. Given bk and the number of parallel paths between states, the fully connected trellis has the minimum number of states. Therefore we focus on the MTC-USTM employing a fully connected trellis with parallel paths by assuming $bk > \nu$. Let (i, j) denote the pair of connected states, $i, j \in \mathbb{Z}_{2^{\nu}}$. For any (i, j), the $2^{bk-\nu}$ parallel k-tuples form a set denoted as $\mathcal{G}_{i,j}$. Let $\boldsymbol{c}_1$ and $\boldsymbol{c}_2$ denote any two k-tuples and $d(\boldsymbol{c}_1, \boldsymbol{c}_2)$ their Hamming distance. The *intra (subset)-Hamming distance* in $\mathcal{G}_{i,j}$ is defined as

$$d(\mathcal{G}_{i,j}) = \min_{\boldsymbol{c}_1, \boldsymbol{c}_2 \in \mathcal{G}_{i,j}, \boldsymbol{c}_1 \neq \boldsymbol{c}_2} d(\boldsymbol{c}_1, \boldsymbol{c}_2). \tag{4.4}$$

The *inter (subset)-Hamming distance* between $\mathcal{G}_{i,j}$ and $\mathcal{G}_{i',j'}, i \neq i'$ and/or $j \neq j'$ is defined as

$$d(\mathcal{G}_{i,j}, \mathcal{G}_{i',j'}) = \min_{\boldsymbol{c}_1 \in \mathcal{G}_{i,j}, \boldsymbol{c}_2 \in \mathcal{G}_{i',j'}} d(\boldsymbol{c}_1, \boldsymbol{c}_2). \tag{4.5}$$

To increase $\ell_{\min}$, one has to maximize $d(\mathcal{G}_{i,j})$ for each (i, j) so as to maximize the length of the shortest error event that covers *one* branch in the trellis diagram. Moreover, to maximize the length of the shortest error event that covers *more than one* branch, one should also maximize the minimum of $d(\mathcal{G}_{i,j}, \mathcal{G}_{i,j'}), j \neq j'$ for subsets emanating from the same state i, defined as

$$d_{i,*} = \min_{0 \leqslant j \neq j' \leqslant 2^{\nu}-1} d(\mathcal{G}_{i,j}, \mathcal{G}_{i,j'}), \tag{4.6}$$

as well as the minimum of all the $d(\mathcal{G}_{i,j}, \mathcal{G}_{i',j}), i \neq i'$ for subsets merging at the same

state j, defined as

$$d_{*,j} = \min_{0 \leqslant i \neq i' \leqslant 2^{\nu}-1} d(\mathcal{G}_{i,j}, \mathcal{G}_{i',j}). \tag{4.7}$$

It is desirable that

$$d_{i,*} + d_{*,j} \geqslant d(\mathcal{G}_{i,j}) \tag{4.8}$$

such that the length of the shortest error event is determined by the intra-Hamming distance $d(\mathcal{G}_{i,j})$. The inequality (4.8) is automatically satisfied for conventional ($k = 1$) TCM or TC-USTM. If $d_{i,*} = d_{*,j}$, then $d_{i,*} = d_{*,j} \geqslant \lceil \frac{d(\mathcal{G}_{i,j})}{2} \rceil$, where $\lceil \cdot \rceil$ denotes the smallest integer not less than $(\cdot)$. As $d(\mathcal{G}_{i,j}) \leqslant k$, we have

Criterion 1. $\ell_{\min} = k$.

In other words, we require that $d(\mathcal{G}_{i,j}) = k$ for each (i, j) under the constraint of (4.8). In the remainder of this section, we assume that Criterion 1 has been satisfied.

Let $\xi(\boldsymbol{c}_1, \boldsymbol{c}_2)$ denote the dissimilarity product between $\boldsymbol{c}_1$ and $\boldsymbol{c}_2$, defined as $\xi(\boldsymbol{c}_1, \boldsymbol{c}_2) = \prod_{r=1, \boldsymbol{c}_1^r \neq \boldsymbol{c}_2^r}^{k} d(\boldsymbol{c}_1^r, \boldsymbol{c}_2^r)$. For the trivial case of $\boldsymbol{c}_1 = \boldsymbol{c}_2$, $\xi(\boldsymbol{c}_1, \boldsymbol{c}_2) = 0$. Since Criterion 1 is assumed to have been satisfied, $d(\mathcal{G}_{i,j}) = k$. Then the *intra (subset)-dissimilarity product* in $\mathcal{G}_{i,j}$ is defined as

$$\xi(\mathcal{G}_{i,j}) = \min_{\boldsymbol{c}_1, \boldsymbol{c}_2 \in \mathcal{G}_{i,j}, \boldsymbol{c}_1 \neq \boldsymbol{c}_2} \xi(\boldsymbol{c}_1, \boldsymbol{c}_2). \tag{4.9}$$

From inequality (4.3), $\xi(\mathcal{G}_{i,j})$ is associated with the highest PEP between two k-tuples in $\mathcal{G}_{i,j}$ and accordingly determines the average PEP in $\mathcal{G}_{i,j}$. Therefore to minimize the average PEP of the shortest error events that cover *one* branch, $\xi(\mathcal{G}_{i,j})$ should be maximized. We have

Criterion 2. $\xi(\mathcal{G}_{i,j})$ should be maximized for every (i, j).

We next consider $\mathcal{G}_{i,j}$ and $\mathcal{G}_{i,j'}, j \neq j'$, which have the same emanating state but distinct merging states. Note that $d_{i,*} \leqslant d(\mathcal{G}_{i,j}, \mathcal{G}_{i,j'}) \leqslant k$. We define a set of k-tuple pairs $\boldsymbol{\vartheta}(\mathcal{G}_{i,j}, \mathcal{G}_{i,j'}) = \{(\boldsymbol{c}_1, \boldsymbol{c}_2) \mid \boldsymbol{c}_1 \in \mathcal{G}_{i,j}, \boldsymbol{c}_2 \in \mathcal{G}_{i,j'}, d(\boldsymbol{c}_1, \boldsymbol{c}_2) = d(\mathcal{G}_{i,j}, \mathcal{G}_{i,j'})\}$. From (3.9) we can see that the pairwise error-event is more likely to happen between $\boldsymbol{c}_1 \in \mathcal{G}_{i,j}, \boldsymbol{c}_2 \in \mathcal{G}_{i,j'}$ for $(\boldsymbol{c}_1, \boldsymbol{c}_2) \in \boldsymbol{\vartheta}(\mathcal{G}_{i,j}, \mathcal{G}_{i,j'})$ rather than between those excluded from $\boldsymbol{\vartheta}(\mathcal{G}_{i,j}, \mathcal{G}_{i,j'})$. Thus the *inter (subset)-dissimilarity product* between $\mathcal{G}_{i,j}$ and $\mathcal{G}_{i,j'}$ is defined as

$$\xi(\mathcal{G}_{i,j}, \mathcal{G}_{i,j'}) = \min_{(\boldsymbol{c}_1, \boldsymbol{c}_2) \in \boldsymbol{\vartheta}(\mathcal{G}_{i,j}, \mathcal{G}_{i,j'})} \xi(\boldsymbol{c}_1, \boldsymbol{c}_2). \tag{4.10}$$

Consider now the case in which $d(\mathcal{G}_{i,j}, \mathcal{G}_{i,j'}) = d_{i,*}$ holds for all $j \neq j' \in \mathbb{Z}_{2^\nu}$. Then the following quantity determines the average PEP for all the k-tuples emanating from state i

$$\xi_{i,*} = \min_{j,j' \in \mathbb{Z}_{2^\nu}, j \neq j'} \xi(\mathcal{G}_{i,j}, \mathcal{G}_{i,j'}). \tag{4.11}$$

For the cases where there exist $d(\mathcal{G}_{i,j}, \mathcal{G}_{i,j'}) > d_{i,*}$ for $j \neq j' \in \mathbb{Z}_{2^\nu}$, the searching space for j, j' in (4.11) should be constrained to the set $\mathcal{J}_{i,*} = \{(j, j') \mid d(\mathcal{G}_{i,j}, \mathcal{G}_{i,j'}) = d_{i,*}, j, j' \in \mathbb{Z}_{2^\nu}, j \neq j'\}$.

Similarly, the above definitions can be extended to $\mathcal{G}_{i,j}$ and $\mathcal{G}_{i',j}, i \neq i'$, which have the same merging state but distinct emanating states, resulting in $\boldsymbol{\vartheta}(\mathcal{G}_{i,j}, \mathcal{G}_{i',j})$, $\xi(\mathcal{G}_{i,j}, \mathcal{G}_{i',j})$, $\xi_{*,j}$ and $\mathcal{J}_{*,j}$. To maximize the dissimilarity product along the path of the shortest error events that cover *more than one* branch, $\xi_{i,*}$ and $\xi_{*,j}$ should also be maximized for every (i, j). Therefore we have:

Criterion 3. $\xi_{i,*}$ and $\xi_{*,j}$ should be maximized for every (i, j).

Criterion 1 forces $\ell_{\min}$ to be maximized when there are parallel paths between states. This criterion is not considered in [35, 36]. For instance, for MTCM with

$k = 3$ [35], the $\ell_{\min}$ can be 2 which is less than k. Therefore with the same information rate and number of states, the error performance of MTCM with $k = 3$ is comparable to that of MTCM with $k = \ell_{\min} = 2$. Thus the benefits of employing a greater k cannot be realized. We avoid this by forcing $\ell_{\min} = k$ in MTC-USTM. Criterion 2 and 3 further reduce the PEP associated with the error events of length $\ell_{\min}$ by forcing the dissimilarity product to be maximized. These three criteria deal with the worst case, i.e., the shortest error events with the least dissimilarity product, which most frequently happen at high SNR. By minimizing the probabilities of these error events, the overall error performance of MTC-USTM can be improved.

Compared with the afore proposed criteria, design criteria for TC-USTM with parallel paths are quite different. In TC-USTM with parallel paths between two consecutive states, $\ell_{\min} = 1$, and therefore error events covering more than one branch, whose length is at least 2, can be neglected at high SNR. Thus design criteria in this case are focused on maximizing the minimum dissimilarity in the subsets formed by signals assigned to the parallel paths between two consecutive states. This issue has been treated in Chapter 3 by applying Ungerboeck's "mapping by set partitioning" to the UST signal set $\mathbf{\Phi}_L$. That is, a set partitioning "tree" is formed for $\mathbf{\Phi}_L$, and it is required that in each layer of the tree, signal subsets have the identical minimum distance $\zeta_{\min}^{(j)}$; in addition, $\zeta_{\min}^{(j)}$ for subsets should increase as rapidly as possible as j increases. For TC-USTM with $\kappa = 2^q, 1 \leqslant q \leqslant b$ parallel paths between two consecutive states, the size-κ subsets in the same layer of the tree should be employed for mapping to the parallel paths between connected states.

We conclude this section by presenting an asymptotic BEP formula for MTC-USTM

$$P_b \approx \frac{1}{kb} \sum_{\ell=\ell_{\min}}^{\ell'} \sum_{j=1}^{J(\ell)} m_{\ell,j} p(\mathbf{\Phi}_{\ell,j}^K \to \hat{\mathbf{\Phi}}_{\ell,j}^K), \tag{4.12}$$

where $J(\ell)$ is the number of the possible error events having the same length ℓ and is often referred to as the *multiplicity* of the error events of length ℓ. In (4.12), $m_{\ell,j}$ is the number of bit-errors associated with the jth error event of length ℓ and $p(\mathbf{\Phi}_{\ell,j}^K \to \hat{\mathbf{\Phi}}_{\ell,j}^K)$ is the PEP associated with this error event, which can be explicitly evaluated by employing equation (4.2). The integer ℓ' is chosen such that most of the dominant error events are included. A BEP lower bound at high SNR can be obtained by only taking the shortest error event into account. By setting $\ell' = \ell_{\min}$ in (4.12), we have

$$P_b \gtrsim \frac{1}{kb} \sum_{j=1}^{J(\ell_{\min})} m_{\ell_{\min},j} p(\mathbf{\Phi}_{\ell_{\min},j}^K \to \hat{\mathbf{\Phi}}_{\ell_{\min},j}^K), \tag{4.13}$$

which gives an accurate estimate of the BEP in the regime of high SNR. The BEP P_b in (4.12) and its lower bound in (4.13) are linear combinations of the PEP's associated with the dominant error events. This indicates that the afore proposed criteria that are aimed at minimizing the PEP will also lead to a good BEP performance.

4.3 Design of MTC-USTM

First we consider $k = 2$. For the 2-fold Cartesian product $\mathbf{\Phi}_L \times \mathbf{\Phi}_L$, we note that $|\mathbf{\Phi}_L \times \mathbf{\Phi}_L| = L^2$, where $|\cdot|$ denotes the dimension of $(\cdot)$. Let $\mathbf{\Psi}_L^0 = \{\Phi_{m_0}, \cdots, \Phi_{m_{L-1}}\}$, where $(m_0, \cdots, m_{L-1})$ is a permutation of the integer sequence $(0, \cdots, L-1)$. Then $\mathbf{\Psi}_L^\lambda = \{\Phi_{m_0 \oplus \lambda}, \cdots, \Phi_{m_{L-1} \oplus \lambda}\}$, $\lambda \in \mathbb{Z}_L$ are the cyclic shifted versions of $\mathbf{\Psi}_L^0$, where $\oplus$

denotes addition modulo-L. We define *ordered Cartesian product* as

$$\mathbf{G}_\lambda = \mathbf{\Phi}_L \otimes \mathbf{\Psi}_L^\lambda = \left\{(\Phi_0, \Phi_{m_0 \oplus \lambda}), \cdots, (\Phi_{L-1}, \Phi_{m_{L-1} \oplus \lambda})\right\}. \tag{4.14}$$

As $|\mathbf{G}_\lambda| = L$, the operator $\mathbf{G}_\lambda$ for $\lambda \in \mathbb{Z}_L$ partitions $\mathbf{\Phi}_L \times \mathbf{\Phi}_L$ into L subsets. This partitioning scheme guarantees that $d(\mathbf{G}_\lambda) = k = 2$. Moreover,

$$d(\mathbf{G}_\lambda, \mathbf{G}_{\lambda'}) = 1 \quad \text{for} \quad \lambda \neq \lambda' \in \mathbb{Z}_L. \tag{4.15}$$

There are $L!$ permutations to form $\mathbf{\Psi}_L^0$. We adopt the method in [36] to form $\mathbf{\Psi}_L^0$ systematically by $\mathbf{\Psi}_L^0 = \{\Phi_{nl} \mid l \in \mathbb{Z}_L\}$, where $n \in \mathbb{Z}_L$ is an *odd* integer. In fact, any integer $n \in \mathbb{Z}_L$ relatively prime to L is a *generator* of the integer group $\mathbb{Z}_L$ under $\oplus$, i.e., for a generator n, $\mathbb{Z}_L = \{nl \mid l \in \mathbb{Z}_L\}$. And we note that the odd integers are all relatively prime to $L = 2^b$. In each $\mathbf{G}_\lambda$, the dissimilarity product between two 2-tuples $(\Phi_l, \Phi_{nl\oplus\lambda})$ and $(\Phi_{l'}, \Phi_{nl'\oplus\lambda}), l \neq l'$ is $\xi\left((\Phi_l, \Phi_{nl\oplus\lambda}), (\Phi_{l'}, \Phi_{nl'\oplus\lambda})\right) = \zeta_{\Delta_{l,l'}} \zeta_{\Delta_{nl,nl'}}$, which is not a function of λ (note that $\zeta_{\Delta_{l,l'}}$ is a simplified notation for $\zeta(\Phi_l, \Phi_{l'})$ due to Property 1 in Section 3.2). Therefore $\xi(\mathbf{G}_\lambda)$ are identical for all λ and can be denoted as ξ_m. To maximize ξ_m, the optimal n, denoted as n_{opt} is

$$n_{\text{opt}} = \arg \max_{n \in \{1,3,\cdots,L-1\}} \min_{0 \leqslant l \neq l' \leqslant L-1} \zeta_{\Delta_{l,l'}} \zeta_{\Delta_{n \cdot l, n \cdot l'}}. \tag{4.16}$$

If $\mathbf{G}_\lambda$, which is formed with n_{opt}, is mapped to $\mathcal{G}_{i,j}$, then $d(\mathcal{G}_{i,j}) = 2$ and $\xi(\mathcal{G}_{i,j})$ is maximized. As $|\mathcal{G}_{i,j}| = |\mathbf{G}_\lambda| = L = 2^{b+1}$ and the fact that there are 2^{2b} branches emanating from each state, the state number is $2^\nu = \frac{2^{2b}}{2^{b+1}} = 2^{b-1}$. For clarity, a $2^\nu \times 2^\nu$ mapping matrix $\mathcal{M}$ can be formed, with entries $\mathcal{M}_{i,j} = \lambda$, which is the subscript of $\mathbf{G}_\lambda$ that is mapped to $\mathcal{G}_{i,j}$. We shall collect two sets of λ's, $\mathbf{\Lambda} \subset \mathbb{Z}_L$ and $\mathbf{\Lambda}' \subset \mathbb{Z}_L$ which satisfy $|\mathbf{\Lambda}| = |\mathbf{\Lambda}'| = 2^\nu, \mathbf{\Lambda} \bigcap \mathbf{\Lambda}' = \emptyset$, and map $\mathbf{\Lambda}$ and $\mathbf{\Lambda}'$ to the first and second rows of $\mathcal{M}$, respectively. Criterion 1 requires that $d(\mathbf{G}_\lambda, \mathbf{G}_{\lambda'}) \geqslant \left\lceil \frac{k}{2} \right\rceil$ for $\lambda \neq \lambda' \in \mathbf{\Lambda}$

(or $\mathbf{\Lambda}'$), which is satisfied for $k = 2$ due to (4.15). We form the even rows of $\mathcal{M}$ by permutations of $\mathbf{\Lambda}$ and the odd rows by permutations of $\mathbf{\Lambda}'$. To allow for arbitrary permutations and in the meantime to ensure that $d_{*,j} \geqslant 1, j \in \mathbb{Z}_{2^\nu}$, we require that for $\lambda \neq \lambda' \in \mathbf{\Lambda} \bigcup \mathbf{\Lambda}'$, $d(\mathbf{G}_\lambda, \mathbf{G}_{\lambda'}) \geqslant \lceil \frac{k}{2} \rceil$. This is also satisfied for the case of $k = 2$ due to (4.15).

Next we attempt to determine $\mathbf{\Lambda}$ and $\mathbf{\Lambda}'$ based on Criterion 3. Consider $(\Phi_l, \Phi_{n_{\text{opt}} l \oplus \lambda})$ $\in \mathbf{G}_\lambda$ and $(\Phi_{l'}, \Phi_{n_{\text{opt}} l' \oplus \lambda'}) \in \mathbf{G}_{\lambda'}$ for $l, l', \lambda, \lambda' \in \mathbb{Z}_L$. Due to (4.15), $\boldsymbol{\vartheta}(\mathbf{G}_\lambda, \mathbf{G}_{\lambda'}) = \boldsymbol{\vartheta}_1 \bigcup \boldsymbol{\vartheta}_2$, where $\boldsymbol{\vartheta}_r = \{(\boldsymbol{c}_1, \boldsymbol{c}_2) \mid \boldsymbol{c}_1 \in \mathbf{G}_\lambda, \boldsymbol{c}_2 \in \mathbf{G}_{\lambda'}, \boldsymbol{c}_1^r = \boldsymbol{c}_2^r\}$ for $r = 1, 2$. Obviously, $\boldsymbol{\vartheta}_1 = \{((\Phi_l, \Phi_{n_{\text{opt}} \cdot l \oplus \lambda}), (\Phi_l, \Phi_{n_{\text{opt}} \cdot l \oplus \lambda'})) \mid l \in \mathbb{Z}_L\}$, resulting in $\xi(\boldsymbol{c}_1, \boldsymbol{c}_2) = \zeta_{\Delta_{\lambda,\lambda'}}$ for $(\boldsymbol{c}_1, \boldsymbol{c}_2) \in \boldsymbol{\vartheta}_1$. To form $\boldsymbol{\vartheta}_2$, let $n_{\text{opt}} l \oplus \lambda = n_{\text{opt}} l' \oplus \lambda'$, which results in $n_{\text{opt}}(l - l') = \lambda' - \lambda$. As n_{opt} is a generator of $\mathbb{Z}_L$, there always exists an integer $a \in \mathbb{Z}_L$ such that $n_{\text{opt}} a = 1$. Accordingly, we have $n_{\text{opt}}(l - l') = n_{\text{opt}} a(\lambda' - \lambda)$ and subsequently $l - l' = a(\lambda' - \lambda)$. Therefore $\boldsymbol{\vartheta}_2 = \{((\Phi_l, \Phi_{n_{\text{opt}} \cdot l \oplus \lambda}), (\Phi_{l - a(\lambda' - \lambda)}, \Phi_{n_{\text{opt}} \cdot l \oplus \lambda})) \mid l \in \mathbb{Z}_L\}$, which results in $\xi(\boldsymbol{c}_1, \boldsymbol{c}_2) = \zeta_{\Delta_{a\lambda', a\lambda}}$. According to (4.10)

$$\xi(\mathbf{G}_\lambda, \mathbf{G}_{\lambda'}) = \min \left\{ \zeta_{\Delta_{\lambda,\lambda'}}, \zeta_{\Delta_{a\lambda, a\lambda'}} \right\}. \tag{4.17}$$

The searching space for $\mathbf{\Lambda}$ is $\mathbb{Z}_L$ due to (4.15). According to (4.11), the optimal $\mathbf{\Lambda}$, denoted as $\mathbf{\Lambda}_{\text{opt}}$ can be searched by

$$\mathbf{\Lambda}_{\text{opt}} = \arg \max_{\mathbf{\Lambda} \subset \mathbb{Z}_L} \min_{\lambda, \lambda' \in \mathbf{\Lambda}, \lambda \neq \lambda'} \xi(\mathbf{G}_\lambda, \mathbf{G}_{\lambda'}). \tag{4.18}$$

Similarly, the optimal $\mathbf{\Lambda}'$, denoted as $\mathbf{\Lambda}'_{\text{opt}}$ is

$$\mathbf{\Lambda}'_{\text{opt}} = \arg \max_{\mathbf{\Lambda}' \subset \overline{\mathbf{\Lambda}_{\text{opt}}}} \min_{\lambda, \lambda' \in \mathbf{\Lambda}', \lambda \neq \lambda'} \xi(\mathbf{G}_\lambda, \mathbf{G}_{\lambda'}). \tag{4.19}$$

where $\overline{(\cdot)}$ denotes the complement of $(\cdot)$ in $\mathbb{Z}_L$. The permutations of $\mathbf{\Lambda}_{\text{opt}}$ and $\mathbf{\Lambda}'_{\text{opt}}$ should be made such that $\xi_{*,j}$ for $j \in \mathbb{Z}_L$ is maximized. We investigate the following examples for elaboration.

Example 1. Consider a MTC-USTM of $T = 2, M = 1, k = 2$ and $R = 1$ where $\mathbf{\Phi}_8$ $(T = 2, M = 1, R = 1.5)$ is employed. By (4.16), $n_{\text{opt}} = 3$ and accordingly $\xi_m = 0.3536$. The 8 subsets of $\mathbf{\Phi}_8 \times \mathbf{\Phi}_8$ are obtained from (4.14) as

$$\begin{aligned} \mathbf{G}_0 = \mathbf{\Phi}_8 \otimes \mathbf{\Psi}_8^0 &= \{(\Phi_0, \Phi_0), \cdots, (\Phi_7, \Phi_5)\}, \\ &\vdots \\ \mathbf{G}_7 = \mathbf{\Phi}_8 \otimes \mathbf{\Psi}_8^7 &= \{(\Phi_0, \Phi_7), \cdots, (\Phi_7, \Phi_4)\}. \end{aligned}$$

As $|\mathbf{G}_\lambda| = 8$ and $2^{kb} = 16$, $2^\nu = \frac{16}{8} = 2$. As $n_{\text{opt}} a = 1$, $a = 3$. According to (4.18) and by referring to Fig. 3.1(a), one can obtain four sets $\mathbf{\Lambda} = \{0, 4\}$, $\mathbf{\Lambda} \oplus 1$, $\mathbf{\Lambda} \oplus 2$ and $\mathbf{\Lambda} \oplus 3$, where $\oplus$ between an integer and a set denotes the addition between the integer with every element in the set. In fact, for $\lambda \neq \lambda' \in \mathbf{\Lambda} \oplus p,\ p \in \mathbb{Z}_4,\ \Delta_{\lambda,\lambda'} = \Delta_{a\lambda',a\lambda} = 4$ and accordingly $\xi(\mathbf{G}_\lambda, \mathbf{G}_{\lambda'}) = \min\{\zeta_4, \zeta_4\} = 1$ is maximized. Without loss of generality, let $\mathbf{\Lambda}_{\text{opt}} = \mathbf{\Lambda}$. From the remaining 3 sets, one should choose the one which maximizes $\xi_{*,0}$ and $\xi_{*,1}$ at the same time. It is not difficult to find that $\mathbf{\Lambda}'_{\text{opt}} = \mathbf{\Lambda} \oplus 2$ is the right choice, as $\xi(\mathbf{G}_0, \mathbf{G}_2) = \xi(\mathbf{G}_4, \mathbf{G}_6) = \min\{\zeta_2, \zeta_6\} = 0.7071$, which leads to $\xi_{*,0} = \xi_{*,1} = 0.7071$, while the other two sets give rise to $\xi_{*,0} = \xi_{*,1} = 0.3827$. Therefore

$$\mathcal{M} = \begin{pmatrix} 0 & 4 \\ 2 & 6 \end{pmatrix}$$

and the trellis diagram is illustrated in Fig. 4.1(a). ■

Example 2. Consider a MTC-USTM of $T = 4, M = 2, k = 2$ and $R = 1$ where $\mathbf{\Phi}_{32}$ $(T = 4, M = 2, R = 1.25)$ is employed. One can determine $n_{\text{opt}} = 15$ and

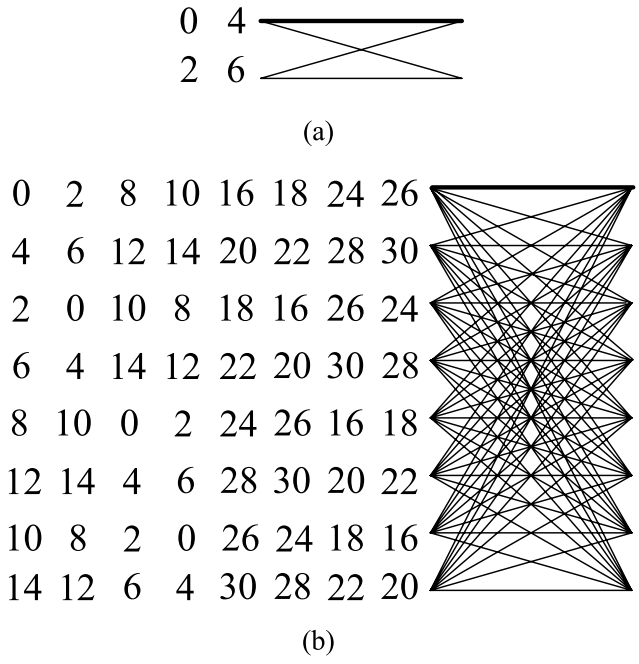

Figure 4.1: Trellis diagrams for MTC-USTM of $R = 1$. (a) $\ell_{\min} = k = 2$, 2 states, $\mathbf{\Phi}_8$ $(T = 2, M = 1, R = 1.5)$ is used; (b) $\ell_{\min} = k = 2$, 8 states, $\mathbf{\Phi}_{32}$ $(T = 4, M = 2, R = 1.25)$ is used.

$\xi_m = 0.1464$. Accordingly, $a = 15$. $\mathbf{\Phi}_{32} \times \mathbf{\Phi}_{32}$ can be partitioned into 32 subsets as

$$\begin{aligned} \mathbf{G}_0 = \mathbf{\Phi}_{32} \otimes \mathbf{\Psi}_{32}^0 &= \{(\Phi_0, \Phi_0), \cdots, (\Phi_{31}, \Phi_{17})\}, \\ &\vdots \\ \mathbf{G}_{31} = \mathbf{\Phi}_{32} \otimes \mathbf{\Psi}_{32}^{31} &= \{(\Phi_0, \Phi_{31}), \cdots, (\Phi_{31}, \Phi_{16})\}. \end{aligned}$$

As $|\mathbf{G}_\lambda| = 32, 2^{kb} = 2^8$, the state number is $2^\nu = \frac{2^8}{32} = 8$. From Fig. 3.1(b) and (4.18) one can determine 4 subset-index sets $\mathbf{\Lambda} = \{0, 2, 8, 10, 16, 18, 24, 26\}$, $\mathbf{\Lambda} \oplus 1$, $\mathbf{\Lambda} \oplus 4$ and $\mathbf{\Lambda} \oplus 5$, which lead to that $\xi_{i,*}, i = 0, 2, 4, 6$ are maximized to be 0.4374. Without loss of generality, let $\mathbf{\Lambda}_{\text{opt}} = \mathbf{\Lambda}$ and subsequently let $\mathbf{\Lambda}'_{\text{opt}} = \mathbf{\Lambda} \oplus 4$. Then $\mathcal{M}$ can be formed and the corresponding trellis diagram is illustrated in Fig. 4.1(b). Note that

the resulting $\xi_{i,*} = 0.4374, \xi_{*,j} = 0.3827, i, j \in \mathbb{Z}_8$ are all maximized. ■

Example 3. We reconsider Example 1 for the case of $R = 2$. For uncoded USTM, $\mathbf{\Phi}_{16}$ $(T = 2, M = 1, R = 2)$ is employed, while for TC-USTM and MTC-USTM, a double-sized signal set $\mathbf{\Phi}_{32}$ $(T = 2, M = 1, R = 2.5)$ is employed. Through (4.16), $n_{\text{opt}} = 7$ and $\xi_m = 0.0622$. Accordingly, $a = 23$. The 32 subsets in $\mathbf{\Phi}_{32} \times \mathbf{\Phi}_{32}$ are

$$\begin{aligned} \mathbf{G}_0 = \mathbf{\Phi}_{32} \otimes \mathbf{\Psi}_{32}^0 &= \{(\Phi_0, \Phi_0), \cdots, (\Phi_{31}, \Phi_{25})\}, \\ &\vdots \\ \mathbf{G}_{31} = \mathbf{\Phi}_{32} \otimes \mathbf{\Psi}_{32}^{31} &= \{(\Phi_0, \Phi_{31}), \cdots, (\Phi_{31}, \Phi_{24})\}. \end{aligned}$$

As $|\mathbf{G}_\lambda| = 32$ and $2^{kb} = 2^8$, the state number is $\frac{2^8}{32} = 8$. Through (4.18), one can obtain $\mathbf{\Lambda} = \{0, 4, 8, 12, 16, 20, 24, 28\}$, $\mathbf{\Lambda} \oplus 1$, $\mathbf{\Lambda} \oplus 2$ and $\mathbf{\Lambda} \oplus 3$, which lead to $\xi_{0,*} = 0.3827$. We let $\mathbf{\Lambda}_{\text{opt}} = \mathbf{\Lambda}$ and $\mathbf{\Lambda}'_{\text{opt}} = \mathbf{\Lambda} \oplus 2$ and form $\mathcal{M}$ as

$$\mathcal{M} = \begin{pmatrix} 0 & 4 & 8 & 12 & 16 & 20 & 24 & 28 \\ 6 & 10 & 14 & 18 & 22 & 26 & 30 & 2 \\ 4 & 0 & 12 & 8 & 20 & 16 & 28 & 24 \\ 10 & 6 & 18 & 14 & 26 & 22 & 2 & 30 \\ 8 & 12 & 0 & 4 & 24 & 28 & 16 & 20 \\ 14 & 18 & 6 & 10 & 30 & 2 & 22 & 26 \\ 12 & 8 & 4 & 0 & 28 & 24 & 20 & 16 \\ 18 & 14 & 10 & 6 & 2 & 30 & 26 & 22 \end{pmatrix}.$$

In this way, $\xi_{i,*} = 0.3827$ and $\xi_{*,j} = 0.1951, i, j \in \mathbb{Z}_8$ are all maximized. ■

To form subsets of dimension $\frac{L}{2}$ in $\mathbf{\Phi}_L \times \mathbf{\Phi}_L$, one can let $\mathbf{\Phi}_{L/2}^0 = \{\Phi_{2l} \mid l \in \mathbb{Z}_{L/2}\}$, $\mathbf{\Phi}_{L/2}^1 = \{\Phi_{2l+1} \mid l \in \mathbb{Z}_{L/2}\}$ and correspondingly, $\mathbf{\Psi}_{L/2}^{0,\lambda} = \{\Phi_{2ln \oplus \lambda} \mid l \in \mathbb{Z}_{L/2}\}$ and $\mathbf{\Psi}_{L/2}^{1,\lambda} = \{\Phi_{(2l+1)n \oplus \lambda} \mid l \in \mathbb{Z}_{L/2}\}$, where $n \in \mathbb{Z}_{L/2}$ is an odd integer, $\lambda \in \mathbb{Z}_L$. The ordered Cartesian products $\mathbf{G}_{\lambda^0} = \mathbf{\Phi}_{L/2}^0 \otimes \mathbf{\Psi}_{L/2}^{0,\lambda}$ and $\mathbf{G}_{\lambda^1} = \mathbf{\Phi}_{L/2}^1 \otimes \mathbf{\Psi}_{L/2}^{1,\lambda}$ will form two subsets

of dimension $\frac{L}{2}$, where $\lambda^q, q = 0, 1$ denotes the subset-index. For $\boldsymbol{c}_1 \neq \boldsymbol{c}_2 \in \mathbf{G}_{\lambda^0}$, $\xi(\boldsymbol{c}_1, \boldsymbol{c}_2) = \zeta_{\Delta_{2l,2l'}} \zeta_{\Delta_{2ln,2l'n}}$; for $\boldsymbol{c}_1 \neq \boldsymbol{c}_2 \in \mathbf{G}_{\lambda^1}$, $\xi(\boldsymbol{c}_1, \boldsymbol{c}_2) = \zeta_{\Delta_{2l\oplus 1,2l'\oplus 1}} \zeta_{\Delta_{(2l\oplus 1)n,(2l'\oplus 1)n}} = \zeta_{\Delta_{2l,2l'}} \zeta_{\Delta_{2ln,2l'n}}$. This implies that the dissimilarity profile in $\mathbf{G}_{\lambda^0}$ is identical to that in $\mathbf{G}_{\lambda^1}$. Therefore it is sufficient to find the optimal n, denoted as n'_{opt} by considering $\mathbf{G}_{\lambda^0}$ to satisfy Criterion 2. This can be searched by using (4.16) (replacing L with $L/2$). If $n'_{\text{opt}} = n_{\text{opt}}$, one can observe that $\mathbf{G}_\lambda = \mathbf{G}_{\lambda^0} \bigcup \mathbf{G}_{\lambda^1}$, i.e., the size-$\frac{L}{2}$ subsets can be obtained by partitioning the size-L subset. In a similar way, one can find size-$\frac{L}{4}$ subsets in $\boldsymbol{\Phi}_L \times \boldsymbol{\Phi}_L$ and so on.

Example 4. We reconsider Example 1 by employing size-4 subsets. Let $\boldsymbol{\Phi}_4^0 = \{\Phi_0, \Phi_2, \Phi_4, \Phi_6\}$, $\boldsymbol{\Phi}_4^1 = \{\Phi_1, \Phi_3, \Phi_5, \Phi_7\}$. As $n'_{\text{opt}} = 3$ by (4.16), we have $\boldsymbol{\Psi}_4^{0,\lambda} = \{\Phi_{2l\cdot 3\oplus\lambda} \mid l \in \mathbb{Z}_4\}$ and $\boldsymbol{\Psi}_4^{1,\lambda} = \{\Phi_{(2l+1)3\oplus\lambda} \mid l \in \mathbb{Z}_4\}$. The resulting subsets are

$$\begin{aligned}
\mathbf{G}_{0^0} &= \{(\Phi_0, \Phi_0), \cdots, (\Phi_6, \Phi_2)\} \\
\mathbf{G}_{0^1} &= \{(\Phi_1, \Phi_3), \cdots, (\Phi_7, \Phi_5)\} \\
&\vdots \\
\mathbf{G}_{7^0} &= \{(\Phi_0, \Phi_7), \cdots, (\Phi_6, \Phi_1)\} \\
\mathbf{G}_{7^1} &= \{(\Phi_1, \Phi_2), \cdots, (\Phi_7, \Phi_4)\}.
\end{aligned}$$

As $|\mathbf{G}_{\lambda^q}| = 4$ and $2^{kb} = 16$, a 4-state trellis is needed. One can observe that $d(\mathbf{G}_{\lambda^q}, \mathbf{G}_{(\lambda\oplus 2p)^{q'}}) = 2$ for $q \neq q' \in \{0, 1\}$ and $p \in \mathbb{Z}_4$. When $p = 0$, $\xi(\mathbf{G}_{\lambda^q}, \mathbf{G}_{\lambda^{q'}}) = 0.3536$ while when $p \neq 0$, $\xi(\mathbf{G}_{\lambda^q}, \mathbf{G}_{(\lambda\oplus 2p)^{q'}}) = 0.1465$. Therefore $\boldsymbol{\Lambda}_{\text{opt}} = \{\lambda^0, \lambda^1, (\lambda \oplus 2p)^0, (\lambda \oplus 2p)^1\}$, with $1 \leqslant p \leqslant 3$ yet to be determined. We note that $d(\mathbf{G}_{\lambda^q}, \mathbf{G}_{(\lambda\oplus 2p)^q}) = 1$ for $1 \leqslant p \leqslant 3$, and when $p = 2$, $\xi(\mathbf{G}_{\lambda^q}, \mathbf{G}_{(\lambda\oplus 4)^q}) = \min\{\zeta_4, \zeta_4\} = 1$, so we have $p = 2$. Without loss of generality, letting $\lambda = 0$, we have $\boldsymbol{\Lambda}_{\text{opt}} = \{0^0, 0^1, 4^0, 4^1\}$. From $\boldsymbol{\Lambda}_{\text{opt}} \oplus 1, \boldsymbol{\Lambda}_{\text{opt}} \oplus 2$ and $\boldsymbol{\Lambda}_{\text{opt}} \oplus 3$, we let $\boldsymbol{\Lambda}'_{\text{opt}} = \boldsymbol{\Lambda}_{\text{opt}} \oplus 2 = \{2^0, 2^1, 6^0, 6^1\}$, because

$\xi(\mathbf{G}_{0^0}, \mathbf{G}_{2^0}) = \min\{\zeta_2, \zeta_6\} = 0.7071$, while $\mathbf{\Lambda}_{\text{opt}} \oplus 1$ and $\mathbf{\Lambda}_{\text{opt}} \oplus 3$ give rise to a smaller value 0.3827. Therefore

$$\mathcal{M} = \begin{pmatrix} 0^0 & 0^1 & 4^0 & 4^1 \\ 2^0 & 2^1 & 6^0 & 6^1 \\ 4^1 & 4^0 & 0^1 & 0^0 \\ 6^1 & 6^0 & 2^1 & 2^0 \end{pmatrix}.$$

As a result, $\xi_{i,*} = 1$ and $\xi_{*,j} = 0.7071$ are all maximized for $i, j \in \mathbb{Z}_4$. ■

For the general case of $k \geqslant 2$, we define the set $\boldsymbol{n} = \{n_q \mid q = 1, \cdots, k-1\}, n_q \in \{1, 3, \cdots, L-1\}$. Let $\mathbf{\Psi}^0_{L,q}, 1 \leqslant q \leqslant k-1$ denote the $k-1$ permutations of $\mathbf{\Phi}_L$. Then there are L^{k-1} subsets as $\mathbf{G}_\lambda = \mathbf{\Phi}_L \otimes \mathbf{\Psi}^{\lambda_1}_{L,1} \otimes \cdots \otimes \mathbf{\Psi}^{\lambda_{k-1}}_{L,k-1}, \lambda_q \in \mathbb{Z}_L$ and $|\mathbf{G}_\lambda| = L$. The subset-index is defined as $\lambda = \sum_{q=1}^{k-1} \lambda_q L^{k-1-q}$. To satisfy Criterion 2, similar to (4.16), the optimal $\boldsymbol{n}$, denoted as $\boldsymbol{n}_{\text{opt}}$ can be determined by:

$$\boldsymbol{n}_{\text{opt}} = \arg \max_{\boldsymbol{n}} \min_{0 \leqslant l \neq l' \leqslant L-1} \zeta_{\Delta_{l,l'}} \prod_{q=1}^{k-1} \zeta_{\Delta_{n_q l, n_q l'}}. \tag{4.20}$$

We observed that if $\mathbf{\Phi}_L$ of dimension $L = 2^{b+1}$ is employed following [32], [35], [38] or [52], in most cases, there are not enough λ's to form $\mathbf{\Lambda}$ and $\mathbf{\Lambda}'$ such that for $\lambda \neq \lambda' \in \mathbf{\Lambda} \bigcup \mathbf{\Lambda}', d(\mathbf{G}_\lambda, \mathbf{G}'_\lambda) \geqslant \lceil \frac{k}{2} \rceil$. To overcome this problem, we employ $\mathbf{\Phi}_L$ with $L = 2^{b+p'}, p' \geqslant 2$. To maintain the same bandwidth, $\mathbf{\Phi}_L$ should be formed by keeping T unchanged while R is increased to $R + \frac{p'}{T}$. The following benefits justify using a larger $\mathbf{\Phi}_L$:

1) $|\mathbf{G}_\lambda| = 2^{b+p'}$, which is $2^{p'-1}$ times greater than 2^{b+1} (the conventional case), thus the state number $2^\nu = \frac{2^{kb}}{2^{b+p'}}$, as well as $|\mathbf{\Lambda}_{\text{opt}} \bigcup \mathbf{\Lambda}'_{\text{opt}}|$, is only a fraction $(\frac{1}{2^{p'-1}})$ of those for the conventional case.

2) The searching space for $\mathbf{\Lambda}_{\text{opt}}$ and $\mathbf{\Lambda}'_{\text{opt}}$ is increased, as now we have in total $L^{k-1} = (2^{b+p'})^{k-1}$ subsets, which is $\frac{2^{(b+p')(k-1)}}{2^{(b+1)(k-1)}} = 2^{(p'-1)(k-1)}$ times greater than that of the conventional case.

Therefore with a larger $\mathbf{\Phi}_L$, Criterion 1 can be more easily satisfied. However, $\mathbf{\Phi}_L$ of a greater dimension with fixed T results in a reduced minimum dissimilarity in $\mathbf{\Phi}_L$, which in turn gives rise to a reduced ξ_m, as well as $\xi_{i,*}$ and $\xi_{*,j}$. Nonetheless, as the slope of the error rate curve is determined by $\ell_{\min}$, it is worthwhile to sacrifice some dissimilarity product in return for an increased $\ell_{\min}$. For elaboration, we consider the following example of $k = 3$.

Example 5. Consider a MTC-USTM ($k = 3, T = 2, M = 1, R = 1$) where by convention $\mathbf{\Phi}_8$ ($T = 2, M = 1, R = 1.5$) is employed. According to (4.20), $\boldsymbol{n}_o = \{1, 3\}$ and correspondingly $\xi_m = 0.1353$. Therefore $\mathbf{\Phi}_8 \times \mathbf{\Phi}_8 \times \mathbf{\Phi}_8$ can be partitioned into 64 3-tuples subsets

$$\begin{aligned} \mathbf{G}_0 = \mathbf{\Phi}_8 \otimes \mathbf{\Psi}^0_{8,1} \otimes \mathbf{\Psi}^0_{8,2} &= \{(\Phi_0, \Phi_0, \Phi_0), \cdots, (\Phi_7, \Phi_7, \Phi_5)\}, \\ &\vdots \\ \mathbf{G}_{63} = \mathbf{\Phi}_8 \otimes \mathbf{\Psi}^7_{8,1} \otimes \mathbf{\Psi}^7_{8,2} &= \{(\Phi_0, \Phi_7, \Phi_7), \cdots, (\Phi_7, \Phi_6, \Phi_4)\}. \end{aligned} \tag{4.21}$$

As $|\mathbf{G}_\lambda| = 8$ and $2^{kb} = 64$, the state number is $2^\nu = \frac{64}{8} = 8$. To satisfy Criterion 1, i.e., to ensure $d_{i,*} = d_{*,j} = \lceil \frac{3}{2} \rceil = 2$ for $0 \leqslant i, j \leqslant 7$, we require that there are at least 16 $\mathbf{G}_\lambda$'s whose inter-Hamming distance is 2. However through an exhaustive search, one can only find at most 7 $\mathbf{G}_\lambda$'s to satisfy this requirement. For example, the subset-index set is $\{2, 8, 17, 29, 35, 47, 62\}$, $\{3, 8, 18, 25, 37, 46, 52\}$, *etc.*. Therefore with $\mathbf{\Phi}_8$, it is impossible to form a MTC-USTM of $\ell_{\min} = k = 3$.

We investigate the case in which $\mathbf{\Phi}_{16}$ ($T = 2, M = 1, R = 2$) is employed instead.

Then $|\mathbf{G}_\lambda| = 16$ and accordingly the state number is $2^\nu = \frac{64}{16} = 4$, which is a half of the former. Moreover, the searching space for λ is $\mathbb{Z}_{256}$, whose dimension is 4 times greater than that of $\mathbb{Z}_{64}$. Therefore Criterion 1 can be more easily satisfied. By (4.20), we have $\mathbf{n}_{\text{opt}} = \{3, 5\}$ and $\xi_m = 0.0901$. Accordingly $\mathbf{\Phi}_{16} \times \mathbf{\Phi}_{16} \times \mathbf{\Phi}_{16}$ is partitioned into 256 subsets

$$\begin{aligned} \mathbf{G}_0 = \mathbf{\Phi}_{16} \otimes \mathbf{\Psi}^0_{16,1} \otimes \mathbf{\Psi}^0_{16,2} &= \{(\Phi_0, \Phi_0, \Phi_0), \cdots, (\Phi_{15}, \Phi_{13}, \Phi_{11})\}, \\ &\vdots \\ \mathbf{G}_{255} = \mathbf{\Phi}_{16} \otimes \mathbf{\Psi}^{15}_{16,1} \otimes \mathbf{\Psi}^{15}_{16,2} &= \{(\Phi_0, \Phi_{15}, \Phi_{15}), \cdots, (\Phi_{15}, \Phi_{12}, \Phi_{10})\}. \quad (4.22) \end{aligned}$$

Through an exhaustive search, one can obtain a 13-element subset-index set {0, 34, 51, 68, 85, 102, 119, 137, 152, 171, 186, 207, 222}, denoted as $\mathbf{U}$. Accordingly, $\mathbf{\Lambda}_{\text{opt}}$ and $\mathbf{\Lambda}'_{\text{opt}}$ are available.

From the definition of the subset index, λ and λ' can be expressed as $\lambda_1 L + \lambda_2$ and $\lambda'_1 L + \lambda'_2$, respectively, for certain $\lambda_1, \lambda'_1, \lambda_2, \lambda'_2 \in \mathbb{Z}_L$. Consider $(\Phi_l, \Phi_{n_1 l \oplus \lambda_1}, \Phi_{n_2 l \oplus \lambda_2}) \in \mathbf{G}_\lambda$ and $(\Phi_{l'}, \Phi_{n_1 l' \oplus \lambda'_1}, \Phi_{n_2 l' \oplus \lambda'_2}) \in \mathbf{G}_{\lambda'}$, where $l, l' \in \mathbb{Z}_L$. To evaluate $\xi(\mathbf{G}_\lambda, \mathbf{G}_{\lambda'})$, we note that $\boldsymbol{\vartheta}(\mathbf{G}_\lambda, \mathbf{G}_{\lambda'}) = \boldsymbol{\vartheta}_1 \bigcup \boldsymbol{\vartheta}_2 \bigcup \boldsymbol{\vartheta}_3$, where $\boldsymbol{\vartheta}_r, r = 1, 2, 3$ denotes the set of the tuple pair $(\boldsymbol{c}_1, \boldsymbol{c}_2) \in \boldsymbol{\vartheta}_r$, where $\boldsymbol{c}^r_1 = \boldsymbol{c}^r_2$. We define $\boldsymbol{a} = \{a_1, a_2\}$ where $a_q n_q = 1$ for $n_q \in \boldsymbol{n}_{\text{opt}}, q = 1, 2$. In this example, $\boldsymbol{a} = \{11, 13\}$. Similar to the case of $k = 2$, one can obtain that $\xi(\boldsymbol{c}_1, \boldsymbol{c}_2) = \zeta_{\Delta_{\lambda_1, \lambda'_1}} \zeta_{\Delta_{\lambda_2, \lambda'_2}}$ for $(\boldsymbol{c}_1, \boldsymbol{c}_2) \in \boldsymbol{\vartheta}_1$, $\xi(\boldsymbol{c}_1, \boldsymbol{c}_2) = \zeta_{\Delta_{a_1\lambda_1, a_1\lambda'_1}} \zeta_{\Delta_{n_2 a_1 \lambda_1 \oplus \lambda'_2, n_2 a_1 \lambda'_1 \oplus \lambda_2}}$ for $(\boldsymbol{c}_1, \boldsymbol{c}_2) \in \boldsymbol{\vartheta}_2$ and $\xi(\boldsymbol{c}_1, \boldsymbol{c}_2) = \zeta_{\Delta_{a_2\lambda_2, a_2\lambda'_2}} \zeta_{\Delta_{n_1 a_2 \lambda_2 \oplus \lambda'_1, n_1 a_2 \lambda'_2 \oplus \lambda_1}}$ for $(\boldsymbol{c}_1, \boldsymbol{c}_2) \in \boldsymbol{\vartheta}_3$, which are denoted as ξ_1, ξ_2 and ξ_3, respectively. Then similar to (4.17), the inter-dissimilarity product is

$$\xi(\mathbf{G}_\lambda, \mathbf{G}_{\lambda'}) = \min\{\xi_1, \xi_2, \xi_3\}. \quad (4.23)$$

Then $\mathbf{\Lambda}_{\text{opt}}$ and $\mathbf{\Lambda}'_{\text{opt}}$ can be searched by (4.18) and (4.19), respectively, however, the

searching space $\mathbb{Z}_L$ is replaced by $\mathbf{U}$. Accordingly, we obtain $\mathbf{\Lambda}_{\text{opt}} = \{0, 34, 68, 102\}$ and $\mathbf{\Lambda}'_{\text{opt}} = \{51, 85, 119, 152\}$, which lead to $\xi_{0,*} = \xi_{2,*} = 0.1464$ and $\xi_{1,*} = \xi_{3,*} = 0.0747$, respectively. $\mathcal{M}$ is formed as

$$\mathcal{M} = \begin{pmatrix} 0 & 34 & 68 & 102 \\ 51 & 85 & 119 & 152 \\ 102 & 68 & 34 & 0 \\ 152 & 119 & 85 & 51 \end{pmatrix}.$$

As a result, $\xi_{*,0} = \xi_{*,2} = 0.0747$ and $\xi_{*,1} = \xi_{*,3} = 0.0381$ are all maximized. ■

As a summary of this section, we list the $\boldsymbol{n}_{\text{opt}}$ and ξ_m for MTC-USTM with different k, T, M, but the same information rate $R = 1$ in Table 4.1.

4.4 Numerical Results

In this section, we compare the BEP performance between the uncoded USTM, TC-USTM and MTC-USTM of the same information rate R. In this comparison, the TC-USTM and MTC-USTM also have the same number of trellis states. We also assume $N = 1$ in all cases.

The BEP performance for MTC-USTM in Example 1 is illustrated in Fig. 4.2. The MTC-USTM starts to outperform the uncoded USTM from 12 dB and the TC-USTM from 19 dB onwards. The error rate curve for MTC-USTM drops off faster than that of the others with increasing SNR. This is because $\ell_{\min} = 2$ for the MTC-USTM while $\ell_{\min} = 1$ for the TC-USTM. The dotted line denotes the BEP lower bound (4.13) in the region of high SNR. As (4.13) is derived under the condition of

Table 4.1: $\boldsymbol{n}_{\text{opt}}$ and ξ_m for MTC-USTM with $R = 1$. ($R' = R + \frac{1}{T}$ for construction of $\boldsymbol{\Phi}_L$)

T	M	k	$[u_1 \cdots u_T]$	R'	L	$\boldsymbol{n}_{\text{opt}}$	ξ_m
2	1	2	[1 2]	1.5	8	[3]	0.3536
2	1	3	[1 2]	1.5	8	[1 3]	0.1353
3	1	2	[1 2 5]	1.333	16	[3]	0.4444
3	1	3	[1 2 5]	1.333	16	[1 3]	0.2963
4	1	2	[1 2 5 14]	1.25	32	[1]	0.5000
4	1	3	[1 2 5 14]	1.25	32	[1 1]	0.3536
4	2	2	[1 1 2 8]	1.25	32	[15]	0.1464
4	2	3	[1 1 2 8]	1.25	32	[3 13]	0.0809
5	1	2	[1 2 4 8 23]	1.2	64	[5]	0.6397
5	1	3	[1 2 4 8 23]	1.2	64	[5 13]	0.5966
5	2	2	[1 8 5 24 19]	1.2	64	[7]	0.3513
5	2	3	[1 8 5 24 19]	1.2	64	[7 11]	0.2513

high SNR, in the region of low and moderate SNR, it is not a strict lower bound. At sufficiently high SNR, this lower bound agrees well with the value obtained from the simulations and therefore can be regarded as an accurate estimate of the BEP. To evaluate (4.13) in an approximate manner, we assume $\boldsymbol{\Phi}^K = \{\Phi_{l_t} = \Phi_0, 1 \leqslant t \leqslant K\}$ is transmitted. Thus the 2-tuples in $\mathcal{G}_{0,0}$ except (Φ_0, Φ_0) form 7 shortest error events that cover *one* branch; additionally, $\{(\Phi_0, \Phi_4), (\Phi_0, \Phi_2)\}$, $\{(\Phi_0, \Phi_4), (\Phi_2, \Phi_0)\}$, $\{(\Phi_4, \Phi_0), (\Phi_0, \Phi_2)\}$ and $\{(\Phi_4, \Phi_0), (\Phi_2, \Phi_0)\}$ form the 4 shortest error events that

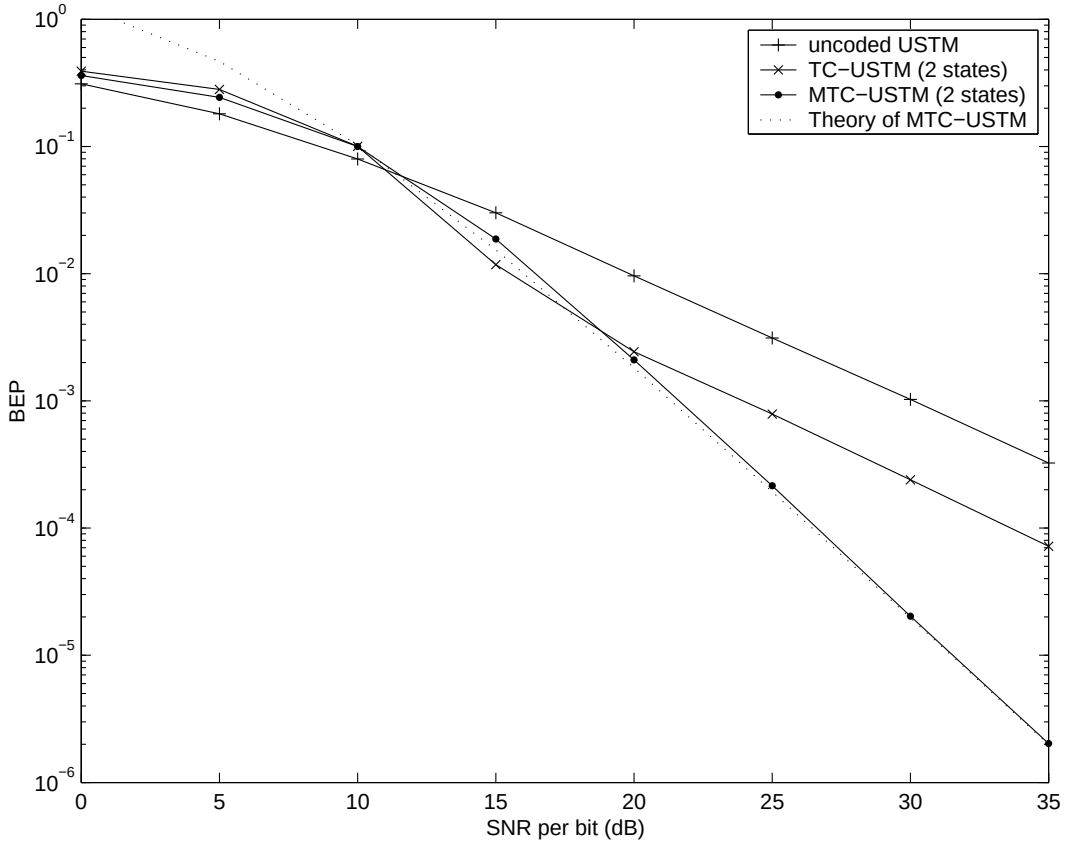

Figure 4.2: BEP comparison between uncoded USTM, TC-USTM and MTC-USTM ($k = 2$). $T = 2, M = 1, R = 1$.

cover 2 branches, as illustrated in Fig. 4.3. So the multiplicity of the shortest error events is $J(2) = 11$. The PEP associated with each of these 11 error events can be evaluated using (4.2). The error bits associated with every error event can be counted from the "mapping by set partitioning" formulated for TC-USTM in Chapter 3. Also note that $b \cdot k = 2 \cdot 2 = 4$.

To justify Criterion 3, we reconsider Example 1 by applying another mapping

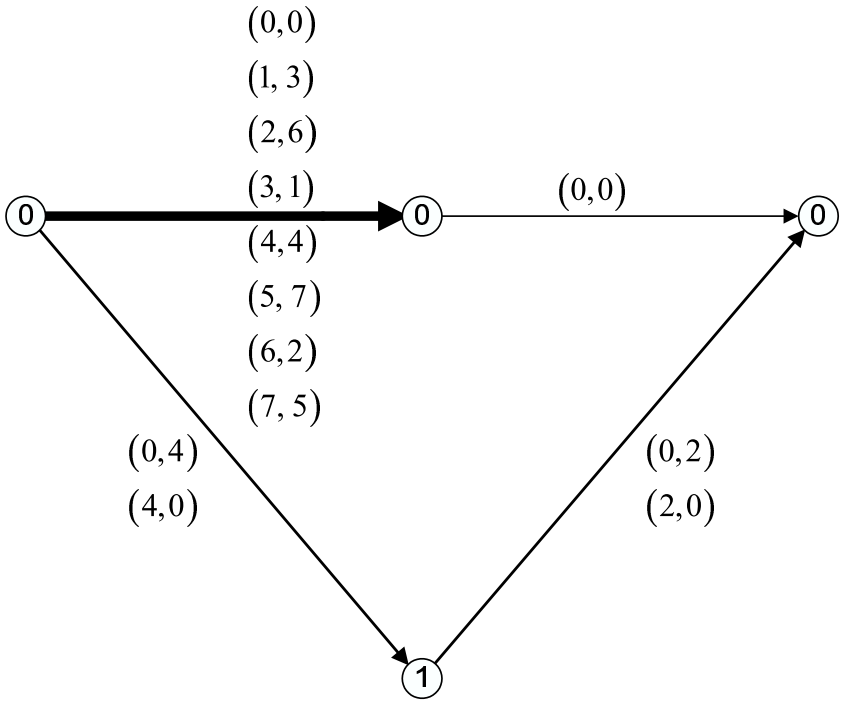

Figure 4.3: The shortest error events of MTC-USTM ($k = 2$) in Example 1, assuming constant sequence Φ_0 is transmitted. Integer l in the parenthesis denotes the the transmitted signal Φ_l.

matrix as

$$\mathcal{M} = \begin{pmatrix} 0 & 1 \\ 3 & 4 \end{pmatrix}.$$

As a result, $\xi_{0,*} = \xi_{1,*} = \min\{\zeta_1, \zeta_5\} = 0.3827 < 1$, and $\xi_{*,0} = \xi_{*,1} = \min\{\zeta_3, \zeta_1\} = 0.3827 < 0.7071$. Fig. 4.4 illustrates that around 1.5 dB coding gain can be obtained by MTC-USTM in Example 1. Analytically, the coding gain obtained by a MTC-USTM over another of the same M, N and $\ell_{\min}$ at high SNR can be derived from (3.12) and (3.9) as

$$\text{Gain} = \frac{10}{-MN\ell_{\min}} \log \frac{\sum_{j=1}^{J_2(\ell_{\min})} m_{2,j} \prod_{t\in\eta_{\min}} \zeta_{1,l_t,\hat{l}_t}^{-2MN}}{\sum_{j=1}^{J_1(\ell_{\min})} m_{1,j} \prod_{t\in\eta_{\min}} \zeta_{2,l_t,\hat{l}_t}^{-2MN}} \quad (\text{d}B), \tag{4.24}$$

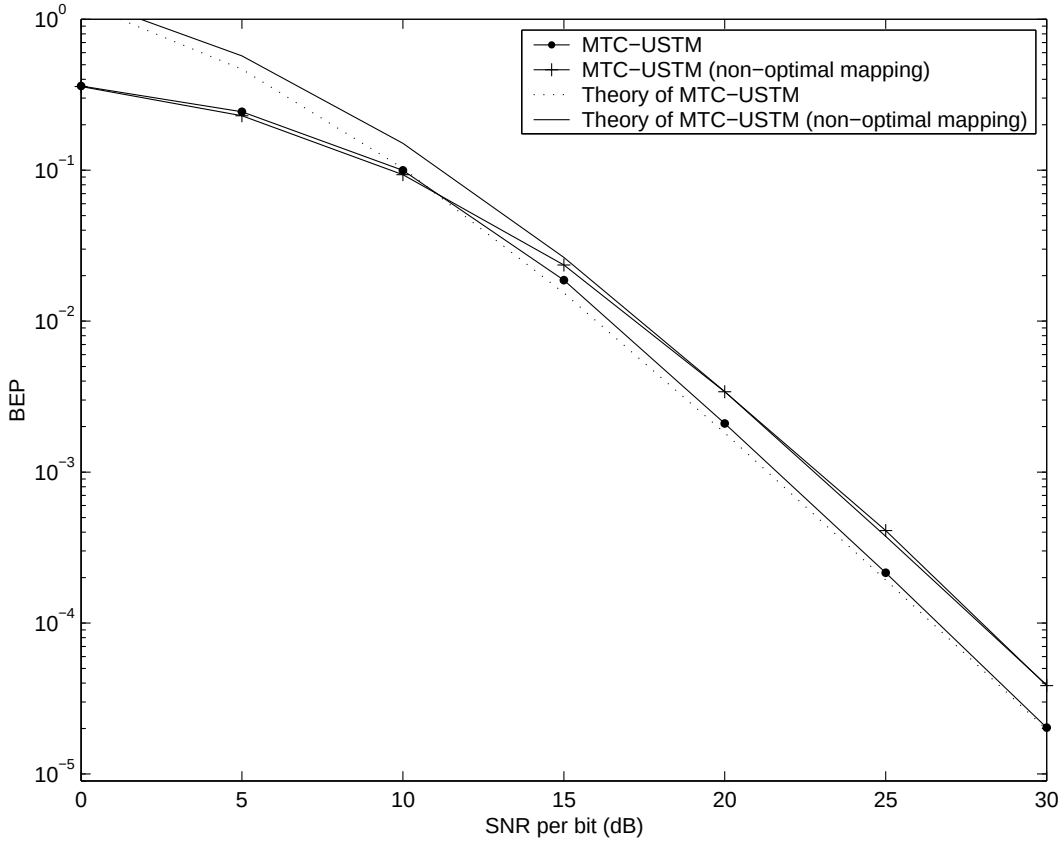

Figure 4.4: BEP comparison between MTC-USTM with and without optimal mapping. $k = 2, T = 2, M = 1, R = 1$.

where $J_\gamma(\ell_{\min}), m_{\gamma,j}$ and $\zeta_{\gamma,l_t,\hat{l}_t}$, $\gamma = 1, 2$ denote the multiplicity of the shortest error events, the associated error bits and the dissimilarity for two distinct MTC-USTM schemes. In comparing the above two MTC-USTM schemes using (4.24), we have a gain of 1.5656 dB for MTC-USTM. This agrees well with the simulation result.

To justify Criterion 2, once again we reconsider Example 1 and let $n_{\text{opt}} = 1$ instead of 3, which results in $\xi_m = 0.1464$. Accordingly $a = 1$. The resulting subsets are $\mathbf{G}_0 = \{(\Phi_0, \Phi_0), \cdots, (\Phi_7, \Phi_7)\}, \cdots, \mathbf{G}_7 = \{(\Phi_0, \Phi_7), \cdots, (\Phi_7, \Phi_6)\}$. With these

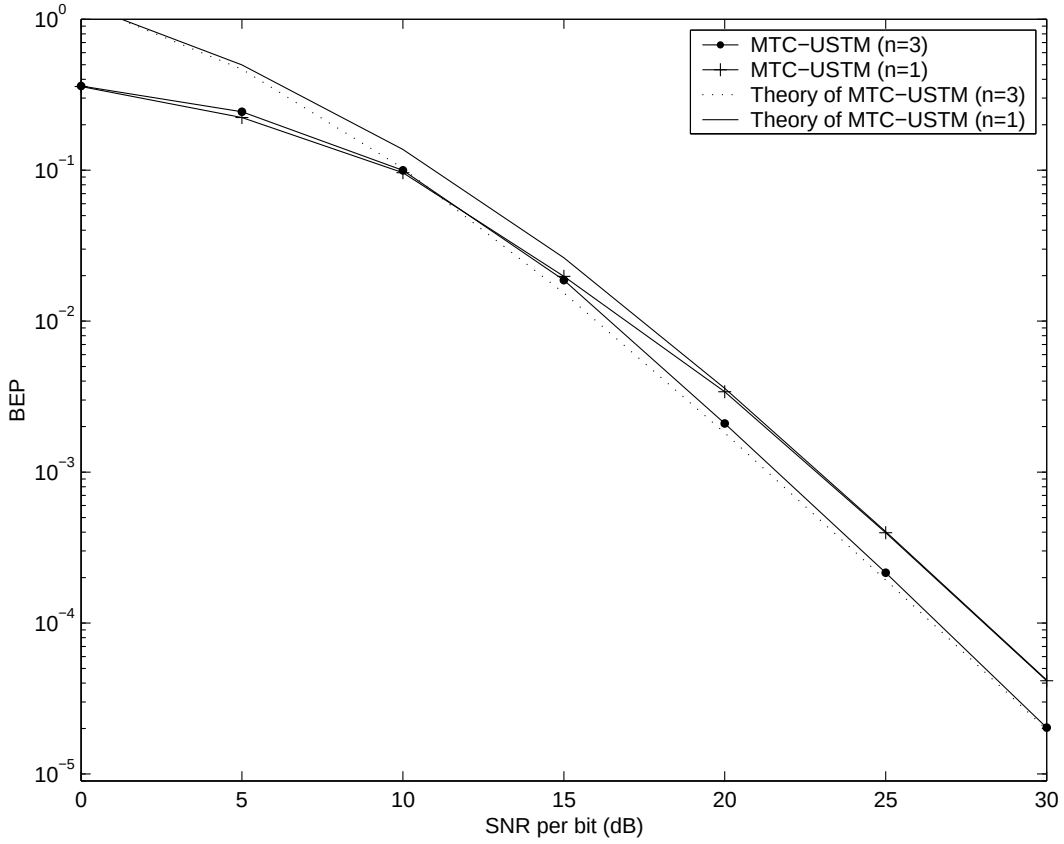

Figure 4.5: BEP comparison between MTC-USTM with optimal $n_{\text{opt}} = 3$ and with $n = 1$. $T = 2, M = 1, R = 1$.

subsets, to satisfy Criterion 3, we have

$$\mathcal{M} = \begin{pmatrix} 0 & 4 \\ 3 & 7 \end{pmatrix},$$

as in this case, $\xi_{0,*} = \xi_{1,*} = \min\{\zeta_4, \zeta_4\} = 1$ and $\xi_{*,0} = \xi_{*,1} = \min\{\zeta_3, \zeta_5\} = 0.9239 > 0.7071$. From Fig. 4.5, we see that MTC-USTM with $n = 1$ is around 1.5 dB worse than the MTC-USTM with n_{opt}. Using (4.24) we also observe that a 1.9785 dB coding gain can be obtained by the MTC-USTM with n_{opt} at high SNR.

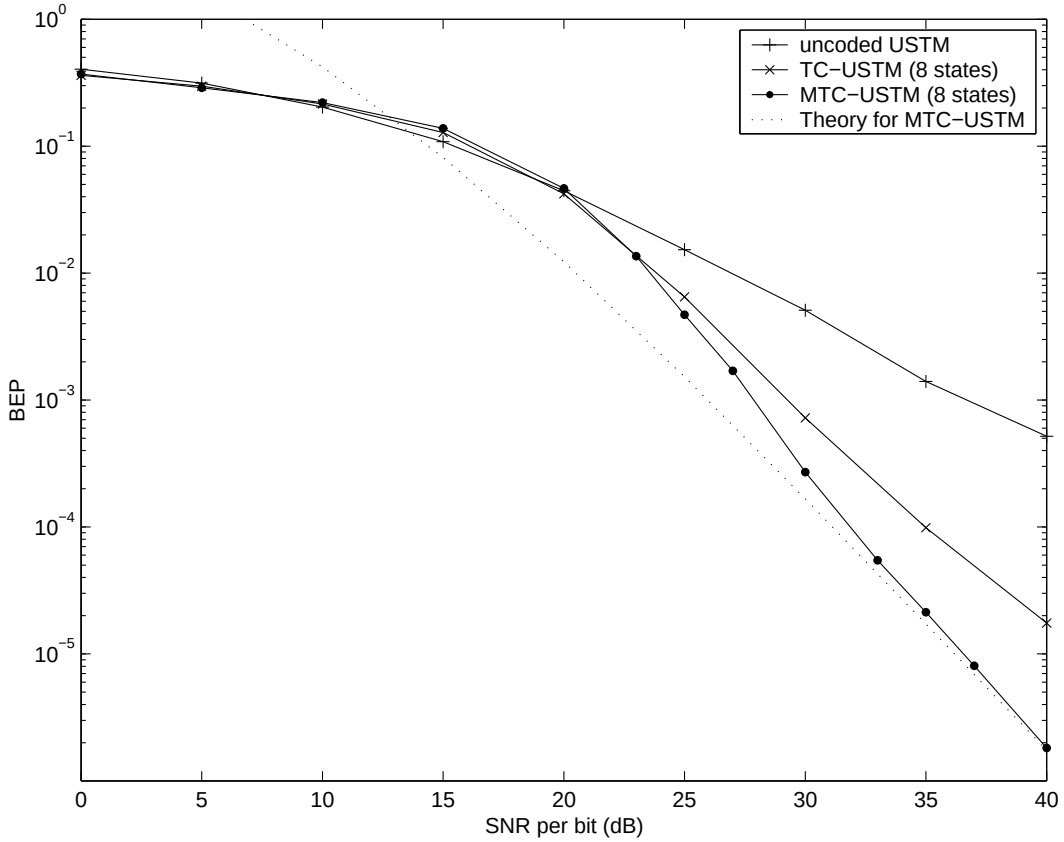

Figure 4.6: BEP comparison between uncoded USTM, TC-USTM and MTC-USTM ($k = 2$). $T = 2, M = 1, R = 2$.

We now consider Example 3, which has a higher information rate $R = 2$ than Example 1. The BEP performance comparison between uncoded USTM, TC-USTM and MTC-USTM is illustrated in Fig. 4.6. Once again, we see that with the same number of states and information rates, MTC-USTM performs better than TC-USTM. For Example 2 with $T = 4, M = 2$, we see in Fig. 4.7 that MTC-USTM outperforms the corresponding TC-USTM from around 18 dB onwards. The simulation result also agrees well with the theoretical lower bound. For Example 4 where smaller-size

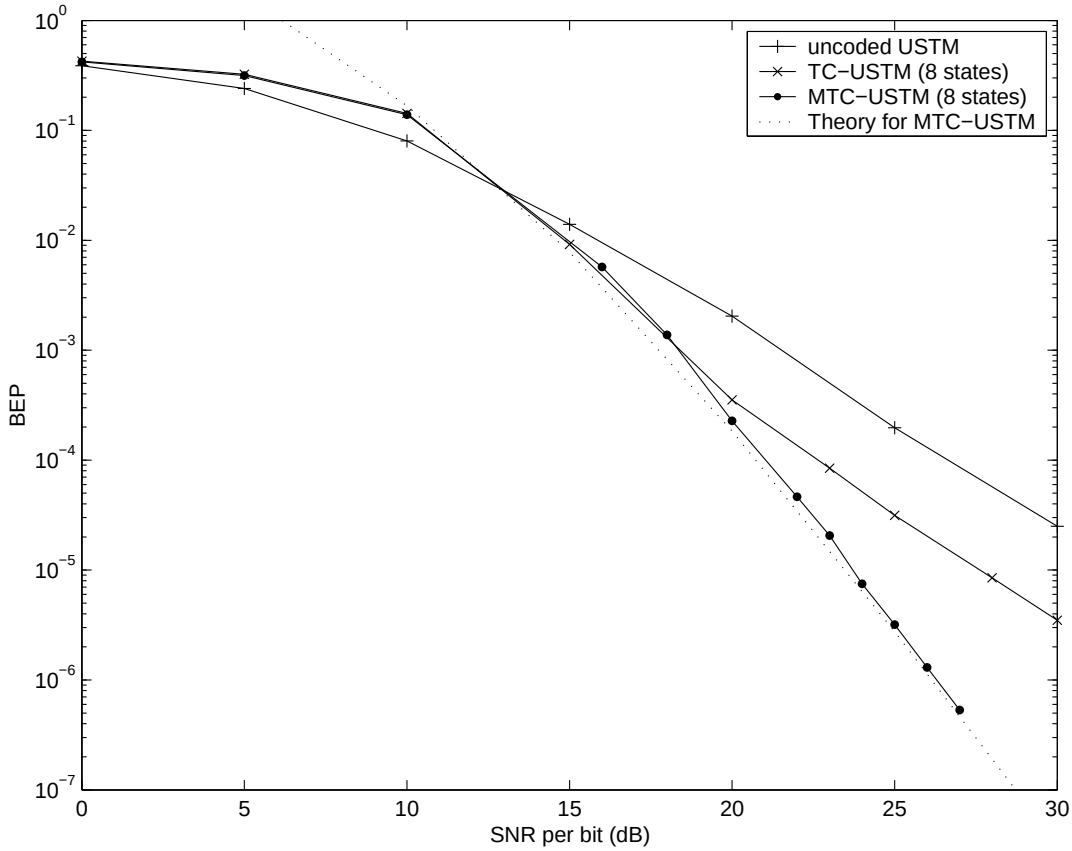

Figure 4.7: BEP comparison between uncoded USTM, TC-USTM and MTC-USTM ($k = 2$). $T = 4, M = 2, R = 1$.

subsets are employed, we show in Fig. 4.8 that the resulting MTC-USTM has approximately the same slope as that in Example 1, as $\ell_{\min} = 2$ for both cases. However MTC-USTM in Example 4 has around 2.5 dB coding gain over that in Example 1 at high SNR, as the former has a less number of multiplicity of the shortest error events.

For Example 5 where $\ell_{\min} = k = 3$, we show in Fig. 4.9 that the resulting MTC-USTM also outperforms the TC-USTM at high SNR, given the same number of trellis states and the same R. We also note that at low SNR, the MTC-USTM

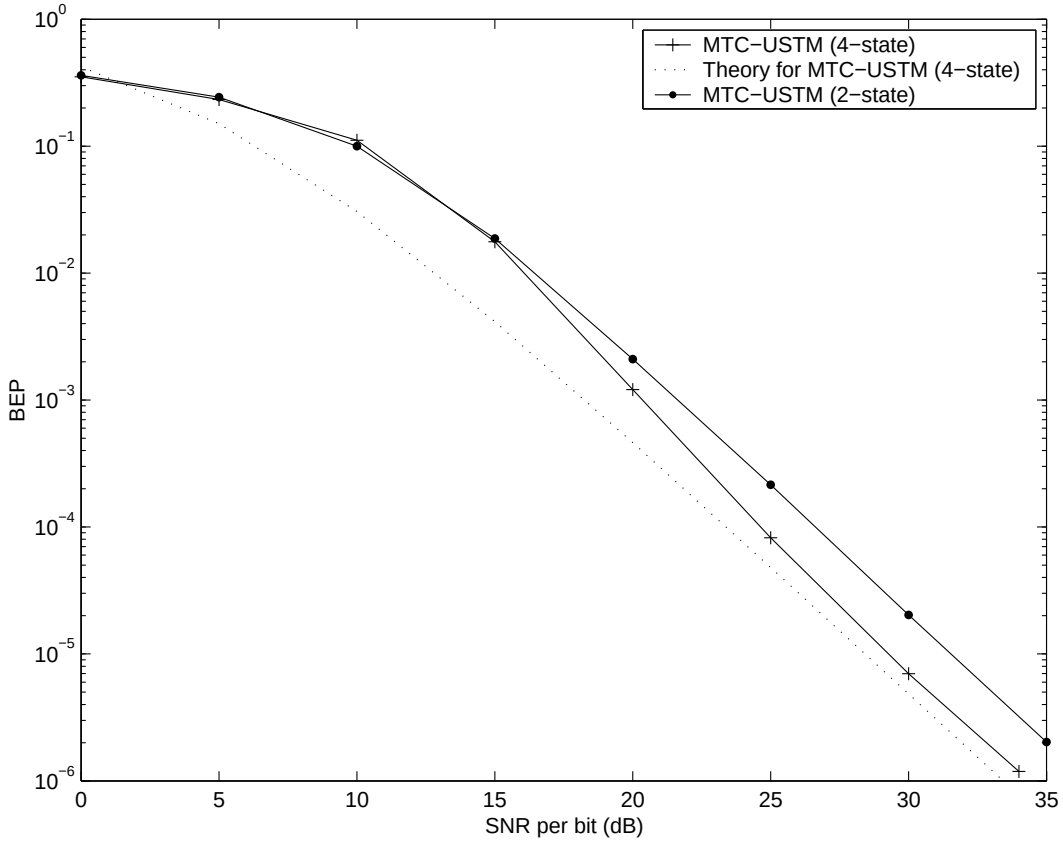

Figure 4.8: BEP comparison between MTC-USTM ($k = 2$) employing $\mathbf{G}_\lambda$ of different dimension and accordingly with different number of states. $T = 2, M = 1, R = 1$.

performs not as good as the corresponding TC-USTM while in the previous several examples, they have approximately the same error performance. In fact, at low SNR, the reduced dissimilarity product for the MTC-USTM of $k = 3$ due to the employment of a greater-dimension $\mathbf{\Phi}_L$ with fixed T, is more prone to error than TC-USTM at the same level of SNR. Therefore, MTC-USTM in Example 5 is not a good choice for a power efficient transmission scheme that operates at low SNR. However, for a bandwidth efficient transmission that operates in the high SNR region, MTC-USTM

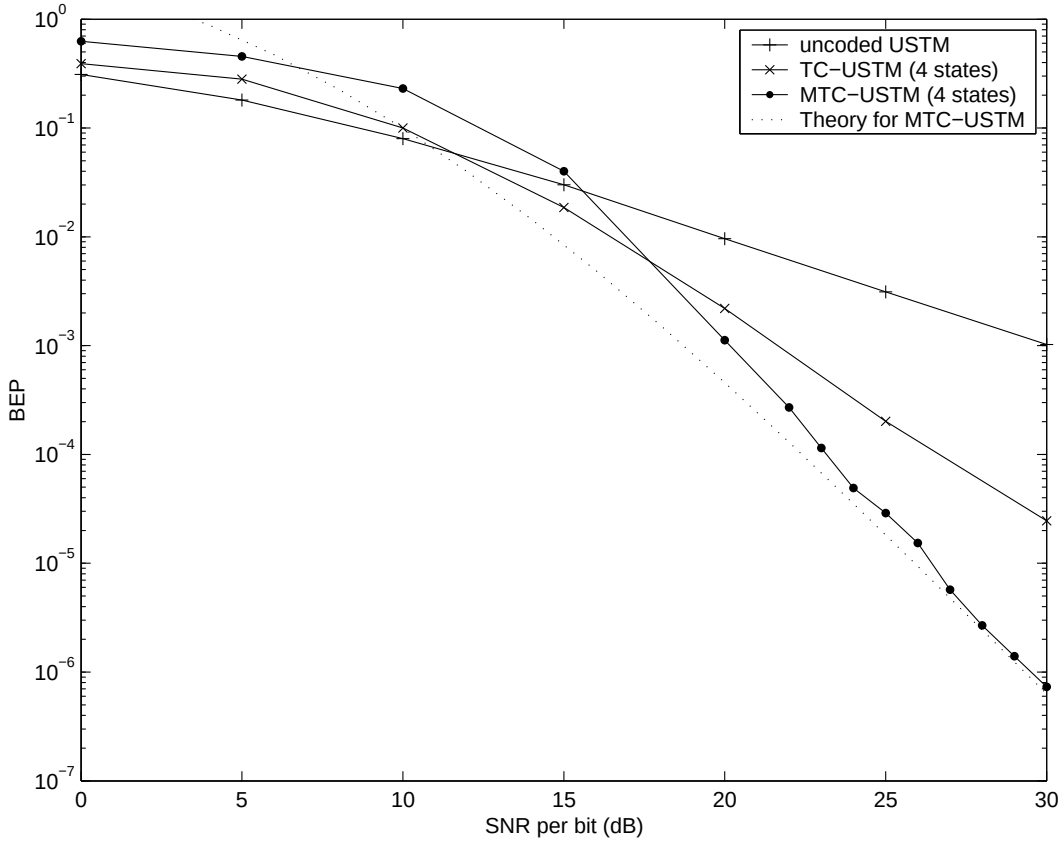

Figure 4.9: BEP comparison between uncoded USTM, TC-USTM and MTC-USTM ($k = 3$). $T = 2, M = 1, R = 1$.

in Example 5 is still attractive for its significant coding gain over its counterparts.

4.5 Summary

We have proposed a MTC-USTM transmission scheme for the Rayleigh flat fading channel where CSI is not known both at the transmitter and the receiver. In comparison with TC-USTM, MTC-USTM has an additional degree of freedom, k, in the design of the trellis diagram to obtain a larger $\ell_{\min}$ with a relatively smaller number

of states. We also provide three design criteria, whose validity are also demonstrated through numerical analysis. Among the three criteria, we found that Criteria 1 is of fundamental importance as it determines the slope of the BEP curves. Criterion 2 and 3 also guarantee additional coding gains. We demonstrate through numerical results that MTC-USTM produces a superior error performance than the TC-USTM of the same information rates and of the same number of states. We also show that the BEP lower bound at high SNR is an accurate estimate of the true BEP.

Chapter 5

Trellis-Coded Differential Unitary Space-Time Modulation

5.1 Background

For the proposed TC-USTM in Chapter 3 and MTC-USTM in Chapter 4, we assume the so-called piecewise constant Rayleigh fading channel model [4, 9] or block fading channel [15]. For these models, the component channel coefficients $h_{i,j}, 1 \leqslant i \leqslant M, 1 \leqslant j \leqslant N$ in the channel matrix H take independent values in every other T-symbol period, and remains constant in that interval. For a real mobile environment, the continuously changing Rayleigh fading channel, such as the Clarke's (or Jakes') model [61], is more appropriate. In this chapter, we propose a trellis coding scheme for the continuously changing Rayleigh fading channel taking into account the Doppler frequency shift effect.

This chapter is based on the differential USTM (DUSTM) proposed by Hochwald and Sweldens in [14], which is suitable for the slow Rayleigh flat fading channel. The signaling scheme for DUSTM has been summarized in Section 2.3. The proposed trellis-coded differential USTM (TC-DUSTM) can be seen as an extension of the TC-USTM, with the signaling scheme replaced by its differential counterpart. In this

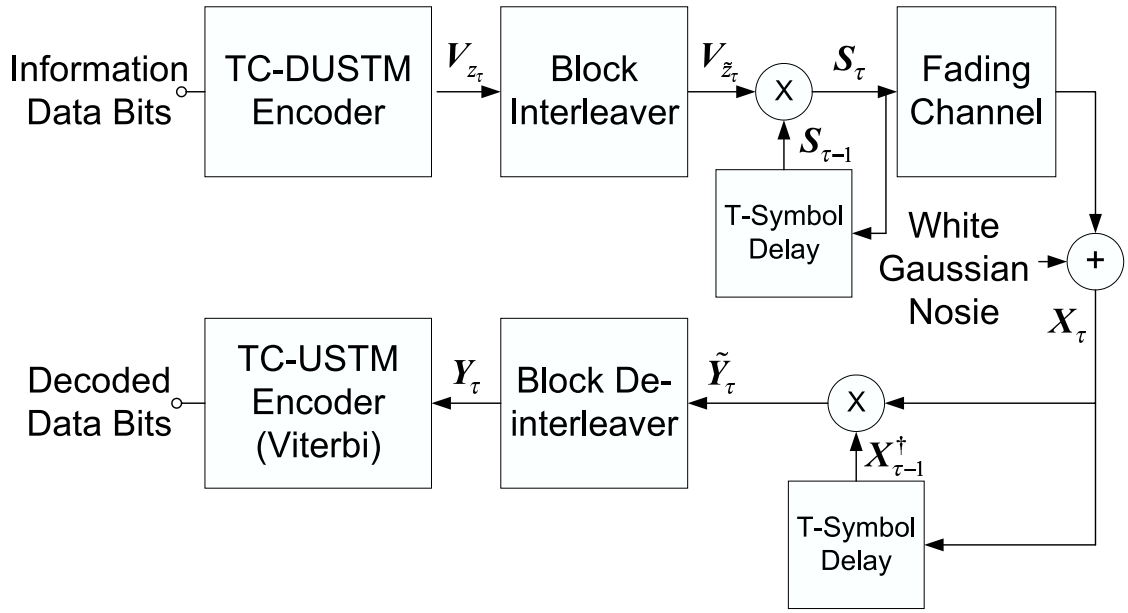

Figure 5.1: Block diagram for TC-DUSTM.

chapter, a performance analysis of the TC-DUSTM is presented and design criteria similar to that given in Chapter 3 are also presented.

5.2 Decision Metric for ML Sequence Decoding of TC-DUSTM

The system model for TC-DUSTM is illustrated in Fig. 5.1. The information bit sequence is divided into blocks of length RM, which is known as the *coding interval*. In every coding interval, the RM data bits are encoded to generate $RM + 1$ coded bits and mapped to a signal in the signal set $\mathbf{V}_L$ by the TC-DUSTM encoder. Before these coded signals are transmitted, they are first block-wise interleaved by the *block interleaver*. Then these signals are differentially modulated and transmitted. The received coded signal blocks are first differentially demodulated and then

de-interleaved. The decoder decides on the coded sequence that is closest to the real sequence, by a ML algorithm (Viterbi decoder). The focus of this chapter is on how to form the TC-DUSTM encoder to realize the minimum error rate performance.

In Fig. 5.1, suppose a trellis-coded sequence $\mathbf{V}^K = \{V_{z_\tau}, \tau = 1, \cdots, K\}$ is fed into the interleaver, with the output interleaved sequence denoted as $\tilde{\mathbf{V}}^K = \{V_{\tilde{z}_\tau}, \tau = 1, \cdots, K\}$. Here τ denotes the time index for each signal block, and the subscripts $z_\tau, \tilde{z}_\tau \in \mathbb{Z}_L$ denote the information delivered by V_{z_τ} and $V_{\tilde{z}_\tau}$, respectively. The differential modulation is realized as follows. Firstly, the constant $M \times M$ identity matrix $S_0 = I_M$ is transmitted. The second transmitted signal is $S_1 = V_{\tilde{z}_1} S_0$. The transmitted signal sequence can be expressed as

$$S_\tau = V_{\tilde{z}_\tau} S_{\tau-1}, \quad \tau = 1, 2, \cdots, K \tag{5.1}$$

The received coded sequence (before differential demodulation) is

$$X_\tau = \sqrt{\frac{\rho}{M}} S_\tau H_\tau + W_\tau, \quad \tau = 1, 2, \cdots, K \tag{5.2}$$

where H_τ denotes the channel matrix at the time index τ. Strictly speaking, in the M-symbol period, $h_{i,j}$ takes different values every other symbol period. However, for a slow Rayleigh flat fading channel, $h_{i,j}$ can be considered as a constant in this period. More over, one can further assume that two consecutive channel matrices are identical, i.e., $H_\tau = H_{\tau-1}$. The entries in H_τ is assumed to be complex Gaussian random variables distributed as $\mathcal{CN}(0, 1)$. The elements in the noise matrix W_τ are also $\mathcal{CN}(0, 1)$ distributed. Therefore ρ is the SNR at each receive antenna. Substituting equation (5.1) into (5.2), one obtains another form of the received signal sequence

$$X_\tau = V_{z_\tau} X_{\tau-1} + W_\tau - V_{z_\tau} W_{\tau-1}, \quad \tau = 1, 2, \cdots, K \tag{5.3}$$

We define the differentially detected signal sequence as

$$\tilde{Y}_\tau = X_\tau X_{\tau-1}^\dagger, \quad \tau = 1, \cdots, K. \tag{5.4}$$

with $\tilde{Y}_\tau$ a $M \times M$ matrix. Substituting (5.1) and (5.3) into (5.4), and neglecting the product terms of W_τ and/or $W_{\tau-1}$, we have

$$\tilde{Y}_\tau = \rho V_{\tilde{z}_\tau} |S_{\tau-1}H|^2 + W'_\tau, \tag{5.5}$$

where

$$W'_\tau = \sqrt{\rho} V_{\tilde{z}_\tau} S_{\tau-1} H W_{\tau-1}^\dagger + \sqrt{\rho} W_\tau H^\dagger S_{\tau-1}^\dagger \tag{5.6}$$

and H is a simplified expression for the approximately identical matrices H_τ and $H_{\tau-1}$. In this chapter, $|A|^2$ denotes $AA^\dagger$ for a matrix A. As $S_{\tau-1}$ is a deterministic unitary matrix, $S_{\tau-1}H$ and H have the same distribution and one can denote the matrix $S_{\tau-1}H$ by a new channel matrix $\mathbf{H}$. As entries in H are i.i.d as $\mathcal{CN}(0,1)$, entries $\mathbf{h}_{i,j}, 1 \leqslant i \leqslant M, 1 \leqslant j \leqslant N$ in $\mathbf{H}$ are also i.i.d as $\mathcal{CN}(0,1)$. Then (5.5) and (5.6) can be equivalently expressed as

$$\tilde{Y}_\tau = \rho V_{\tilde{z}_\tau} |\mathbf{H}|^2 + W'_\tau, \tag{5.7}$$

$$W'_\tau = \sqrt{\rho} V_{\tilde{z}_\tau} \mathbf{H} W_{\tau-1}^\dagger + \sqrt{\rho} W_\tau \mathbf{H}^\dagger. \tag{5.8}$$

As the component channel coefficients are assumed to be independent, $E\{\mathbf{h}_{m,n}\mathbf{h}_{p,q}\} = \Delta_{m,p}\Delta_{n,q}$, where Δ denotes the Kroneker product. Therefore the conditional mean of $\tilde{Y}_\tau$ can be expressed as

$$E\{\tilde{Y}_\tau | V_{\tilde{z}_\tau}\} = \rho N V_{\tilde{z}_\tau}. \tag{5.9}$$

The variance of $\tilde{Y}_\tau$ given $V_{\tilde{z}_\tau}$ is $\Lambda = E\{(\tilde{Y}_\tau - \rho N V_{\tilde{z}_\tau})(\tilde{Y}_\tau - \rho N V_{\tilde{z}_\tau})^\dagger\}$ and can be derived as

$$\Lambda = \rho M N (\rho + 2) I_M. \tag{5.10}$$

Derivations of the equations (5.9) and (5.10) can be found in Appendix B and C, respectively. Therefore the pdf of $\tilde{Y}_\tau$ given $V_{\tilde{z}_\tau}$ is

$$p(\tilde{Y}_\tau|V_{\tilde{z}_\tau}) = \frac{\exp\left\{-\mathrm{tr}\left(\Lambda^{-1}(\tilde{Y}_\tau - \rho N V_{\tilde{z}_\tau})(\tilde{Y}_\tau - \rho N V_{\tilde{z}_\tau})^\dagger\right)\right\}}{\pi^{M\times N}\det^N(\Lambda)}. \tag{5.11}$$

Assuming an ideal interleaving-deinterleaving, each element in $\mathbf{Y}^K = \{Y_\tau, \tau = 1, \cdots, K\}$ is independent. Therefore the joint pdf of $\mathbf{Y}^K$ given $\mathbf{V}^K$ is $p(\mathbf{Y}^K|\mathbf{V}^K) = \prod_{\tau=1}^K p(Y_\tau|V_{z_\tau})$. Note that $p(Y_\tau|V_{z_\tau}) = p(\tilde{Y}_\tau|V_{\tilde{z}_\tau})$. Hence the ML sequence decoder can be developed as

$$\begin{aligned}
\mathbf{V}_{ml}^K &= \arg\max_{\mathbf{V}^K} p(\mathbf{Y}^K \mid \mathbf{V}^K) \\
&= \arg\max_{V_{z_\tau}\in\{V_0,\cdots,V_{L-1}\}} \sum_{\tau=1}^K \mathrm{tr}\left\{Y_\tau V_{z_\tau}^\dagger + V_{z_\tau} Y_\tau^\dagger\right\}. \qquad (5.12)
\end{aligned}$$

This ML algorithm can be efficiently implemented by a Viterbi decoder. We note that equation (5.5) is under the assumption that the product terms $W_\tau W_\tau^\dagger$, $W_\tau W_{\tau-1}^\dagger$ and $W_{\tau-1}W_{\tau-1}^\dagger$ are neglected in the derivation. Though in this way the resulting decision metric loses some information, especially at low SNR, we obtained a most important benefit as that a much simplified expression is obtained. We will continue to examine a full decision metric comprising these product terms and put it as our future work.

5.3 Performance Analysis for the TC-DUSTM

Suppose $\mathbf{V}^K$ is transmitted, while the decoder decides on a different sequence $\hat{\mathbf{V}}^K = \{V_{\hat{z}_\tau}, \tau = 1, \cdots, K\}$ in place of $\mathbf{V}^K$. The length of an error event is defined as the Hamming distance between $\mathbf{V}^K$ and $\hat{\mathbf{V}}^K$. From (5.12), the PEP $p(\mathbf{V}^K \to \hat{\mathbf{V}}^K)$ of mistaking $\mathbf{V}^K$ for $\hat{\mathbf{V}}^K$ or vice versa is

$$p(\mathbf{V}^K \to \hat{\mathbf{V}}^K) = p(\sum_{\tau=1}^K D_\tau > 0) \tag{5.13}$$

where $D_\tau = \mathrm{tr}\{Y_\tau(V_{\hat{z}_\tau} - V_{z_\tau})^\dagger + (V_{\hat{z}_\tau} - V_{z_\tau})Y_\tau^\dagger\}$. In [14], D_τ is the quadratic form used to derive the pairwise block error probability (PBEP) between V_{z_τ} and $V_{\hat{z}_\tau}$ and we know that when $V_{z_\tau} \neq V_{\hat{z}_\tau}$, the characteristic function of the quadratic form D_τ is [9, 14]

$$\Phi_{D_\tau}(\omega) = \prod_{m=1}^{M} \left[\frac{1+2\rho}{\rho^2 \sigma_{m,\tau}^2 [(\omega - i/2)^2 + a_{m,\tau}^2]} \right]^N \tag{5.14}$$

where

$$a_{m,\tau} = \sqrt{\frac{1}{4} + \frac{1+2\rho}{\rho^2 \sigma_{m,\tau}^2}} \tag{5.15}$$

and $\sigma_{m,\tau}$ is the mth singular value of the matrix $V_{z_\tau} - V_{\hat{z}_\tau}$. When $V_{z_\tau} = V_{\hat{z}_\tau}$, $\Phi_{D_\tau}(\omega) = 1$. Assuming an ideal interleaving-interleaving, the quadratic forms D_τ's are independent for different τ's. Therefore the characteristic function of $D = \sum_{\tau=1}^{K} D_\tau$ is $\Phi_D(\omega) = \prod_{\tau \in \eta} \Phi_{D_\tau}(\omega)$, where η is the set of τ for which $V_{z_\tau} \neq V_{\hat{z}_\tau}$. We can invert the characteristic function to find the pdf of D and the PEP can be derived as

$$p(\mathbf{V}^K \to \hat{\mathbf{V}}^K) = \frac{1}{4\pi} \int_{-\infty}^{\infty} d\omega \frac{1}{\omega^2 + 1/4} \prod_{\tau \in \eta} \prod_{m=1}^{M} \left[\frac{1+2\rho}{\rho^2 \sigma_{m,\tau}^2 (\omega^2 + a_{m,\tau}^2)} \right]^N \tag{5.16}$$

An upper bound of the PEP can be found as

$$p(\mathbf{V}^K \to \hat{\mathbf{V}}^K) \leqslant \prod_{\tau \in \eta} \Gamma_\tau \tag{5.17}$$

where

$$\Gamma_\tau = \frac{1}{2} \prod_{m=1}^{M} \left[1 + \frac{\rho^2 \sigma_{m,\tau}^2}{4(1+2\rho)} \right]^{-N} \tag{5.18}$$

is the Chernoff upper bound for the PBEP between V_{z_τ} and $V_{\hat{z}_\tau}$ [14]. Suppose the size of the set η, i.e., the length of the associated error event is ℓ. The inequality (5.17) suggests that the error events with long length ℓ can be neglected while the error event with the shortest length ℓ_{min} plays the main role in determining the PEP. At

sufficiently high SNR, Γ_τ is upper bounded by $\Gamma_\tau \leqslant \frac{1}{2}\left(\frac{8}{\rho}\right)^{MN}\prod_{m=1}^{M}\sigma_{m,\tau}^{-2N}$. Therefore when only the shortest error event is taken into account, we have

$$p(\mathbf{V}^K \to \hat{\mathbf{V}}^K) \leqslant \left(\frac{1}{2^{\ell_{min}}}\left(\frac{8}{\rho}\right)^{MN\ell_{min}}\right)\cdot\left(\prod_{\tau\in\eta_{min}}\prod_{m=1}^{M}\sigma_{m,\tau}^{-2N}\right) \tag{5.19}$$

where η_{min} denotes the set of τ for which $V_{z_\tau} \neq V_{\hat{z}_\tau}$ along the shortest error event. The part in the first bracket in inequality (5.19) suggests that the error curve of the PEP varies as $\rho^{-MN\ell_{min}}$. Thus not only a *diversity gain* of MN is obtained from the space-time signal design, but also a coding gain of $\ell_{\min}$ from the trellis-coding design. Therefore one should choose a TC-DUSTM scheme with as large a value of $\ell_{\min}$ as computational complexity allows.

An additional coding gain comes from the second part of (5.19). Recalling (1), we have

$$\prod_{\tau\in\eta_{min}}\prod_{m=1}^{M}\sigma_{m,\tau}^{-2N} = 2\prod_{\tau\in\eta_{min}}\zeta_{z_\tau,\hat{z}_\tau}^{-2MN}, \tag{5.20}$$

which suggests that in the shortest error event, the corresponding two signals along the path should be selected such that the product of the *dissimilarities* should be maximized.

An asymptotic BEP formula can be expressed as

$$P_b \approx \frac{1}{R\cdot M}\sum_{\ell=\ell_{\min}}^{\ell'}\sum_{j=1}^{J(\ell)} m_{\ell,j}\, p(\mathbf{V}_{\ell,j}^K \to \hat{\mathbf{V}}_{\ell,j}^K) \tag{5.21}$$

where $J(\ell)$ is the number of error events having the same length ℓ. $m_{\ell,j}$ is the number of bit-errors associated with the jth error event of length ℓ and $p(\mathbf{V}_{\ell,j}^K \to \hat{\mathbf{V}}_{\ell,j}^K)$ is the PEP between these two coded sequences along that path. ℓ' is chosen so that the amount of computation will not be excessive and yet most of the dominant error events are included. A BEP lower bound at high SNR can be obtained by only

taking the shortest error event into account, i.e., by setting $\ell' = \ell_{\min}$ in (5.21), one can have

$$P_b \gtrsim \frac{1}{R \cdot M} \sum_{j=1}^{J(\ell_{min})} m_{\ell_{\min},j} p(\mathbf{V}^N_{\ell_{min},j} \to \hat{\mathbf{V}}^N_{\ell_{\min},j}). \tag{5.22}$$

At a sufficiently high SNR, (5.22) gives an accurate estimation of the BEP.

5.4 Mapping by Set Partitioning for TC-DUSTM

5.4.1 Design Criteria

In Section 3.3, design criteria for TC-USTM have been given. On the one hand, those criteria guarantee that the minimum BEP can be obtained; on the other hand, if there are parallel paths between any two consecutive states, those criteria guarantee that the BEP performance analysis can be simplified by investigating the PEP between parallel paths between any two consecutive states.

In this section, we follow the proposed criteria given in Section 3.3. We still focus on the TC-DUSTM where there exist parallel paths between consecutive states. Let $b = RM$, then $L = 2^b$. Let $\mathbf{V}_L$ be in layer-1 of the set partitioning tree and the single signals $V_l, l \in \mathbb{Z}_L$ be in the layer-$(b+1)$. Correspondingly, in layer-$j, 1 \leqslant j \leqslant b+1$, there are 2^{j-1} subsets, denoted as $\boldsymbol{v}_i^{(j)}, 0 \leqslant i \leqslant \mathbb{Z}_{2^{j-1}-1}$, and each subset contains 2^{b-j+1} signals. The definition of congruent subsets follows the definition in Section 3.3. Therefore Criterion 1 can be formulated as

Criterion 1. All the subsets in the same layer are congruent subsets, that is, $\boldsymbol{v}_0^{(j)} \cong \cdots \cong \boldsymbol{v}_{2^{j-1}-1}^{(j)}$ for $2 \leqslant j \leqslant b$.

As a result of Criterion 1, subsets in the same layer have identical minimum dissimilarity, denoted as $\zeta_{\min}^{(j)}$. The following criterion guarantees that the best BEP

performance can be obtained by the TC-DUSTM.

Criterion 2. $\zeta_{\min}^{(j)}$ should be maximized for each j.

Set partitioning satisfying both criteria is referred to as *optimal set partitioning* for TC-DUSTM.

5.4.2 Properties of DUSTM Signal Set

We focus on the systematically designed DUSTM, which has been introduced in Section 2.3. As $V_l = V_1^l, V_{l'} = V_1^{l'}$, we have $\det(V_l - V_{l'}) = \det(V_1(I_M - V_1^{l'-l}))$. Therefore

$$\det(V_l - V_{l'}) = \det(I_M - V_1^{l'-l}). \tag{5.23}$$

Recalling equation (2.16), we conclude that the dissimilarity between V_l and $V_{l'}$ is a function of the *index interval* $(l'-l) \bmod L$, denoted as $\Delta_{l,l'}$, and accordingly $\zeta(V_l, V_{l'})$ can be denoted as $\zeta_{\Delta_{l,l'}}$. Thus any two signals with the same index interval have the same value of dissimilarity.

Fixing the *reference signal* V_l, when the index l' of $V_{l'}$ runs over the whole integer set $\mathbb{Z}_L$, we obtain the set of signal index intervals, denoted as $\mathbf{\Delta}_{\mathbf{V}_L}(l) = \{\Delta_{l,l'} \mid l', l \in \mathbb{Z}_L, l' \neq l\}$. It follows that the $\mathbf{\Delta}_{\mathbf{V}_L}(l)$ is identical with different reference signal V_l, which is $\{1, 2, \cdots, L-1\}$. The dissimilarity set corresponding to the index interval set is defined as the *dissimilarity profile*, $\mathcal{P}_{\mathbf{V}_L}(l) = \{\zeta_{\Delta_{l,l'}} \mid \Delta_{l,l'} \in \mathbf{\Delta}_{\mathbf{V}_L}\}$. For $\mathbf{\Delta}_{\mathbf{V}_L}(l)$, we have the following property.

Property 1. $\mathbf{\Delta}_{\mathbf{V}_L}(l)$ is identical for different reference l.

Therefore $\mathbf{\Delta}_{\mathbf{V}_L}(l)$ and $\mathcal{P}_{\mathbf{V}_L}(l)$ can be simplified as $\mathbf{\Delta}_{\mathbf{V}_L}$ and $\mathcal{P}_{\mathbf{V}_L}$, respectively. As a result, for simplicity, one can investigate the $\zeta_{\Delta_{0,l}}, l \in \mathbb{Z}_L$, instead of $\zeta_{\Delta_{l,l'}}, l, l' \in \mathbb{Z}_L$

for a full view of the dissimilarities in a DUSTM signal set. For two signals V_l and $V_{l'}$, we note that $(l'-l)\ \mathrm{mod} L = L-(l-l')\ \mathrm{mod} L$. It follows that in the dissimilarity profile, $\Delta_{l,l'}$ and $L-\Delta_{l,l'}$ correspond to the identical dissimilarity. Therefore we have the following property.

Property 2. $\mathbf{\Delta}_{\mathbf{V}_L}$ is symmetrical about the central point $\Delta_{l,l'} = \frac{L}{2}$, i.e., $\zeta_{\Delta_{l,l'}} = \zeta_{\Delta_{l',l}}$.

The above two properties also hold for USTM. For DUSTM, additionally, we have

Property 3. $\mathbf{\Delta}_{\mathbf{V}_L}$ has its maximum value 1 at the central point $L/2$, i.e., $\zeta_{L/2} = 1$.

In fact, we know $\zeta_{\Delta_{0,1}} = |\prod_{m=1}^{M} \sin(\pi u_m l/L)|^{1/M}$ and that $u_m, m = 1, \cdots, M$ are all odd integers [14], which indicates that $\zeta_{\Delta_{0,1}}$ has its maximum value 1 at $\Delta_{l,l'} = L/2$.

For the purpose of illustration, Fig. 5.2 displays four dissimilarity profiles for signal set $\mathbf{V}_4$ $(M = 2, R = 1)$, $\mathbf{V}_8$ $(M = 3, R = 1)$, $\mathbf{V}_{16}$ $(M = 4, R = 1)$ and $\mathbf{V}_{32}$ $(M = 5, R = 1)$. The above three properties can be demonstrated by these examples.

5.4.3 A Systematic and Universal Set Partitioning Strategy for TC-DUSTM

The systematic set partitioning strategy for TC-USTM in Chapter 3 can be exploited in this section for the set partitioning of the DUSTM signal sets. One can observe that the properties listed in Section 5.4.2 are similar to those for USTM in Section 3.2; more over, the design criteria proposed for TC-DUSTM in Section 5.4.1 are similar to those for TC-USTM in Section 3.4 as well. From these facts, we can justify that the optimal set partitioning scheme for the USTM in Section 3.5 can be

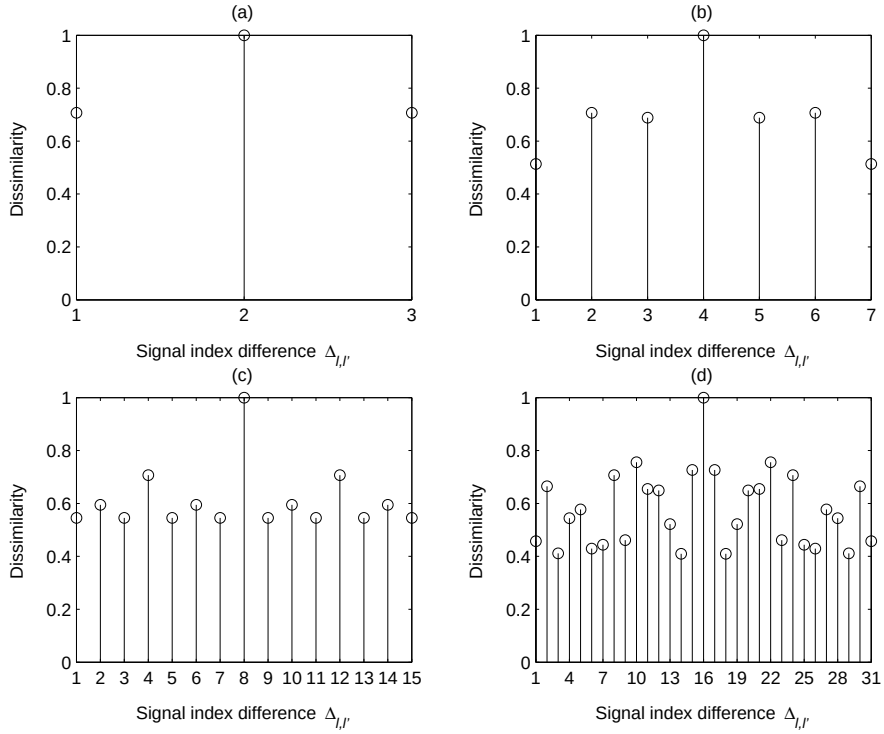

Figure 5.2: $\mathcal{P}_{\mathbf{V}_L}$ for signal sets $\mathbf{V}_4$ ($M = 2$), $\mathbf{V}_8$ ($M = 3$), $\mathbf{V}_{16}$ ($M = 4$) and $\mathbf{V}_{32}$ ($M = 5$). $R = 1$.

applied to the DUSTM signal sets. In summary, set partitioning can be realized in two steps: 1) Formulate all the possible realizations of set partitioning tree which guarantee subsets in the same layer are congruent subsets (Criterion 1 is satisfied); 2) Choose one realization which guarantees $\zeta_{\min}^{(j)}$ increases as rapidly as possible as j increases(Criterion 2 is satisfied).

A systematic set partitioning scheme for the UST signal set can be realized following the same line of the Proposition in Section 3.5.4, which is known as the subset-pairing. After some modifications to that proposition, one can obtain a new proposition to suit for the DUSTM signals sets. We also let $\mathbf{\Delta}_{\mathcal{A}}(a)$ denote the index interval set of the integer set $\mathcal{A}$ with respect to the reference $a \in \mathcal{A}$. If $\mathcal{A}$ is a group under $\oplus$,

$\mathbf{\Delta}_{\mathcal{A}}(a)$ will be identical for different $a \in \mathcal{A}$ and can be simplified as $\mathbf{\Delta}_{\mathcal{A}}$.

We consider an arbitrary integer group $\mathcal{S} = 2^p\mathbb{Z}_{2^{b-p}}, 0 \leqslant p \leqslant b-1$ and an arbitrary $\Delta \in \mathbf{\Delta}_{\mathcal{S}}$. We define $\Delta = \frac{\Delta}{2^p}$ as the *normalized* index interval. If Δ is an odd integer, $\mathcal{S}$ can be partitioned into congruent size-2 subsets $\{2^{p+1}i, 2^{p+1}i \oplus \Delta\}, i \in \mathbb{Z}_{2^{b-p-1}}$, where the *reference set* is defined as $\mathcal{R} = \{2^{p+1}i \mid i \in \mathbb{Z}_{2^{b-p-1}}\}$. This integer-pairing operation in $\mathcal{S}$ is defined as *Operation* I. If Δ is an even integer, $\{2^{p+p'+1}i \oplus m, 2^{p+p'+1}i \oplus \Delta \oplus m\}, i \in \mathbb{Z}_{2^{b-p-p'-1}}, m \in 2^p\mathbb{Z}_{2^{p'}}$ form congruent size-2 subsets in $\mathcal{S}$, where $p', 1 \leqslant p' \leqslant b-p-1$ is chosen such that $\frac{\Delta}{2^{p'}}$ is an odd integer. In this case, the reference set is defined as $\mathcal{R} = \{2^{p+p'+1}i \mid i \in \mathbb{Z}_{2^{b-p-p'-1}}\}$. This integer-pairing operation in $\mathcal{S}$ is defined as *Operation* II. Operation I and II are fundamental operations in the subset-pairing procedure.

Setting $\mathcal{S}^{(0)} \leftarrow \mathbb{Z}_L$, congruent size-2 subsets in $\mathbb{Z}_L$ and the corresponding reference set $\mathcal{R}^{(0)}$ can be obtained by Operation I or II. By definition, $\mathcal{R}^{(0)}$ is also an integer group under $\oplus$. Then for an arbitrary integer $\Delta \in \mathbf{\Delta}_{\mathcal{R}}$, setting $\mathcal{S}^{(1)} \leftarrow \mathcal{R}^{(0)}$, one can obtain the congruent size-2 subsets in $\mathcal{R}^{(0)}$, which leads to congruent size-4 integer subsets and a new $\mathbb{Z}_L$. Thus through the critical step $\mathcal{S}^{(k)} \leftarrow \mathcal{R}^{(k-1)}, k \geqslant 1$, one achieves a recursive subset-pairing procedure. When Operation II has been applied, there should be a redefinition of the reference set corresponding to this Operation II.

The above recursive subset-pairing scheme presents a framework to realize step 1). To realize step 2), an exhaustive search for the optimal $\Delta^* \in \mathbf{\Delta}_{\mathcal{S}^{(k)}}$ must be done by the following function

$$\Delta^* = \arg \max_{\Delta \in \mathbf{\Delta}_{\mathcal{S}^{(k)}}} \zeta_{\min}\left(\boldsymbol{v}(0) \bigcup \boldsymbol{v}(\Delta)\right) \tag{5.24}$$

where $\boldsymbol{v}(0)$ and $\boldsymbol{v}(\Delta)$ denote the signal sets in $\mathbf{V}_L$ associated with the reference integer 0 and $\Delta \in \mathbf{\Delta}_{\mathcal{S}^{(k)}}$, respectively, and $\zeta_{\min}(\cdot)$ denotes the minimum dissimilarity

in the signal set $(\cdot)$. Therefore we have the following proposition for an optimal set partitioning of the DUSTM signal set.

Proposition. The subset-pairing for an arbitrary DUSTM signal set $\mathbf{V}_L$ can be formulated as follows:

1) (*Initialization*) Set $k \leftarrow 0$, $\mathcal{S}^{(k)} \leftarrow \mathbb{Z}_L$ and $\oplus \leftarrow \oplus_b$;

2) (*Subset-pairing*) Obtain $\Delta^* \in \mathbf{\Delta}_{\mathcal{S}^{(k)}}$ through (5.24) and determine the corresponding normalized integer interval δ. Depending on δ, employ Operation I or Operation II based on $\oplus$ to make congruent size-2 subsets in $\mathcal{S}^{(k)}$, which results in $\mathcal{R}^{(k)}$;

3) If $\mathcal{R}^{(k)} = \{0\}$, go to step 4); otherwise set $k \leftarrow k+1$, $\mathcal{S}^{(k)} = \mathcal{R}^{(k-1)}$ and go to step 2);

4) (*Redefinition*) If $|\boldsymbol{v}(0)| = L$, go to step 5); otherwise redefine $\mathcal{R}^{(k)}$ and determine Q for $\oplus_Q$. Set $k \leftarrow k+1$, $\mathcal{S}^{(k)} = \mathcal{R}^{(k-1)}$ and $\oplus \leftarrow \oplus_Q$, then go to step 2);

5) (*Termination*) The subset-pairing procedure terminates.

Due to Property 3, when $k = 0$, the optimal $\Delta^* = L/2 = 2^{b-1}$, which is an even integer. Then Operation II is always firstly applied on $\mathbf{V}_L$ and redefinition of the reference set is always a necessary step in the set partitioning for $\mathbf{V}_L$.

5.5 Examples and Numerical Results

In this section, we consider examples of TC-DUSTM and compare their BEP with the uncoded DUSTM. We assume a Rayleigh flat fading channel with the maximum normalized Doppler frequency shift as 0.0025. The number of receiver antenna is

Table 5.1: Subset-pairing for $\mathbf{V}_8$ $(M = 2, R = 1.5)$.

Layer-j	$\lvert\boldsymbol{v}_i^{(j)}\rvert$	$\zeta_{\min}^{(j)}$	Δ^*	δ	k	$\mathcal{S}^{(k)}$	$-$ Operation $\rightarrow$	$\mathcal{R}^{(k)}$
1	8	0.51	$\sim$	$\sim$	3	$\sim$	$\sim$	$\sim$
2	4	0.71	1	1	2	$\mathbb{Z}_2$	I	$2\mathbb{Z}_1$
3	2	1.00	2	2	1	$\mathbb{Z}_4$	II	$\mathbb{Z}_2$
4	1	∞	4	4	0	$\mathbb{Z}_8$	II	$\mathbb{Z}_4$

Table 5.2: Subset-pairing for $\mathbf{V}_{16}$ $(M = 3, R = 1.33)$.

Layer-j	$\lvert\boldsymbol{v}_i^{(j)}\rvert$	$\zeta_{\min}^{(j)}$	Δ^*	δ	k	$\mathcal{S}^{(k)}$	$-$ Operation $\rightarrow$	$\mathcal{R}^{(k)}$
1	16	0.45	$\sim$	$\sim$	4	$\sim$	$\sim$	$\sim$
2	8	0.51	1	1	3	$\mathbb{Z}_2$	I	$2\mathbb{Z}_1$
3	4	0.71	2	2	2	$\mathbb{Z}_4$	II	$\mathbb{Z}_2$
4	2	1.00	4	4	1	$\mathbb{Z}_8$	II	$\mathbb{Z}_4$
5	1	∞	8	8	0	$\mathbb{Z}_{16}$	II	$\mathbb{Z}_8$

set to be 1. We also apply a 500×5 block interleaver which interleaves the signal block-wisely.

5.5.1 TC-DUSTM with $\mathbf{V}_8$ $(M = 2, R = 1.5)$

We consider DUSTM signal set $\mathbf{V}_8$ $(M = 2, R = 1.5)$. $\mathcal{P}_{\mathbf{V}_8}$ is illustrated in Fig. 5.2(b). Following the Proposition, we set $\mathcal{S}^{(0)} \leftarrow \mathbb{Z}_8$, then determine $\Delta = \Delta^* = 4 \in \mathbf{\Delta}_{\mathcal{S}^{(0)}}$ according to (5.24). We choose $p' = 2$ such that $\frac{4}{2^1} = 1$ is an odd integer. The corresponding cosets in $\mathcal{S}^{(0)}$ are $\{0, 4\} \oplus_3 m, m \in \mathbb{Z}_4$. In $\{0, 4\}$, integer-pairing is straightforward, leading to $\mathcal{R}^{(0)} = \{0\}$. Then we redefine $\mathcal{R}^{(0)} = \mathbb{Z}_4$ according to the Proposition.

Then we set $\mathcal{S}^{(1)} \leftarrow \mathbb{Z}_4$. By (5.24), we find $\delta = \Delta^* = 2$ is still an even integer. Then we choose $p' = 1$ such that $\frac{2}{2} = 1$ is an odd integer. Then we have cosets $\mathcal{S}_{\text{in}}^{(1)} \oplus m, m \in \mathbb{Z}_2$, where $\mathcal{S}_{\text{in}}^{(1)} = \{0, 2\}$. Integer-pairing in $\{0, 2\}$ is straightforward,

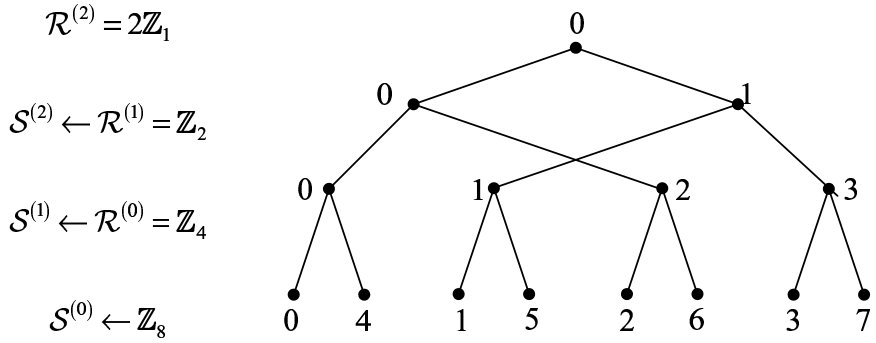

Figure 5.3: Set partitioning for $\mathbf{V}_8$ $(M = 2, R = 1.5)$.

leading to $\mathcal{R}^{(1)} = \{0\}$, which is redefined as $\mathcal{R}^{(1)} = \mathbb{Z}_2$. We set $\mathcal{S}^{(2)} \leftarrow \mathbb{Z}_2$, in which the integer-pairing is straightforward. We recorded the pertinent parameters in Table 5.1 and in Fig. 5.3 we can find the structure of the set partitioning tree.

This set partitioning can be applied to the TC-DUSTM of $M = 2, R = 1$. One realization of the trellis encoder and the resulting trellis diagram are illustrated in Fig. 5.4, from which we can see $\ell_{\min} = 1$. The BEP comparison between the TC-DUSTM and the uncoded DUSTM $(M = 2, R = 1)$ is given in Fig. 5.5. One can observe that a coding gain of around 5dB can be obtained by the TC-DUSTM over the uncoded DUSTM at moderate and high SNR. However, at low SNR, TC-DUSTM may produce worse error performance than the uncoded DUSTM. This phenomenon is similar to that of TCM [32]. We also note that at relatively high SNR, the BEP lower bound gives an accurate estimate of the BEP performance.

5.5.2 TC-DUSTM with $\mathbf{V}_{16}$ $(M = 3, R = 1.33)$

In this section, we examine the TC-DUSTM of $M = 3, R = 1$. Therefore the signal set employed should be $\mathbf{V}_{16}$ for which $M = 3, R = 1.333$. The set partitioning procedure follows the Proposition in Section 5.4.3. The operations and the pertinent

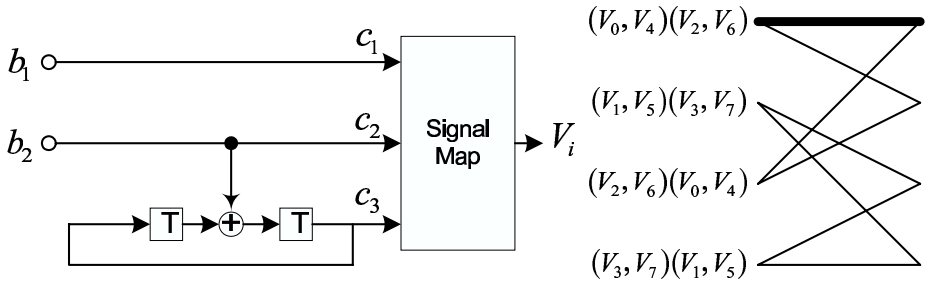

Figure 5.4: Trellis encoder and trellis diagram for TC-DUSTM ($M = 2, R = 1$).

parameters are recorded in Table 5.2 and the set partitioning tree is illustrated in Fig. 5.6. We illustrate the BEP comparison in Fig. 5.7 between TC-DUSTM and the uncoded DUSTM ($M = 3, R = 1$). The achieved coding gain can be observed to be greater than 8dB at the BEP of 10^{-5}. The lower bound also agrees well with the BEP, especially in the high SNR region.

5.6 Summary

Based on the PEP and BEP analysis, a trellis coding scheme for the DUSTM has been proposed in this chapter for a continuously changing mobile environment. The PEP and the BEP analysis also suggest the design criteria for the TC-DUSTM to obtain a best BEP performance. Simulations and theoretical analysis demonstrate that significant coding gain can be obtained by the TC-DUSTM over the uncoded DUSTM.

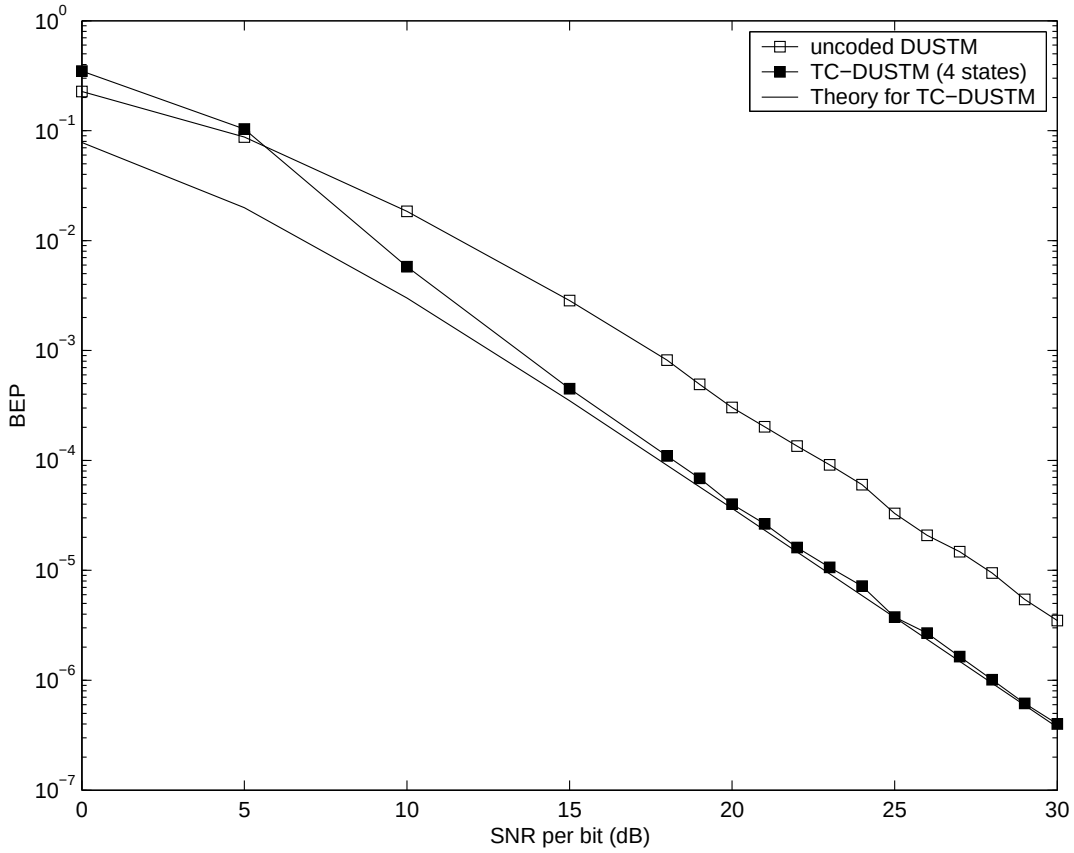

Figure 5.5: BEP comparison between TC-DUSTM and uncoded DUSTM ($M = 2, R = 1$).

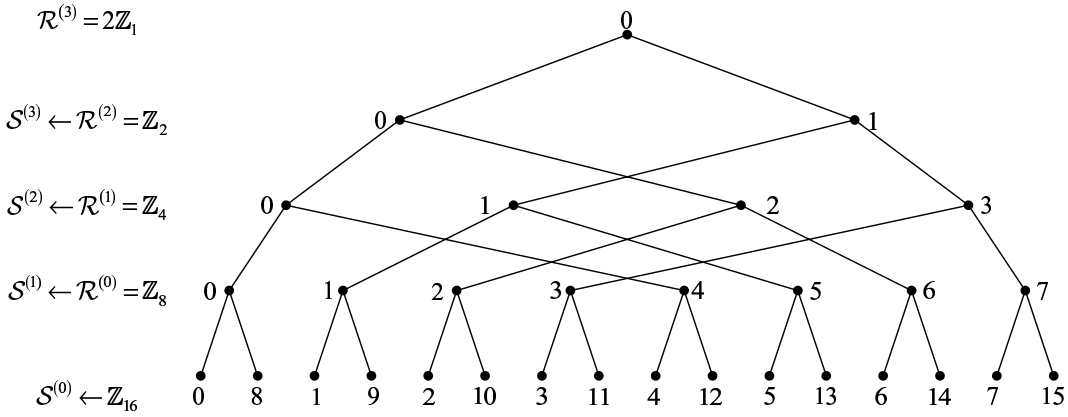

Figure 5.6: Set partitioning tree for $\mathbf{V}_{16}$ ($M = 3, R = 1.33$).

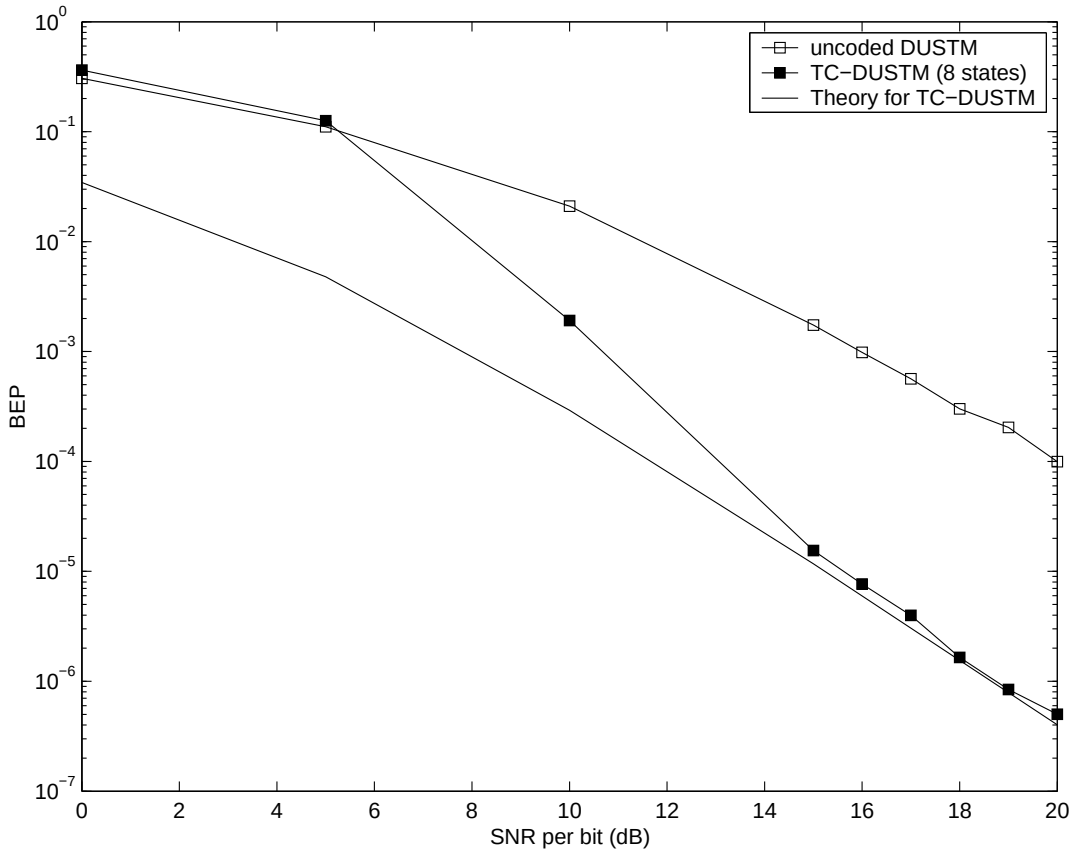

Figure 5.7: BEP comparison between TC-DUSTM and uncoded DUSTM ($M = 3, R = 1$).

Chapter 6

Conclusions and Future Works

In this thesis, we have examined a large class of trellis coded unitary space-time modulation schemes for the non-coherent MIMO system, namely, the trellis-coded USTM in Chapter 3, the multiple trellis-coded USTM in Chapter 4 and the trellis-coded differential USTM in Chapter 5. To carry out the research in these topics, we have followed the same approach: firstly, we proceed with the error performance of the proposed coding scheme; then we come up with the design criteria to minimize the PEP or BEP performance; lastly, we realize these criteria in a systematic way. We also carry out simulation as well as use BEP lower bound to demonstrate the validity of these coding scheme. Mainly, we have obtained the following results.

6.1 Completed Work

6.1.1 TC-USTM

We have proposed a bandwidth and power efficient TC-USTM coding scheme, which combines modulation and coding into one step for the non-coherent MIMO system, operated in the piecewise constant Rayleigh fading channel. Following the line of

Ungerboeck's celebrated "mapping by set partitioning" for the 2-D signal set, we formulate a systematic "mapping by set partitioning" technique for the UST signal set, which can be realized through a systematic recursive way. This approach can greatly simplify the searching procedure for a good coding scheme, and is implementable in a computer search. The resulting TC-USTM has significant coding gains over the uncoded USTM, due to the increased diversity gain and coding gain by the coding process. Computer simulations show that the theoretical analysis is accurate as they agree well with the BEP curves obtained through simulations, especially at high SNR.

6.1.2 MTC-USTM

We also assign multiple UST signals to one trellis branch, resulting in the so-called MTC-USTM. Though parallel paths exist in this scheme, the $\ell_{\min}$ can be as long as k, which is the length of the tuple associated with each trellis, and this gives another degree of freedom in the design of the coding scheme. We implement a systematic partitioning of the k-fold Cartesian product, that produces equal-size and identically structured k-fold UST signal subsets. We focus on the case where $\ell_{\min} = k$. We found that a larger UST signal set (four-times greater instead of two-times greater as usual) is usually employed when $k \geqslant 3$. Given the same information rates and same number of states, the MTC-USTM outperforms the TC-USTM, especially at high SNR.

6.1.3 TC-DUSTM

We extend the TC-USTM to the case where the continuous Rayleigh fading channel is employed instead of the piecewise constant fading channel. To suit this channel model, differential UST signal set is used, which requires a new error performance analysis to obtain the design criteria for TC-DUSTM, though we arrive at a similar

result to that in TC-USTM. Therefore the systematic and recursive "mapping by set partitioning" can be borrowed from TC-USTM and modified to suit for TC-DUSTM. The results also conforms with the analysis.

6.2 Future Work

Several issues, which are discovered during this work and listed below, can be further investigated.

For TC-DUSTM, when we derived the decision metric in Section 5.2, we only considered the condition that the operating SNR is high enough such that the product terms of the white Gaussian noise matrices $W_\tau W_\tau^\dagger$, $W_\tau W_{\tau-1}^\dagger$ and $W_{\tau-1} W_{\tau-1}^\dagger$ were neglected in the derivation. Though we obtained a most important benefit as that a much simplified expression is obtained, some useful information is also lost. Therefore it is interesting to continue to examine a full decision metric comprising these product terms, especially in the low SNR region. We believe in this way by sacrificing some decoding complexity, the decision metric would be more accurate and therefore give rise to a better error rate performance.

For MTC-USTM, when $k \geqslant 3$, the condition under which the availability of the subsets in the k-fold Cartesian product that ensures $\ell_{\min} \geqslant k$, need to be further studied. In this work, the searching for such kind of subsets is conducted simply by computer search, which is cumbersome and time consuming. Therefore theoretical analysis on the availability of such subsets is desirable.

Another important issue to explore is to incorporate the state-of-the-art coding

technique into this trellis coded USTM, *e.g.*, turbo codes and iterative decoding process, and the low density parity check codes. These codes are powerful and can approach channel capacity even at low SNR. Therefore it is of great interest to evaluate the error performance for these combined coding system.

The UST signal set also lends itself for the purpose of blind channel estimation. Since the subspace delivered by the UST signal set will not change due to the multiplicative fading coefficients between antenna pairs, one can first obtain the channel matrix (CSI) through a ML algorithm. Then this channel matrix can be taken as the real channel matrix and subsequently a coherent decoding algorithm can be obtained. Thus, a *hybrid* transmission and detection scheme can be proposed.

It is also interesting to put the USTM signaling in a time dispersive channel environments to study the error rate performance. Each component channel is now characterized by a FIR filter. For the purpose of implementing the ML decoding, deconvolution techniques have to be employed to demodulate the received UST signal set.

Appendix A

Derivation of Pairwise Error Event Probability P_{event}

Based on equation (3.5), the PEP of mistaking $\mathbf{\Phi}^K$ for $\hat{\mathbf{\Phi}}^K$, or vice versa can be derived in a integral form as

$$\begin{aligned} P_{\text{event}} &= p\left(\mathbf{\Phi}_L \rightarrow \hat{\mathbf{\Phi}}_L \mid \mathbf{\Phi}_L \text{transmitted}\right) \\ &= p\left(\hat{\mathbf{\Phi}}_L \rightarrow \mathbf{\Phi}_L \mid \hat{\mathbf{\Phi}}_L \text{transmitted}\right) \\ &= p\left(\sum_{t=1}^{K} \text{tr}\left\{X_t^\dagger \Phi_{l_t} \Phi_{l_t}^\dagger X_t\right\} < \sum_{t=1}^{K} \text{tr}\left\{X_t^\dagger \Phi_{\hat{l}_t} \Phi_{\hat{l}_t}^\dagger X_t\right\} \mid \mathbf{\Phi}_L\right) \\ &= p\left(\sum_{t=1}^{K} \text{tr}\left\{X_t^\dagger \left(\Phi_{l_t} \Phi_{l_t}^\dagger - \Phi_{\hat{l}_t} \Phi_{\hat{l}_t}^\dagger\right) X_t\right\} < 0 \mid \mathbf{\Phi}_L\right) \\ &= p\left(D = \sum_{t=1}^{K} D_t > 0 \mid \mathbf{\Phi}_L\right) \end{aligned} \tag{A.1}$$

where the random variable D_t is defined as $D_t = X_t^\dagger \left(\Phi_{\hat{l}_t} \Phi_{\hat{l}_t}^\dagger - \Phi_{l_t} \Phi_{l_t}^\dagger\right) X_t$. To evaluate P_{event}, which is the probability that the sum of K independent random variables D_t is greater than 0, a common approach is to find the characteristic function of D, denoted as $\Psi_D(\omega)$, then invert $\Psi_D(\omega)$ to find the pdf of D [62].

When $\Phi_{l_t} \neq \Phi_{\hat{l}_t}$, the characteristic function of D_t is [9]

$$\Psi_{D_t}(\omega) = \prod_{m=1, d_{m,t}<1}^{M} \left(\frac{1+\rho T/M}{(\rho T/M)^2(1-d_{m,t}^2)((\omega - i/2)^2 + a_{m,t}^2)} \right)^N, \tag{A.2}$$

where

$$a_{m,t} = \sqrt{\frac{1}{4} + \frac{1+\rho T/M}{(\rho T/M)^2(1-d_{m,t}^2)}} \tag{A.3}$$

and $d_{m,t}$ is the mth singular value of the correlation matrix $\Phi_{l_t}^{\dagger}\Phi_{\hat{l}_t}$. When $\Phi_{l_t} = \Phi_{\hat{l}_t}$, $\Psi_{D_t}(\omega) = 1$. As H_t's are independent for different t's, the D_t's are independent. Therefore the characteristic function of D is $\Psi_D(\omega) = \prod_{t\in\ \eta} \Psi_{D_t}(\omega)$, where η is the set of t for which $\Phi_{l_t} \neq \Phi_{\hat{l}_t}$. Note that the region of convergence for $\Psi_{D_t}(\omega)$ is $1/2 - a_{m,t} < \Im(\omega) < 1/2 + a_{m,t}$, where $\Im(\cdot)$ denote the imaginary part of the complex number $(\cdot)$. We can invert the characteristic function $\Psi_D(\omega)$ to find the pdf of D by selecting an integration contour within the region of the convergence as $-\infty + \frac{i}{2}$ to $+\infty + \frac{i}{2}$

$$P_D(z) = \frac{1}{2\pi} \int_{\omega=-\infty+i/2}^{\infty+i/2} d\omega\ \exp(i\omega z) \prod_{t\in\eta} \Psi_{D_t}(\omega). \tag{A.4}$$

Accordingly, the PEP can be derived as

$$\begin{aligned}
P_{\text{event}} &= \int_{z=0}^{\infty} P_D(z)dz \\
&= \int_{z=0}^{\infty} \frac{1}{2\pi} \int_{\omega=-\infty+i/2}^{\infty+i/2} d\omega\ \exp(i\omega z) \prod_{t\in\eta} \Psi_{D_t}(\omega) dz \\
&= \frac{1}{2\pi} \int_{\omega=-\infty+i/2}^{\infty+i/2} d\omega \prod_{t\in\eta} \Psi_{D_t}(\omega) \int_{z=0}^{\infty} \exp(i\omega z) dz \\
&= \frac{1}{2\pi} \int_{\omega=-\infty}^{\infty} \frac{d\omega}{\omega^2 + 1/4} \prod_{t\in\eta} \prod_{m=1, d_{m,t}<1}^{M} \left[\frac{1+\rho T/M}{(\rho T/M)^2(1-d_{m,t}^2)(\omega^2 + a_{m,t}^2)} \right]^N
\end{aligned}$$

$$= \frac{1}{2\pi}\int_{\omega=-\infty}^{\infty}\frac{d\omega}{\omega^2+1/4}\left\{\prod_{t\in\eta}\prod_{m=1,d_{m,t}<1}^{M}\left[1+\frac{(\rho T/M)^2(1-d_{m,t}^2)(\omega^2+1/4)}{1+\rho T/M}\right]^{-N}\right\}. \tag{A.5}$$

Appendix B

Derivation of Conditional Mean of $\tilde{Y_\tau}$

The conditional mean of the received signal $\tilde{Y_\tau}$ is

$$\begin{aligned} E\{\tilde{Y_\tau} \mid V_{\tilde{z}_\tau}\} &= \rho V_{\tilde{z}_\tau} E\{|\mathbf{H}|^2\} + E\{\mathbf{W}_\tau^{'}\} \\ &= \rho V_{\tilde{z}_\tau} E\{|\mathbf{H}|^2\} \end{aligned} \tag{B.1}$$

Let $\mathbf{K} = \mathbf{H}\mathbf{H}^\dagger$. Then each entry in $\mathbf{K}$ can be expressed as $\mathbf{k}_{i,j} = \sum_{p=1}^{N} \mathbf{h}_{i,p}\mathbf{h}_{j,p}^*, 1 \leqslant i, j \leqslant M$. So

$$E\{\mathbf{k}_{i,j}\} = \sum_{p=1}^{N} E\{\mathbf{h}_{i,p}\mathbf{h}_{j,p}^*\} = \sum_{p=1}^{N} \delta_{i,j} = N\delta_{i,j}. \tag{B.2}$$

Therefore

$$E\{\mathbf{K}\} = NI_M. \tag{B.3}$$

As a result

$$E\{\tilde{Y_\tau} \mid V_{\tilde{z}_\tau}\} = \rho N V_{\tilde{z}_\tau}. \tag{B.4}$$

Appendix C

Derivation of Conditional Variance of $\tilde{Y}_\tau$

Let $\mathbf{A} = \mathbf{K}\mathbf{K}^\dagger$, where $\mathbf{K}$ is defined in Appendix B. Each element in $\mathbf{A}$ is expressed as $\mathbf{a}_{i,j} = \sum_{l=1}^{M} \mathbf{k}_{i,l}\mathbf{k}_{j,l}^*, 1 \leqslant i,j \leqslant M$. When $i \neq j$,

$$\begin{aligned} E\{\mathbf{a}_{i,j}\} &= \sum_{l=1}^{M} E\{\mathbf{k}_{i,l}\mathbf{k}_{j,l}^*\} = \sum_{l=1}^{M}\sum_{k=1}^{N}\sum_{k'=1}^{N} E\{\mathbf{h}_{i,k}\mathbf{h}_{l,k}^*\mathbf{h}_{j,k'}^*\mathbf{h}_{l,k'}\} \\ &= \sum_{k=1}^{N} E\{\mathbf{h}_{i,k}\mathbf{h}_{i,k}^*\mathbf{h}_{j,k}^*\mathbf{h}_{i,k}\} + \sum_{k=1,k\neq k'}^{N}\sum_{k'=1}^{N} E\{\mathbf{h}_{i,k}\mathbf{h}_{i,k}^*\mathbf{h}_{j,k}^*\mathbf{h}_{i,k}\} \\ &\quad + \sum_{l=1,i\neq l}^{M}\sum_{k=1}^{N}\sum_{k'=1}^{N} E\{\mathbf{h}_{i,k}\mathbf{h}_{i,k}^*\mathbf{h}_{j,k}^*\mathbf{h}_{i,k}\} \\ &= 0. \end{aligned} \tag{C.1}$$

When $i = j$,

$$\begin{aligned} E\{\mathbf{a}_{i,j}\} &= \sum_{l=1}^{M} E\{\mathbf{k}_{i,l}\mathbf{k}_{i,l}^*\} = \sum_{l=1}^{M}\sum_{k=1}^{N}\sum_{k'=1}^{N} E\{\mathbf{h}_{i,k}\mathbf{h}_{l,k}^*\mathbf{h}_{i,k'}^*\mathbf{h}_{l,k'}\} \\ &= \sum_{k=1}^{N} E\{\mathbf{h}_{i,k}\mathbf{h}_{i,k}^*\mathbf{h}_{i,k}^*\mathbf{h}_{i,k}\} + \sum_{k=1,k\neq k'}^{N}\sum_{k'=1}^{N} E\{|\mathbf{h}_{i,k}|^2\}E\{|\mathbf{h}_{i,k'}|^2\} \\ &\quad + \sum_{l=1,l\neq i}^{M}\sum_{k=1}^{N}\sum_{k'=1}^{N} E\{\mathbf{h}_{i,k}\mathbf{h}_{l,k}^*\mathbf{h}_{i,k'}^*\mathbf{h}_{l,k'}\} \end{aligned}$$

$$
\begin{aligned}
&= \sum_{k=1}^{N} E\{|\mathbf{h}_{i,k}|^4\} + N(N-1) + \sum_{l=1,l\neq i}^{M}\sum_{k'=1}^{N} E\{|\mathbf{h}_{i,k'}|^2\}E\{|\mathbf{h}_{l,k'}|^2\} \\
&\quad + \sum_{l=1,l\neq i}^{M}\sum_{k=1,k\neq k'}^{N}\sum_{k'=1}^{N} E\{\mathbf{h}_{i,k}\}E\{\mathbf{h}_{l,k}^*\}E\{\mathbf{h}_{i,k'}^*\}E\{\mathbf{h}_{l,k'}\} \\
&= N(2\times 2\times \frac{1}{4} + 2^2\frac{1}{4}) + N(N-1) + (M-1)N + 0 \\
&= N^2 + MN \qquad \text{(C.2)}
\end{aligned}
$$

Therefore,

$$E\{\mathbf{A}\} = (N^2 + NM)I_M \qquad \text{(C.3)}$$

With the above results, one can readily derive the variance of $\tilde{Y}_\tau$ as

$$
\begin{aligned}
\Lambda &= E\left\{\left(\tilde{Y}_\tau - \rho N V_{\tilde{z}_\tau}\right)\left(\tilde{Y}_\tau - \rho N V_{\tilde{z}_\tau}\right)^\dagger\right\} \\
&= E\left\{\left(\rho V_{\tilde{z}_\tau}\left(\mathbf{H}\mathbf{H}^\dagger - NI_M\right) + \mathbf{W}_\tau^{'}\right)\left(\rho V_{\tilde{z}_\tau}\left(\mathbf{H}\mathbf{H}^\dagger - NI_M\right) + \mathbf{W}_\tau^{'}\right)^\dagger\right\} \\
&= \rho^2 MNI_M + E\left\{\mathbf{W}_\tau^{'}\mathbf{W}_\tau^{'\dagger}\right\}
\end{aligned}
$$

Let $\mathbf{W}_1 = \sqrt{\rho}V_{\tilde{z}_\tau}\mathbf{H}\mathbf{W}_{\tau-1}^\dagger$ and $\mathbf{W}_2 = \sqrt{\rho}\mathbf{W}_\tau\mathbf{H}^\dagger$, then

$$E\{\mathbf{W}_\tau^{'}\mathbf{W}_\tau^{'\dagger}\} = E\left\{\mathbf{W}_1\mathbf{W}_1^\dagger\right\} + E\left\{\mathbf{W}_2\mathbf{W}_2^\dagger\right\} \qquad \text{(C.4)}$$

Let $\mathbf{Z} = \mathbf{H}\mathbf{W}_{\tau-1}^\dagger$, then each entry in $\mathbf{Z}$ is $\mathbf{z}_{i,j} = \sum_{k=1}^{N}\mathbf{h}_{i,k}\mathbf{w}_{j,k}^\dagger, 1 \leqslant i,j \leqslant M$, where $\mathbf{w}_{j,k}$ denotes the entry in $\mathbf{W}_{\tau-1}$. Then entries in $\mathbf{Z}\mathbf{Z}^\dagger$ will have the form

$$
\begin{aligned}
\sum_{k=1}^{M}\mathbf{z}_{i,k}\mathbf{z}_{j,k}^* &= \sum_{k=1}^{M}\left(\sum_{k'=1}^{N}\mathbf{h}_{i,k'}\mathbf{w}_{k,k'}^*\right)\left(\sum_{k''=1}^{N}\mathbf{h}_{j,k''}^*\mathbf{w}_{k,k''}\right) \\
&= \sum_{k=1}^{M}\sum_{k'=1}^{N}\sum_{k''=1}^{N}\mathbf{h}_{i,k'}\mathbf{w}_{k,k'}^*\mathbf{h}_{j,k''}^*\mathbf{w}_{k,k''}
\end{aligned}
$$

Thus,

$$\begin{aligned} E\left\{\sum_{k=1}^{M}\mathbf{z}_{i,k}\mathbf{z}_{j,k}^{*}\right\} &= \sum_{k=1}^{M}\sum_{k'=1}^{N}\sum_{k''=1}^{N} E\left\{\mathbf{h}_{i,k'}\mathbf{h}_{j,k''}^{*}\right\} E\left\{\mathbf{w}_{k,k'}^{*}\mathbf{w}_{k,k''}\right\} \\ &= \sum_{k=1}^{M}\sum_{k'=1}^{N} E\{\mathbf{h}_{i,k'}\mathbf{h}_{j,k'}^{*}\} \\ &= \begin{cases} MN & 1 \leqslant i = j \leqslant M \\ 0 & \text{otherwise} \end{cases} \end{aligned} \tag{C.5}$$

As a result,

$$E\left\{\left|\mathbf{H}\mathbf{W}_{\tau-1}^{\dagger}\right|^{2}\right\} = MNI_{M}. \tag{C.6}$$

Similarly, $E\{|\mathbf{W}_{\tau}\mathbf{H}^{\dagger}|^{2}\} = MNI_{M}$. Therefore the conditional variance is

$$\Lambda = \rho^{2}MNI_{M} + 2\rho MNI_{M}. \tag{C.7}$$

Appendix D

Author's Publications

1. Zhenyu Sun and T.T. Tjhung, "On performance analysis and design criteria for trellis coded unitary space-time modulation," *IEEE Commun. Letters*, pp. 156-158, April 2003.

2. Zhenyu Sun and T.T. Tjhung, "Multiple trellis coded unitary space-time modulation in Rayleigh flat fading," accepted as regular paper by *IEEE Trans. Wireless Commun.*.

3. Zhenyu Sun and T.T. Tjhung, "A systematic set partitioning for unitary space-time signal set," submitted to *IEEE Trans. Inform. Theory*.

4. Zhenyu Sun and T.T. Tjhung, "On performance analysis and design criteria for trellis coded differential unitary space time modulation," in *Proc. of ICC*, pp. 3477 -3481, Alaska, US, May 2003.

5. Zhenyu Sun and T.T. Tjhung, "Multiple trellis coded differential unitary space time modulation in Rayleigh flat fading," in *Proc. of ICASSP*, pp. IV_353 - 356, Hong Kong, April 2003.

6. Zhenyu Sun and T.T. Tjhung, "On performance analysis and design criteria for trellis coded unitary space-time modulation," in *Proc. of WCNC*, pp. 262 -267, New Orleans, US, March 2003.

7. Zhenyu Sun and T.T. Tjhung, "Multiple trellis coded unitary space time modulation in Rayleigh flat fading," in *Proc. of VTC Spring*, pp. 47-51, Jeju, Korea, April, 2003.

8. Zhenyu Sun and T.T. Tjhung, "Trellis coded differential unitary space-time modulation: performance analysis and design criteria," in *Proc of ICCS*, pp.198-202, Singapore, Nov. 2002.

9. Zhenyu Sun and T.T. Tjhung, "Trellis-coded unitary space-time modulation," in *Proc of the* $3G$ *Wireless Conf.*, pp.196-201, San Francisco, USA, May 2002.

Bibliography

[1] G. J. Foschini, "Layered space-time architecture for wireless communication in a fading environment when using multi-element antennas," *AT & T Bell Labs. Tech. J.*, vol. 1, no. 2, pp. 41-59, 1996.

[2] G. J. Foschini and M. Gans, "On limits of wireless communications in fading enironment when using multiple antennas," *Wireless Personal Commun.*, vol. 6, pp. 311-335, 1998.

[3] I. Telatar, "Capacity of multi-antenna Gaussian channels," *European Trans. Telecommun.*, vol. 10, pp. 585-595, Nov./Dec. 1999.

[4] T. L. Marzetta and B. M. Hochwald, "Capacity of a mobile multiple-antenna communication link in Rayleigh flat fading," *IEEE Trans. Inform. Theory*, vol. 45, pp. 139-157, Jan. 1999.

[5] G. D. Golden, G. J. Foschini, R. A. Valenzuela and P. W. Wolniansky, "Detection Algorithm and Initial Laboratory Results using the V-BLAST Space-Time Communication Architecture," *Electronics Letters*, pp. 14-15, Jan. 7, 1999.

[6] Lizhong Zheng and D. Tse, "Communication on the Grassmann manifold: a geometric approach to the noncoherent multiple-antenna channel," *IEEE Trans. Inform. Theory*, vol. 48, pp. 359-383, Feb. 2002.

[7] Lizhong Zheng and D. Tse, "Diversity and multiplexing: A fundermantal tradeoff in multiple-antenna channels," *IEEE Trans. Inform. Theory*, vol. 49, pp. 1073-1096, May 2003.

[8] B. Hassibi and T. L. Marzetta, "Multiple-antennas and isotropically random unitary inputs: the received signal density in closed forms," *IEEE Trans. Inform. Theory*, vol. 48, pp. 1473-1484, June 2002.

[9] B. M. Hochwald and T. L. Marzetta, "Unitary space-time modulation for multiple-antenna communications in Rayleigh flat fading," *IEEE Trans. Inform. Theory*, vol. 46, pp. 543-564, Mar. 2000.

[10] B. M. Hochwald, T. L. Marzetta, T. J. Richardson, W. Sweldens and R. Urbanke, "Systematic design of unitary space-time constellations," *IEEE Trans. Inform. Theory*, vol. 46, pp. 1962-1973, Sep. 2000.

[11] B. M. Hochwald, T. L. Marzetta and B. Hassibi, "Space-time autocoding," *IEEE Trans. Inform. Theory*, vol. 47, pp. 2761-2781, Nov. 2001.

[12] T. L. Marzetta, B. Hassibi and B. M. Hochwald, "Structured unitary space-time autocoding constellations," *IEEE Trans. Inform. Theory*, vol. 48, pp. 942-950, Apr. 2002.

[13] D. Agrawal, T. J. Richardson and R. L. Urbanke, "Multiple-antenna signal constellations for fading channels," *IEEE Trans. Inform. Theory,* vol. 47, pp. 2618-2626, Sept. 2001.

[14] B. M. Hochwald and W. Sweldens, "Differential unitary space time modulation," *IEEE Trans. Commun.*, vol. 48, pp. 2041-2052, Dec. 2000.

[15] E. Biglieri, J. Proakis and S. Shamai (Shitz), "Fading Channels: Information-Theoretic and Communications Aspects," *IEEE Trans. Inform. Theory*, vol. 44, pp. 2619-2692, Oct. 1998.

[16] B. L. Hughes, "Differential space-time modulation," *IEEE Trans. Inform. Theory*, vol. 46, pp. 2567-2578, Nov. 2000.

[17] V. Tarokh, N. Seshadri and A. R. Calderbank, "Space-time codes for high data rate wireless communication: perforance criterion and code construction," *IEEE Trans. Inform. Theory*, vol. 44, pp. 744-765, Mar. 1998.

[18] S. M. Alamouti, "A simple transmitter diversity scheme for wireless communications," *IEEE J. Select. Areas Commun.* vol. 16, pp. 1451-1458, Oct. 1998.

[19] V. Tarokh, H. Jafakhani and A. R. Calderbank, "Space-time block codes from orthogonal designs," *IEEE Trans. Inform. Theory*, vol. 45, pp. 1456-1467, July 1999.

[20] V. Tarokh, A. Naguib, N. Seshadri and A. R. Calderbank, "Combined array processing and space-time coding," *IEEE Trans. Inform. Theory*, vol. 45, pp. 1121-1128, May 1999.

[21] V. Tarokh, H. Jafarkhani and A. R. Calderbank, "Space-time block coding for wireless communications: performance results," *IEEE J. Selet. Areas Commun.*, vol. 17, NO. 3, pp. 451-460, July 1999.

[22] V. Tarokh and H. Jafarkhani, "A differential detection scheme for transmit diversity," *IEEE J. Select. Areas Commun.*, vol. 18, pp. 1169 -1174, July 2000.

[23] H. Jafarkhani and V. Tarokh, "Multiple transmit antenna differential detection from generalized orthogonal designs," *IEEE Trans. Inform. Theory,* vol. 47, pp. 2626-2630, Sept. 2001.

[24] S. L. Ariyavisitakul, "Turbo space-time processing to improve wireless channel capacity," *IEEE Trans. Commun.*, pp. 1347–1359, Aug. 2000.

[25] Z. Liu, G. B. Giannakis and B. L. Hughes, "Double differential space-time block codign for time selective fading channels," *IEEE Trans. Commun.*, vol. 49, pp. 1529-1539, Sept. 2001.

[26] H. Jafarkhani and N. Seshadri, "Super-orthogonal space-time trellis codes," *IEEE Trans. Inform. Theory*, vol. 49, pp. 937-950, Apr. 2003.

[27] Yi Gong and Ben Letaief, K., "Concatenated space-time block coding with trellis coded modulation in fading channels," *IEEE Trans. Wireless Commun.*, vol. 1, pp. 580-590, Oct. 2002.

[28] B. M. Hochwald and S. ten Brink, "Achieving near-capacity on a multiple-antenna channel," *IEEE Trans. Commun.*, vol. 51, pp. 389-399, Mar. 2003.

[29] E. Biglieri, J. Proakis and S. Shamai (Shitz), "Fading channels: Information-theoretic and communications aspects," *IEEE Trans. Inform. Theory*, vol. 44, pp. 2619-2692, Oct. 1998.

[30] L. H. Ozarow, S. Shamai (Shitz) and A. D. Wyner, "Information theoretic considerations for cellular mobile radio," *IEEE Trans. Veh. Technol.*, vol. 43, pp. 359-378, May 1994.

[31] D. Slepian, "Group codes fro the Gaussian channel," *Bell Syst. Tech. J.*, vol. 47, pp. 575-602, Apr. 1968.

[32] G. Ungerboeck, "Channel coding with multilevel/phase signal," *IEEE Trans. Inform. Theory*, vol. IT-28, pp. 55-66, Jan. 1982.

[33] G. Ungerboeck, "Trellis-coded modulation with redundant signal sets; Part I: Introduction; Part II: State of the art," *IEEE Commun. Mag.*, vol. 25, pp. 5-21, Feb. 1987.

[34] D. Divsalar and M. K. Simon, "The design of trellis coded MPSK for fading Channels: Performance criteria," *IEEE Trans. Commun.*, vol. 36, pp. 1004-1012, Sept. 1988.

[35] D. Divsalar and M. K. Simon, "Multiple trellis coded modulation (MTCM)," *IEEE Trans. Commun.*, vol. 36, pp. 410-419, Apr. 1988.

[36] D. Divsalar and M. K. Simon, "The design of trellis coded MPSK for fading Channels: Set partitioning for optimum code design," *IEEE Trans. Commun.*, vol. 36, pp. 1013-1021, Sept. 1988.

[37] J. K. Cavers and P. Ho, "Analysis of the error performance of trellis coded modulations in Rayleigh fading channels," *IEEE Trans. Commun.*, vol. 40, pp. 74-83, Jan. 1992.

[38] I. Bahceci and T. M. Duman, "Trellis coded unitary space-time modulation," in *Proc. of IEEE GlobeCom*, pp. 1108-1112, San Antonio, Texas, Nov. 2001.

[39] I. Bahceci and T. M. Duman, "Combined turbo coding and unitary space-time modulation," *IEEE Trans. Commun.*, vol. 50, pp. 1244-1249, Aug. 2002.

[40] W. Zhao, G. Leus, and G. B. Giannakis, "Algebraic design of unitary constellations for uncoded and trellis coded modulation of non-coherent space-time systems," submitted to *IEEE Trans. Inform. Theory*, July 2002.

[41] Tao Li and K.B. Letaief, "Bit-interleaved trellis coded unitary space-time modulation with iterative decoding," in *Proceedings of WCNC*, pp. 84-88, Mar. 2002.

[42] Meixia Tao and R. S. Cheng, "Trellis-coded differential unitary space-time modulation over flat fading channels," *IEEE Trans. Commun.*, pp. 587-596, Apr. 2003.

[43] Xiaotong Lin and Rick S. Blum, "Systematic design of space-time codes employing multiple trellis coded modulation," *IEEE Trans. Commun.*, pp. 608-615, April 2002.

[44] Z. Sun and T.T. Tjhung, "On performance analysis and design criteria for trellis coded unitary space-time modulation," *IEEE Commun. Letters*, pp. 156-158, April 2003.

[45] Z. Sun and T.T. Tjhung, "Multiple trellis coded unitary space-time modulation in Rayleigh flat fading," Accepted by *IEEE Trans. Wireless Commun.*.

[46] Z. Sun and T.T. Tjhung, "Set partitioning for trellis coded unitary space-time modulation," submitted to *IEEE Trans. Inform. Theory*.

[47] Z. Sun and T.T. Tjhung, "On performance analysis and design criteria for trellis coded differential unitary space time modulation," in *Proc. Int. Conf. on Commun. (ICC)*, Anchorage, Alaska, US, May, 2003.

[48] Z. Sun and T.T. Tjhung, "Multiple trellis coded differential unitary space time modulation in Rayleigh flat fading," in *Proc. of ICASSP*, Hong Kong, April 2003.

[49] Z. Sun and T.T. Tjhung, "On performance analysis and design criteria for trellis coded unitary space-time modulation," in *Proc. of WCNC*, New Orleans, US, March 2003.

[50] Z. Sun and T.T. Tjhung, "Multiple trellis coded unitary space time modulation in Rayleigh flat fading," in *Proc. of VTC* Spring, Jeju, Korea, April, 2003.

[51] Z. Sun and T.T. Tjhung, "Trellis coded differential unitary space-time modulation: performance analysis and design criteria," in *Proc of ICCS*, pp.198-202, Singapore, Nov. 2002.

[52] Z. Sun and T.T. Tjhung, "Trellis-coded unitary space-time modulation," in *Proc of the* $3G$ *Wireless Conf.*, pp.196-201, San Francisco, USA, May 2002.

[53] G. D. Forney, "Coset codes - Part I: Binary lattices and related codes," *IEEE Trans. Inform. Theory*, vol. 34, no. 6, pp. 1152-1187, Sept. 1988.

[54] G. D. Forney, "Geometrically uniform codes," *IEEE Trans. Inform. Theory*, vol. 37, pp. 1241-1260, Sept. 1991.

[55] C. E. Shannon, "A mathematical theory of communication," *Bell Syst. Tech. J.*, vol. 27, pp. 379-423 and pp. 623-656, July and Oct. 1948.

[56] G. D. Forney and G. Ungerboeck, "Modulation and coding for linear Gaussian channels," *IEEE Trans. Inform. Theory*, vol. 44, pp. 2384-2415, Oct. 1998.

[57] L.-F. Wei, "Trellis-coded mouldaiton using multidimensional constellations," *IEEE Trans. Inform. Theory*, vol. 33, pp. 483-501, July 1987.

[58] L.-F. Wei, "Rotationally invariant trellis-coded mouldaitons with multidimensional M-PSK," *IEEE J. Select. Areas Commun.*, vol. 7, pp. 1281-1295, Dec. 1989.

[59] A. J. Viterbi, "Error bounds for convolutional codes and an asymptotically optimum decoding algorithm," *IEEE Trans. Inform. Theory*, pp. 260-269, Apr. 1967.

[60] G. D. Forney, Jr., "The Viterbi algorithm", *Proc. IEEE*, vol. 61, pp. 268-278, 1973.

[61] W. C. Jakes, *Microwave Mobile Communications*, New York, Wiley, 1974.

[62] J. G. Proakis, *Digital Communications*, Third Edition, McGraw-Hill, 1995.

[63] E. Biglieri, D. Divsalar, P. J. McLane and M. K. Simon, *Introduction to Trellis-Coded Modulation with Applications*, Maxwell MacMillan Int. Editions, New York, 1991.

[64] J. H. Conway and N. J. A. Sloane, *Sphere Packings, Lattices and Groups*, Springer-Verlag, New York, 1988.

[65] L. Hanzo, T. H. Liew and B. L. Yeap, *Turbo Coding, Turbo Equalisation and Space-Time Coding for Transmission over Fading Channels*, John Wiley & Sons, 2002.